A Cognitive Radio Compressive Sensing Framework

Thesis

A Cognitive Radio Compressive Sensing Framework

Dimitrios Karampoulas
BEng (Hons), MSc

A Thesis submitted in partial fulfilment of
the requirements for the degree of Doctor of Philosophy

School of Computing and Communications
Faculty of Science, Technology, Engineering and Mathematics
The Open University
Milton Keynes
Submitted on 18th August 2017

Acknowledgements

I would like to express my deepest and sincerest gratitude to my supervisor Professor Laurence S. Dooley for his constant academic and moral support. His guidance, advice, comments and suggestions were tremendously valuable throughout this journey. His in-depth technical knowledge, expertise in scientific writing and unique ability to identify areas for improvement provided invaluable help to crystallization of ideas and production of this thesis. I am also immensely indebted to my co-supervisor Dr. Soraya Kouadri M. for her support and extremely valuable comments and advices. Her ability to look from a different perspective was crucial throughout the entire research.

My sincere gratitude also goes to Dr. Patrick Wong and the current and past members of the *neXt Generation Multimedia Technologies* (XGMT) research group at the Open University. They created a friendly environment for discussion and provided valuable comments during our Monday meetings. I am grateful especially to Parminder and Alam for their help they gave when I asked them for.

I would like also to thank my mini viva examiners Dr. Alan Jones and Dr. Tony Nixon for their comments and feedback during the initial phases of this project.

I also thank my children for their positive attitude and helping to focus on things other than research. In particular I also thank my son Sean for his advice with software packages.

Last but not least, I am deeply grateful to my adorable wife Nancy. She was instrumental to encourage and convince me to undertake this journey. The love, patience, compassion, support, flexibility and support were such, that it would be almost impossible to complete the thesis without them.

Abstract

With the proliferation of wireless devices and services, allied with further significant predicted growth, there is an ever increasing demand for higher transmission rates. This is especially challenging given the limited availability of radio spectrum, and is further exacerbated by a rigid licensing regulatory regime. Spectrum however, is largely underutilized and this has prompted regulators to promote the concept of opportunistic spectrum access. This allows unlicensed *secondary users* to use bands which are licensed to *primary users*, but are currently unoccupied, so leading to more efficient spectrum utilization.

A potentially attractive solution to this spectrum underutilisation problem is *cognitive radio* (CR) technology, which enables the identification and usage of vacant bands by continuously sensing the radio environment, though CR enforces stringent timing requirements and high sampling rates. *Compressive sensing* (CS) has emerged as a novel sampling paradigm, which provides the theoretical basis to resolve some of these issues, especially for signals exhibiting sparsity in some domain. For CR-related signals however, existing CS architectures such as the *random demodulator* and *compressive multiplexer* have limitations in regard to the signal types used, spectrum estimation methods applied, spectral band classification and a dependence on Fourier domain based sparsity.

This thesis presents a new generic *CS framework* which addresses these issues by specifically embracing three original scientific contributions: i) seamless embedding of the concept of *precolouring* into existing CS architectures to enhance signal sparsity for CR-related digital modulation schemes; ii) integration of the *multitaper* spectral estimator to improve sparsity in CR narrowband modulation schemes; and iii) exploiting sparsity in an alternative, non-Fourier (Walsh-Hadamard) domain to expand the applicable CR-related modulation schemes.

Critical analysis reveals the new *CS framework* provides a consistently superior and robust solution for the recovery of an extensive set of currently employed CR-type signals encountered in wireless communication standards. Significantly, the generic and portable nature of the framework affords the opportunity for further extensions into other CS architectures and sparsity domains.

Declaration

The work presented in this thesis is an original contribution of he author. Parts of the thesis have appeared in the following:

Peer-Reviewed Publications:

Karampoulas, D., Dooley, L. and Mostéfaoui, S. (2013a) "Precolouring in Compressive Spectrum Estimation for Cognitive Radio", In *IEEE EUROCON*, pp. 1715-1720, Zagreb, Croatia, 1-4 July.

Karampoulas, D., Kouadri, S. and Dooley, L. (2013b) "A Novel Precolouring-Random Demodulator Architecture for Compressive Spectrum Estimation", In *IET Intelligent Signal Processing*, pp. 1-6, London, UK, 2-3 December.

Karampoulas, D., Dooley, L. and Kouadri, S. (2014) "Integration of a precolouring matrix in the random demodulator model for improved compressive spectrum estimation", In *IEEE GlobalSIP*, pp. 1209-1213, Atlanta, USA, 3-5 December.

Karampoulas, D., Dooley, L. and Kouadri, S. (2015) "A multitaper-random demodulator model for narrowband compressive spectral estimation", In IEEE *GlobalSIP*, pp. 1362-1366, Orlando, USA, 14-15 December.

Table of Contents

List of Figures

List of Tables

List of Abbreviations

1G	1st generation
2G	2nd generation
3G	3rd generation
4G	4th generation
5G	5th generation
ADC	Analog to Digital Conversion/ter
AIC	Akaike Information Criterion
AM	Amplitude Modulation
AR	Autoregressive
AR-CM	Autoregressive with Compressive Multiplexer
AR-RD	AutoRegressive with Random Demodulator
ARMA	AutoRegressive Moving Average
AWGN	Additive White Gaussian Noise
BPSK	Binary Phase Shift Keying
BS	Base Station
CAT	Criterion Autoregressive Transfer
CDMA	Code Division Multiple Access
CM	Compressive Multiplexer
CR	Cognitive Radio
CS	Compressive Sensing
DFT	Discrete Fourier Transform
DSA	Dynamic Spectrum Access
ED	Energy Detector
FB	Filter Bank
FCC	Federal Communications Commission
FFT	Fast Fourier Transform
FM	Frequency Modulation
FPE	Final Prediction Error
GPS	Global Positioning System
IoT	Internet of Things
iid	independent & identically distributed

*i*PM-RD	integrated PM to RD
*i*PM-CM	integrated PM to CM
LAN	Local Area Network/s
LTE	Long Term Evolution
MAN	Metropolitan Area Network/s
MDL	Minimum Description Length
MLE	Maximum Likelihood Estimation
MS	Mobile Station
MT	Multitaper
MT-CM	Multitaper with Compressive Multiplexer
MT-RD	Multitaper with Random Demodulator
MTS	Mobile Telephone Service
MWC	Modulated Wideband Converter
Ofcom	Office of Communications
OFDM	Orthogonal Frequency Division Multiplexing
PM	Precolouring Matrix
PM-MT	Precolouring - Multitaper
PN	Pseudorandom Number
PSD	Power Spectral Density
PSK	Phased Shift Keying
PU	Primary User/s
QAM	Quadratur Amplitude Modulation
QoS	Quality of Service
QPSK	Quadrature Phase Shift Keying
RAN	Regional Area Networks
RD	Random Demodulator
RIP	Restrictive Isometry Property
RMS	Root mean square
SCF	Spectral Correlation Function
SDR	Software Defined Radio
SNR	Signal to Noise Ratio
SPS	Sequency Power Spectrum
SU	Secondary User/s
SVD	Singular Value Decomposition

TDL	Time Delay
TVWS	TV White Spaces
UNI-CS	Unified with Compressive Sensing
WH-CS	Walsh Hadamard with Compressive Sensing
WH-CM	Walsh Hadamard with Compressive Multiplexer
WH-RD	Walsh Hadamard with Random Demodulator
WHT	Walsh Hadamard Transform

List of Variables

a	Signal representation in the Fourier domain
a_k	The k^{th} AR filter coefficient
Δf	Frequency resolution
Δt	Sampling interval
λ_m	The m^{th} eigenvalue of the MT spectral estimator
σ_w^2	White noise variance
Φ	Measurement matrix in a CS framework/architecture
Φ_j	The j^{th} diagonal measurement matrix of a CM
Ψ	Sparse basis in a CS framework
b	Bandwidth per carrier
B	Signal bandwidth
c_k	The k^{th} element of the precolouring matrix
C	Precolouring matrix
f	Frequency
f_C	The precoloured frequency vector
f_{CMT}	The PM-MT frequency vector
f_{MT}	The MT frequency vector
f^l	The l^{th} frequency vector
f_k^l	The k^{th} element of the l^{th} frequency vector
F	DFT matrix
F_C	Precoloured DFT matrix
F_{MT}	MT DFT matrix
G	Recovery matrix of the classical RD
G_C	Recovery matrix of the AR-RD and *i*PM-RD
G_{CMT}	Recovery matrix of the UNI-RD
G_H	Recovery matrix of the WH-RD

G_{MT}	Recovery matrix of the MT-RD
G^{CM}	Recovery matrix of the classical CM
G_{C}^{CM}	Recovery matrix of the *i*PM-CM
G_{CMT}^{CM}	Recovery matrix of the UNI-CM
G_{H}^{CM}	Recovery matrix of the WH-CM
G_{MT}^{CM}	Recovery matrix of the MT-CM
h	Signal representation in the WH domain
H	WHT matrix
$H(f)$	Filter frequency response
H_N	Hadamard matrix of order N
J	Number of channels in a CS architecture
K	Number of non-zero coefficients (signal sparsity)
L	Number of Slepian sequencies
M	Number of CS measurements
$M\alpha$	Sampling rate of the RD
N	Number of signal samples taken at Nyquist frequency
$N\alpha$	Sampling rate at least equal to Nyquist rate
$\mathbb{N}$	The set of natural numbers
p	The AR filter order
p_c	Chipping sequence
P	Power Spectral Density (PSD) vector
P_C	The precoloured PSD vector
P_{CS}	Signal power recovered by CS architectures
P_{CMT}	The PM-MT PSD vector
P_H	The Sequency Power Spectrum (SPS) vector
P_{MT}	The MT PSD vector
P_{Nyq}	Signal power derived at rates equal or above Nyquist
P_{occ}	Power within the occupied frequencies

P_{total}	Signal plus noise power
q	Combined representation of the CM input in the Fourier domain
q_C	Combined representation of the *i*PM-CM input in the Fourier domain
q_{CMT}	Combined representation of UNI-CM input in the Fourier domain
q_H	Combined representation of WH-CM the input in the WH domain
q_{MT}	Combined representation of MT-CM the input in the Fourier domain
$r_i^{H_N}$	The i^{th} row of Hadamard matrix of order N
s	Signal representation in a sparse basis/domain
S	The MT matrix
t	Signal duration
T	Random demodulator data period
T_1	Average input noise level
T_2	RMS of signal PSD
v_{cs}	Spectral classification vector
v_{ref}	Reference vector
V^l	The l^{th} eigenvector determined by the MT spectral estimator
w	White noise process
W	Resolution of the MT spectral estimator
y	Measurement vector of the output of a CS architecture

1 Introduction

1.1. Overview

In the last decade, wireless communication has been undergoing rapid development, with mobile devices becoming an essential element of people's daily lives. As new technologies emerge, wireless services and applications are commensurately expanding, with mobile data traffic having grown 4000-fold over the past decade and 400 million times over the last 15 years (CISCO, 2016). Almost half a billion mobile devices and connections were added in 2016, with smartphones accounting for the most of that growth, raising the total global number of mobile devices to 8 billion in 2016 (CISCO, 2017a). More growth is anticipated in the future as global Internet traffic is predicted to increase nearly threefold by 2021, while traffic from wireless and mobile devices will account for almost two-thirds of this expansion (CISCO, 2017b).

This condition will dramatically increase the need for high data transmission rates, thus making it increasingly challenging to accommodate this expanding and emergent wireless world using the existing finite available spectrum, and deliver the required *quality of services* (QoS). The problem is further aggravated by the inflexible licensing of the wireless spectrum by the regulatory bodies to the telecommunications operators, the so-called *licensed* or *primary users* (PU) in the sense that the licensing is exclusive and no violation is allowed by *unlicensed* or *secondary users* (SU) (Ben Letaief & Zhang, 2007).

As a result, spectrum is an extremely scarce and valuable resource. It is estimated that in the US the licensed spectrum available for the mobile wireless industry is valued around US$500 billion (CTIA, 2016). In the UK the annual contribution in the spectrum to the economy was in 2014 over £50bn and is expected to double by 2025 (Real Wireless, 2015). Despite the spectrum scarcity and rigid regulations, the available spectrum is highly underutilized (Federal Communications Commission, 2002; Broderson et al. 2004) In particular, the degree of spectrum utilization ranges from 15% to 85% (Federal Communications Commission, 2002) in New York City

the maximum total spectrum occupancy is 13.1% from 30MHz to 3GHz (McHenry, 2005), while in the UK the Wi-Fi spectrum usage reaches 16% (Ofcom, 2013).

The observed spectrum underutilization allied with key technology developments in digital radio and computer software (Tuttlebee, 2002; Milligan, 2003), have prompted regulatory bodies like the *Federal Communications Commission* (FCC) (FCC, 2004) and the *Office of Communications* (Ofcom, 2007) to promote a completely different approach, where SU are allowed to *opportunistically* access and utilize unused licensed bands, referred to as *spectrum holes* or *white spaces* (Nekovee, 2010). This concept is called *dynamic spectrum access* (DSA) (Nekovee, 2006; Marcus, 2005) and leads to a more efficient utilization of the available spectrum. A special IEEE committee was established in 2005 to develop the IEEE 1900 regulatory series standards for DSA networks (IEEE DySPAN, 2017). Moreover, OFCOM proposed a spectrum sharing framework which introduced regulatory tools that facilitated spectrum sharing and evaluated the potential of sharing frequencies between PU and SU (OFCOM, 2015; OFCOM, 2016). Likewise, FCC introduced a 3-tier spectrum sharing framework where both PU and SU were assigned a priority spectrum access status and then subsequently placed into one of the 3 tiers (FCC, 2015).

A promising technology which offers mechanisms to improve spectrum utilization is *cognitive radio* (CR) (Mitola & Maguire, 1999; Mitola, 2000). The spectrum utilization is implemented in an autonomous manner (Haykin, 2005) by firstly, identifying the unused licensed radio spectrum and then, rendering this spectrum available for SU, while not causing any harmful interference to the PU, thereby respecting, at all times, their rights as the licensed operators. In order to facilitate this opportunistic spectrum access to SU, a CR transceiver needs to be aware of its radio environment and using this information it can then select and accordingly adapt its various communication parameters e.g., bandwidth, carrier frequency, modulation scheme, transmit power and networking parameters (Hossain & Bhargava, 2007).

There exist three methods for a CR transceiver to reliably identify white spaces (spectrum holes) without generating PU interference (Nekovee 2010; Brown, 2005): i) beacon signals, ii) geolocation with database, and iii) spectrum sensing. The beacon method requires dedicated infrastructure to be installed and maintained, while beacon signals can be lost due to mechanisms similar to the hidden node problem which may arise in wireless networks (Nekovee 2010). In contrast, the geolocation with database

approach is regarded by the regulators as offering a better short-term solution (Nekovee 2010; Webb, 2012), however, it requires modifications to the licensed systems and additional costly infrastructure for database construction and maintenance (Nekovee 2010; Ghasemi & Sousa, 2008). In addition, extra connectivity is required for information exchange between the SU and databases, as well as considerable management of participating parties (Webb, 2012). Crucially, as with the beacon signal solution, this method compromises the autonomous nature of a CR system, since the PU are under no obligation to share information regarding their operating parameters (Sun et al., 2013).

In the spectrum sensing approach, the identification of the spectral holes is accomplished solely by the SU in an autonomous manner (Haykin et al., 2009; Ghasemi & Sousa, 2008). After sensing a *vacant* licensed band, the SU can transmit on this band of frequencies provided the PU is not transmitting, so avoiding harmful interference. The infrastructure overheads are low and there is no need for any modification to the licensed systems. Consequently this has provided considerable impetus to investigate spectrum sensing by both researchers and industry, as evidenced by its inclusion in the IEEE 802.22, 802.11.af standards (Stevenson, 2009; Shellhammer, 2008; IEEE 802.22 Working Group, 2017; Flores et al., 2013). The spectrum sensing approach, its techniques and challenges is the subject of the following Section.

1.2. Spectrum Sensing for Cognitive Radio

Spectrum sensing is one of the critical components in CR technology (Ghasemi & Sousa; Ben Letaief & Zhang, 2007; Sun et al., 2013; Lundén et al., 2015) in enabling the successful identification of frequency bands for SU to gain access to any vacant channels. Moreover, spectrum awareness and by implication, spectrum sensing is crucial to adapting CR communication parameters (Lundén et al., 2015).

Spectrum sensing, due to its importance, has to perform robustly and reliably even in severe communication environments (Ghasemi & Sousa, 2008). This coupled with the variable and random nature of wireless channels (Haykin et al. 2009), presents many challenges to CR spectrum sensing, including uncertainties due to noise,

sensitivity, interference and the hidden node problem (Nekovee, 2010), as well as the strict requirements governing sensing time, awareness, adaptability and reliability (Ghasemi & Sousa, 2008; Fette, 2004; Ben Letaief & Zhang, 2007).

These challenges and strict requirements could be relaxed if a *cooperative* sensing strategy was to be employed, where multiple transceivers share their sensing results and mutually decide about the status of the spectrum bands (Ghasemi & Sousa, 2008; Ian F. Akyildiz et al., 2011). Even so, this incurs overheads like extra sensing time, delay, energy and infrastructure to accommodate the exchange of sensing information (Ghasemi & Sousa, 2008; Ian F. Akyildiz et al., 2011). In any case, the overall spectrum sensing performance of a CR network, even in a cooperative environment, is dependent on the performance of each of the CR transceivers of the network and the effectiveness of the spectrum techniques employed by them.

The most well-known techniques are matched filtering, energy detection, and cyclostationarity feature detection (Cabric et al., 2004; Yucek & Arslan, 2009; Sun et al., 2010). Energy-based detection is the most popular due to its simplicity and also does not require *a priori* knowledge of the input signal (Ben Letaief & Zhang, 2007; Hossain & Bhargava, 2007; Cabric et al., 2006; Doyle, 2009). This approach however, is considered as narrowband, in that the corresponding receiver systems are only capable of processing signals within a narrow bandwidth channel (Sun et al., 2013; Yucek & Arslan, 2009). Another common feature of these techniques is that the detection of the spectrum holes is a binary decision (Ben Letaief & Zhang, 2007; Haykin et al. 2009; Sun et al., 2013), meaning spectral bands are classified as either vacant or not.

However, to more efficiently exploit the presented spectrum opportunities, a CR network must also manage wideband signals operating over far wider frequency range from hundreds of megahertz to several gigahertz (Yucek & Arslan, 2009; Sun et al., 2013). This mandates the signal processing at much higher sampling rates, which may not be feasible if conventional techniques are applied (Tian & Giannakis, 2007; Yu & Hoyos, 2009). In addition, the stringent system requirement of very short sensing times (Ghasemi & Sousa, 2008; Tian & Giannakis, 2007), means only a limited number of samples can be collected, which may be insufficient for reliable sensing performance (Tian, 2008).

Moreover, the binary decision for spectral band classification implies that the only possible decisions are for a band to be *vacant* (white) or *occupied (black*). However, a

band could also be classified as *partially occupied* (*gray)*. Examples of such cases include low-power interfering signals (Haykin et al. 2009), underutilized channels (Cabric et al., 2006; Arianananda et al., 2009), or even mobile networks where PU transmissions are weak in an area where a SU is situated (Haykin et al. 2009). If only two occupancy states are considered, vacant or occupied, then these gray spectral bands would be identified as occupied and not as opportunities for the SU, certainly impacting the QoS of the CR network. Therefore, in order to also include the possibility of existence of gray bands and subsequently provide an accurate and efficient spectral classification, it is important to resort to sensing techniques that include *spectrum estimation* (Haykin et al. 2009).

Compressive sensing (CS) (Candès et al., 2006; Donoho, 2006) has emerged as a new signal acquisition paradigm. It is considered a type of sampling theory (Fornassier & Rauhut, 2015; Baraniuk et al., 2017), where signals which are *sparse* in some domain, can be efficiently be acquired and subsequently recovered in the sparse domain using relatively few measurements, with a sampling rate below that dictated by the Nyquist theorem (Kotelnikov, 1933; Nyquist, 1928). As the wireless communications signals are inherently sparse in the Fourier domain due to the spectrum underutilization, CS has the potential to address the challenges of the high sampling rates and the limited number of available signal samples. As the signal recovery is accomplished in the frequency domain, CS has also the potential to incorporate spectrum estimation. Collectively these CS opportunities underpin the key motivation for this research thesis.

1.3. Research Motivation

Much research activity has followed the emergence of CS theory and the field has attracted considerable attention in various disciplines including wireless communications and CR (Baraniuk et al., 2017; Fornassier & Rauhut, 2015; Duarte & Eldar, 2011; Hayashi et al., 2013). Several architectures have been presented and implemented as hardware prototypes, such as the *random demodulator* (RD), the *modulated wideband converter* (MWC) and the *compressive multiplexer* (CM) (Ragheb et al., 2008; Mishali et al., 2011; Slavinsky et al., 2011). They have also been

tested with communications signals and been evaluated to have a potential impact for spectrum sensing for CR type signals (Lexa et al., 2012; Tropp et al., 2010; Eldar & Kutyniok, 2012).

Despite existing CS solutions, which could provide the basis for novel more efficient spectrum sensing schemes, in particular in combination with spectrum estimation methods, there are still many challenges to be resolved in achieving efficient and reliable spectrum sensing in CR networks. Some of these include:

a. Several CS architectures assume specific input signal types e.g. narrowband and their performance becomes ineffectual for signals with different features. This has major spectral sensing implications for the different type of signal encountered in wireless applications, where diverse modulation and access schemes are frequently applied.

b. The underlying spectrum estimation technique adopted in many CS architectures is based on the classical *periodogram*, which while simple to realise has a number of major deficiencies including being an inconsistent and biased estimator (Manolakis et al., 2005). Consequently, more sophisticated spectrum estimation methods have to be considered.

c. Given the low spectrum utilization, almost all the CS techniques exploit signal sparsity in the frequency domain. As CS for CR improves spectrum utilization, the sparsity level of wireless signals is reduced and it may not be sufficient enough to facilitate satisfactory CS performance. It is therefore a challenge to perform CS exploiting possible signal sparsities in domains other than Fourier.

d. Although several architectures have been presented with the aim to improve performance of the existing CS structures, these have come at the cost of additional complexity (Yu & Hoyos, 2009; Taheri & Vorobyov, 2011; Y. Lu et al., 2011; Zhao et al., 2011; Harms et al., 2013; Mangia et al., 2011). Moreover, due to the wideband nature of the

signals involved, there is always a need to achieve as low sampling rates as possible.

e. The ultimate aim of spectrum sensing for CR purposes is the classification of the spectrum. Since there is the possibility of the existence of three occupancy states, the binary decision is no longer applicable, so the CS-based designs must be capable of assigning three possible occupancy states to the spectral bands.

These challenges along with the general aim of improving sensing performance and robustness of CS-based designs for a range of diverse signals in CR, without crucially increasing processing complexity, were the main motivations for this research. These are important requirements to be addressed if CS is going to be effectively employed in CR networks, since they are related with crucial issues such as inclusion of diverse range of signals, exploitation of spectrum estimation methods, consideration of sparsities other than Fourier, reliable spectral classification and complexity. This provided the context for the overarching thesis research question and the related objectives which are presented in the next Section.

1.4. Research Question and Objectives

From the above discussion, the following research question was framed:

How can spectrum sensing for Cognitive Radio-based be best achieved?

After a detailed literature survey and critical evaluation of existing CS techniques, a strategy *combining energy-based spectrum sensing with CS* was identified as a particularly promising area for further investigation, as it has considerable potential to achieve efficient and reliable classification of the spectral bands in CR applications. Such a strategy would lead to the design and development of novel spectrum sensing architectures that successfully address the challenges identified in Section 1.3, without

concomitantly imposing unfavourable overheads or trade-offs with the computational cost, hardware complex and the PU access.

A set of three research objectives were subsequently distilled to address the main overarching research question:

1. *To develop and critically analyse new compressive sensing architectures for cognitive radio applications.*

   Justification: This objective focuses on investigating and designing novel CS architectures for wireless communication signals by particularly, exploiting their structure so to increase frequency sparsity. This will seek to address the challenge of very high sampling rate requirements which often push current *analog to digital conversion* (ADC) technology to its limits, especially for wideband signals. It also addresses the stringent timing requirements, which means that only a very limited number of signal samples are able
   to be acquired. Furthermore, the CS architecture design must be flexible so it can handle different CR related signals as well as diverse modulation and radio access schemes. Finally it must be able to perform accurate and efficient spectral classification considering three occupancy states instead of two.

2. *To critically synthesize spectrum estimation into the compressive sensing architectures.*

   Justification: This objective seeks to enhance the capabilities of the CS architectures in *Objective 1* by integrating parametric spectrum estimation techniques into the spectrum sensing process for CR. The application of alternative non-parametric spectrum estimation methods instead of the established, but inconsistent periodogram provides the opportunity for more accurate and reliable information regarding spectrum utilization and occupation. There are in the literature spectrum estimators which are considered promising to be employed for spectrum sensing in CR applications, thanks to their favourable properties.

3. *To design and critically assess the CS architectures so to perform sensing for signals which are not sparse in the frequency domain.*

   Justification: The *Objectives 1 and 2* above, assume that the signals are frequency sparse. As CR improves spectrum utilization the spectrum becomes less sparse, which is not a favourable CS scenario because the basis for efficient sensing performance depends on the existence of sufficient signal sparsity in the frequency domain. Moreover, there are cases where wireless signals are not frequency sparse, as in the case of spread spectrum signal types like CDMA. Hence this objective seeks to extend the capabilities of the new CS architectures by examining the viability of performing CS for signals which are characterised by being sparse in other domains, rather than only the frequency domain.

The overall aim is to develop a new flexible CS framework, which provides consistently efficient and robust performance by exploiting signal structure and incorporating sophisticated spectrum estimation as well as extending CS functionality to domains other than frequency. The outcome is enhanced signal sparsity, which depending on the CS domain, can also be viewed as a noise reduction process.

1.5. Contributions

To accomplish the aforementioned objectives, this thesis presents a novel robust and flexible *generic Compressive Sensing framework*, which comprises four original scientific contributions to the field of compressive sensing for CR networks. Initially a novel CS model exploits the structure of several signals typical in telecommunications in order to enhance their sparsity and subsequently provide some important framework performance enhancements. Then another novel CS model employs spectrum estimation more sophisticated than the periodogram to improve performance. The performance is further increased by unifying the two models and is also expanded by introducing sparsity domains other than frequency. The outcome of

the models is employed in spectral/channel classification which considers the existence of three occupancy states.

The four original scientific contributions of this thesis are as follows:

a. A new *autoregressive* (AR)-based CS model is introduced and critically analysed as a realisation of the research objective 1. The model addresses the challenge to extend the scope of the existing CS designs so to handle various signal types encountered in CR by utilizing their structure to increase their sparsity, thereby improving performance. The sparsity enhancement is accomplished by seamlessly integrating *precolouring* to the existing CS architectures.

b. A new *multitaper* (MT)-based CS model is also presented and critically analysed as a fulfilment of the Objective 2. The model seamlessly integrates the MT *spectral estimator* to existing CS architectures, thereby exploiting the inherent advantages of the MT method to enhance performance. Moreover, thanks to the non-parametric nature of the MT method, the performance does not depend on the signal structure.

c. The third contribution is the development of a *Walsh-Hadamard* (WH)-*based* CS model, which attempts to address the Objective 3. It is based on signal sparsity in the *Walsh-Hadamard* (WH) domain and not the Fourier/frequency domain. WH sparse signals are encountered in wireless communications and they exhibit insufficiently low frequency sparsity to be handled by the conventional frequency-based CS architectures. It can be stated therefore that for such types of signals the WH-based CS model can considered as a sparsity enhancer. Due to the type of the sparsity, the model performs channel classification instead of spectrum, by extracting the structure of the signal in the WH domain. This facilitates the identification of the occupied and vacant channels, where the latter could be employed by a SU.

d. The fourth contribution is the *unification* of the AR-based and MT-based models resulting in an extended and more flexible *unified* CS (UNI-CS) model, which accordingly exploits the advantages offered by the precolouring process and the MT spectral estimator. The standard operation of the UNI-CS model is based on the MT estimator, while, depending on the type of the incoming signal, the precolouring process is activated.

The generic CS framework is realised by the parallel operation of the UNI-CS and WH-based models, as depicted in Figure 1.1. The RF input signal is firstly down-converted to the baseband before sampling, so the signal content is now between dc and some maximum frequency. The baseband signal is then used as the input to the appropriate CS models which generate information about the spectral and channel occupancy status respectively.

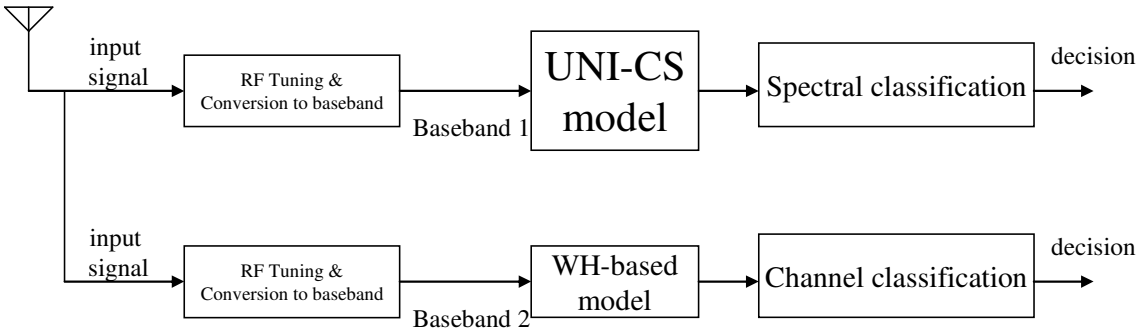

Figure 1.1: Block diagram of the generic CS framework.

1.6. Thesis Structure

The rest of the thesis is organised as follows:

a. *Chapter 2* presents a historical background of CR systems, before a thorough literature review of different CR tasks and challenges is

presented, especially those pertaining to spectrum sensing. It also focuses on compressive sensing and presents and discusses the strengths and weaknesses of the most promising CS designs to be employed in CR applications.

b. *Chapter 3* presents the research methodology employed in this thesis, including the description of the various CS architectures which constitute the proposed CS framework and their associated parameters. The chapter also presents and discusses the choice of the simulation platform, the different testing scenarios employed, along with performance metrics and software validation methods used.

c. *Chapter 4* details the formulation of the AR-based CS model which is based on the precolouring process and for CS structures, the RD and CM. It describes the formulation and integration of a specific *precolouring matrix* and elaborates on the choice of the relevant parameters. The performance is critically evaluated and compared against the classic RD and CM. Work from this Chapter has been published in (Karampoulas et al., 2013a; (Karampoulas et al., 2013b; Karampoulas et al., 2014).

d. *Chapter 5* presents the MT-based CS model which integrates the sophisticated, nonparametric MT spectrum estimation method to it for both RD and CM. The formulation and integration of a specific *MT matrix* is described. The resulting RD and CM versions of the MT-based model are also critically evaluated and compared with the original RD and CM architectures. Work from this Chapter has been published in (Karampoulas et al., 2015).

e. *Chapter 6* presents the WH-based CS model which is also based on the RD or CM structures, but instead of frequency, exploits sparsity in the WH domain, termed *sequency*. The performance of the resulting RD and CM versions of the model is investigated, critically evaluated and

compared against the frequency sparsity based counterparts and for non-frequency sparse signals.

f. *Chapter 7* leverages from the key findings of *Chapter 4* and *Chapter 5* to propose the unified UNI-CS model able to exploit the advantages of both the precolouring process and MT spectrum estimator. The MT matrix is seamlessly integrated into the model, with precolouring determined from the input signal characteristics. The model is also critically evaluated as a spectral band classifier. Finally, the generic CS framework is presented as a parallel structure, where its branches are the UNI-CS and WH-based models respectively.

g. *Chapter 8* presents some future directions and new research avenues that the new *compressive sensing framework for CR systems* provides.

h. *Chapter 9* summarises the key findings emanating from the thesis.

1.7. Summary

In this Chapter, the overarching research question and the three main research objectives have been framed to address some of the main challenges in spectrum sensing for CR, in particular those arising from the high sampling rates and stringent timing requirements. The next Chapter will present a comprehensive literature review of CR technologies and compressive sensing, and the role they play in intelligent spectrum sensing for wireless applications.

Chapter 2

Compressive Sensing for Cognitive Radio: A Literature Review

2.1 Introduction

Over the last decade, the wireless devices and services have been ubiquitous and a vital component in every day life almost all over the globe (Scwhartz, 2005); Zheng & Cao, 2007). This pattern will continue over the span of the next 5 years and even greater expansion of services and growth of the number of the devices is anticipated. For instance, around 29 billion connected devices are forecast by 2022, of which around 18 billion will be related to Internet of Things (IoT), while the number of smartphones will jump from 3.9 billion in 2016 to around 6.8 billion by 2022. As a result, the mobile data traffic will increase sevenfold between 2016 and 2021 (CISCO, 2017c).

Consequently, the arising demand for higher capacity and transmission rates will likewise dramatically increase the need for extra bandwidth, thus putting huge pressure to the spectrum resources. The situation is getting worse if the conventional approach to spectrum management continues to be in force. It is very inflexible in the sense that each operator is granted by the government agencies an exclusive license to operate in a certain frequency band (Ghasemi & Sousa, 2008) rendering the spectrum a scarce resource. Since most of the available spectrum is already allocated (Ben Letaief & Zhang, 2007), if the conventional approach persisted, the spectrum would become even scarcer.

Despite the spectrum scarcity and inflexible regulations, the available spectrum is highly underutilized, which has driven the regulatory organizations to introduce the concept of unlicensed users who borrow or share the spectrum assigned to the license

holders (Marcus, 2005; Federal Communications Commission, 2004). The CR technology has the potential to exploit this more flexible regulatory concept, thereby solving the spectrum underutilization problem. However, the implementation of a CR network presents its own challenges pertaining to high sampling rates and strict timing requirements, respectively due to the nature of the wireless signals and the constraints imposed by the spectrum regulators.

The CS paradigm has come into view over the last few years and provides the theoretical framework to resolve the above issues pertain to the CR implementation, though the existing CS architectures have their own problems and limitations. This Chapter provides an overview of the CR, presenting the major tasks and challenges, while it discusses CS highlighting its potential and its own challenges to be employed in CR.

2.2. A Brief Historical Review of Wireless Communications

The advent of wireless communications can be traced back in the late 19th century when Heinrich Hertz in 1888 successfully demonstrated the generation and detection of electromagnetic waves and also in 1896-97 when Guglielmo Marconi successfully transmitted signals over hundreds of miles and demonstrated radio's ability to provide continuous contact with ships sailing the English Channel (Miao, 2007; Rahman & Ibnkahla, 2005). The next important contributions to the field were the pioneering work of Nyquist in 1927, which was later followed by advances made by Shannon in 1948. The combination of their works gave birth to the field of information theory and is collectively known as the Nyquist-Shannon sampling theorem (Miao, 2007; Nyquist 1928; Shannon, 1949).

During the 20th century several milestones regarding wireless communications took place: The commercial *amplitude modulation* (AM) broadcast in the 20s, the invention of *frequency modulation* (FM) in the 30s, the first TV broadcast in the USA in 1929, the first BBC TV broadcast in 1936. Radio navigation systems have been already deployed in the 20's, while the first satellite communication satellite was launched in 1963 (Maral & Bousquet, 2009).

In regards to mobile communications, the first commercialized system was the *Mobile Telephone Service* (MTS) by AT&T in 1947, while the 1st generation analog (1G) cellular system was introduced in 1978 in the USA. A turning point was the adoption of digital technology by the 2nd generation (2G) system introduced in 1991. The shift to digital technology and the application of advanced signal processing which was not possible in the analog domain, paved the way for higher data rates, lower costs and greater channel and power efficiency. Moreover, in addition to the voice services, data services were introduced such as short messaging, email and internet access, while new mobile applications emerged. The new services coupled with lower costs, made the mobile devices popular and affordable for wider population.

The introduction of the 3rd (3G) generation systems in 2001, further enhanced the functional capabilities and enriched the array of the services provided to include among others multimedia and video streaming (Smith & Collins, 2007). Today the 4th generation (4G) systems are in operation with the first commercial system deployed in 2009, with even better operational characteristics and more services available such as mobile web access, video conferencing, mobile/IP TV, entertainment, cloud storage and others (Boccuzzi, 2008; Dahlman et al., 2014). In 2015 the *next generation mobile networks* (NGMN) Alliance published a white paper outlining the requirements and capabilities for the 5th (5G) generation system (Afif Osseiran et al., 2016), which is expected to make its appearance in 2020 (NGMN Alliance, 2015).

Analogous developments have taken place in the field of wireless networking. The wireless *local area networks* (LAN) have gone through a long way of development since the 1971 and today are every where from home to business applications. In addition the LAN concept has geographically expanded to included *metropolitan area network*s (MAN) as well as *regional area networks* (RAN) (Stallings, 2014; Guizani et al., 2015).

The proliferation of services and applications and their great market potential has led to the development of a great number of different standards for the above mentioned systems, which are not compatible with each other (Goldsmith, 2005). This situation along with the need to maintain and even improve *quality of service* (QoS) provided by the wireless communication systems, led to the emergence and realization of *software defined radio* (SDR) technology (Miao, 2007; Boccuzzi, 2008). The SDR devices are reprogrammable and reconfigurable and permit seamless

wireless connectivity and interface between wireless network services regardless of the standards applied (Miao, 2007; Boccuzzi, 2008; Grayver, 2013).

Despite the fact that the wireless technologies and systems described so far provide ever increasing data rates, the ever growing data rate demands stemming from the emergence of new applications and services, makes it increasingly difficult for them to keep up with the pace (Guizani et al., 2015). The manner the available spectrum is used makes matters worse, rendering it a valuable and scarce natural resource (Tomar et al., 2017). The CR technology and concept is a promising solution to address these challenges.

2.3. Cognitive Radio

There are two developments which contributed to the advent of CR. The first pertains to the findings reported by the FCC in 2002 (Federal Communications Commission, 2002; Kolodzy, 2001), according to which the radio spectrum was underutilized, namely:

a. Some bands are largely unoccupied most of the time
b. Others are only partially occupied
c. The remaining bands are heavily used

The spectrum underutilization implies the existence of spectrum holes as discussed in Section 1.1. In (Kolodzy, 2001), a spectrum hole is defined as a "*band of frequencies assigned to a PU, but at a particular time and specific geographical location, the band is not being utilized by the user*". As also mentioned in Section 1.1, the partially occupied bands are called *gray bands* and the heavily used ones are called black.

The observed spectrum underutilization has prompted FCC (Federal Communications Commission, 2002) and other regulatory bodies like Ofcom (Ofcom, 2007) to investigate and promote a radically different access paradigm, where unlicensed systems (SU) are allowed to opportunistically utilize the unused licensed (primary) bands assigned to a PU. The bands are commonly referred as white spaces.

The second development is the today's realization of the SDR, thanks to sophisticated signal processing and the convergence of the key technologies of digital radio and computer software (Tuttlebee, 2002; Milligan, 2003), in the sense that the properties of carrier frequency, signal bandwidth, modulation and network access are defined by software (Fette, 2009).

CR, exploiting the already existing SDR platform, has been proposed as the means to promote the efficient use of the spectrum by exploiting the existence of spectrum holes (Mitola & Maguire, 1999; Mitola, 2000; Grayver, 2013; Tomar et al., 2017).

2.3.1. The CR Concept and Tasks

The concept of CR was first proposed by Joseph Mitola III in a seminar at the Royal Institute of Technology in Stockholm in 1998 and was published in an article (Mitola & Maguire, 1999). Later Mitola, in his dissertation (Mitola, 2000) described how a CR could enhance the flexibility of personal wireless services through a new language called the radio knowledge representation language. He followed his dissertation with the publication (Mitola, 2006) of a book on CR architecture. According to Mitola, a CR is software control and could orient itself by establishing priorities, create plans, decide and finally take the appropriate action in response to sensing of the RF environment of the outside world (Hossain & Bhargava, 2007).

Another CR approach was presented (Haykin, 2005), where the focus was in signal processing and communication aspects, rather in software. According to this approach, a CR is an intelligent wireless communication system that is aware of its surrounding environment. It is able to learn from its environment and adapts according to the incoming RF stimuli by making the necessary changes in certain operating parameters (transmit-power, carrier-frequency, modulation strategy) in real time. The objectives are highly reliable communications and efficient utilization of the radio spectrum. Based on this description, the following tasks are identified (Akyldiz et al., 2006):

a. *RF sensing* which basically encompasses the detection of the spectrum holes. It employs information about the RF stimuli of the surrounding radio environment.

b. *Spectrum analysis* is based on information about the RF stimuli and spectrum holes to build a model for the estimation of channel state information in order to predict the channel capacity to be used by the CR device.

c. *Spectrum* decision, where the information about channel capacity and spectrum holes is used to determine the parameters of the transmitted signal as well as the transmission time.

Through interaction with the RF environment, these three tasks form a CR cycle, which is depicted in its most basic form in Figure 2.1 (Haykin, 2005).

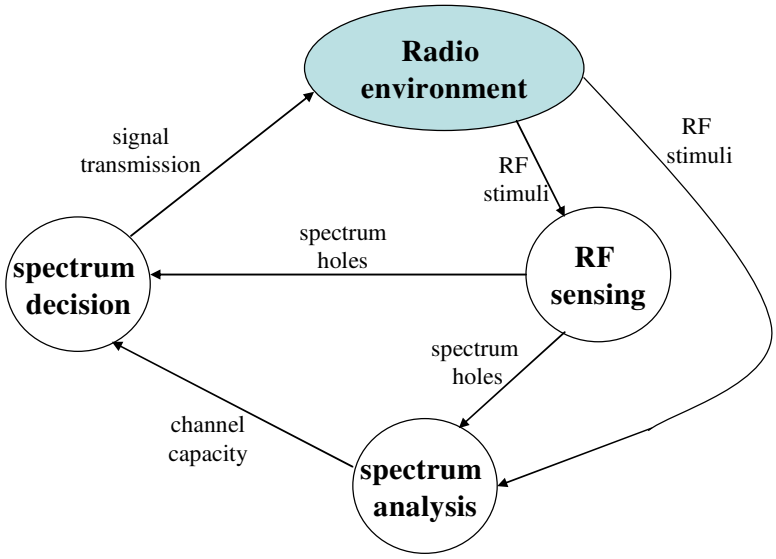

Figure 2.1: Basic Cognitive Radio cycle.

For the CR cycle to be successfully implemented, a CR must build upon an SDR system and add the capabilities of sensing, agility, flexibility and networking (Kolodzy, 2004). RF sensing is needed for the CR to be aware of its environment and gather the necessary information to detect the spectrum holes in order to change its operation parameters. A CR device needs to be agile so to be able to change the operating spectral band, while flexibility is required to change its waveform and configuration. Networking is useful for the CR devices to communicate with each other, cooperate, better understand the environment and thus make a more efficient

use of the spectrum resources (Fette, 2009; Ian F. Akyildiz et al., 2011). It is also important to stress that in principle, a CR must be able to
operate autonomously, since the PUs are not obliged to dispense their operating parameters (Sun et al., 2013; Haykin et al., 2009; Hossain & Bhargava, 2007).

2.3.2. Spectrum Sensing for CR

The task of detection of spectrum holes has acquired major importance in CR, since FCC (Federal Communications Commission, 2004) and Ofcom (Ofcom, 2009) have expressed their interest in permitting unlicensed access to TV white spaces (TVWS). Building on this interest, the IEEE has formed the IEEE 802.22 working group (IEEE 802.22 Working Group, 2017) to develop an interface for opportunistic secondary access to the TV spectrum.

In order to protect the primary systems from the adverse effects of SU's interference, white spaces across frequency, in time and space should be reliably identified (Yucek & Arslan, 2009). The following approaches have been proposed to address this challenge (Nekovee, 2010; Brown, 2005):

a. *Beacon signals*. With the beacon method, unlicensed devices only transmit if they receive a control signal (beacon) identifying vacant channels within their service areas. The signal can be received from a TV station, FM broadcast station, or even a TV unlicensed transmitter. One issue with the control signal method is that it requires a beacon infrastructure to be in place, which needs to be maintained and operated. Another issue is that beacon signals can be lost due to effects similar to the hidden node problem (Nekovee, 2010), which occurs when the CR device is shadowed, in severe multipath fading or inside buildings which have high penetration losses, while a PU is operating in the vicinity (Nekovee, 2010; Ben Letaief & Zhang, 2007).

b. *Geolocation Combined with Database*: In this method, a secondary device determines its location and accesses a database to determine the channels that are vacant in a given location (Webb, 2012; (Carvalho et

al., 2015). The database is accessed by the primary devices systems and contains information about their locations, their transmitted power, current operating band and expected duration of its usage. This method is regarded by the regulators as a suitable short-term solution (Nekovee, 2010; Ofcom, 2012). However, there are a number of limitations associated with this method (Nekovee, 2010): Firstly, there is a need to build and maintain the database. Secondly, both primary and secondary devices need to know their locations with a prescribed accuracy, so they rely on accuracy and availability of systems like the GPS. Finally, additional connectivity and complexity is needed so the devices can access the database, either for updating or for getting information. In order to address these issues, additional costly modifications and infrastructure is required from the PU side (Ghasemi & Sousa, 2008). In addition, considerable management of the participating parties is required (Webb, 2012). Therefore, as with the beacon signal solution discussed in part a., this method compromises the autonomous nature of CR systems (see section 2.3.1).

c. *Spectrum Sensing:* Spectrum sensing for CR can be defined (Haykin et al., 2009; Tomar et al., 2017) as the task of finding spectrum holes and detecting interference by sensing the radio spectrum in the local neighbourhood of a CR receiver in an autonomous manner. By sensing and adapting to the environment, a CR is able to serve its users without causing harmful interference to the licensed user. Unlike the first two approaches, spectrum sensing, on the other hand, relies only on the secondary system to identify the spectrum holes, by directly sensing the licensed bands and switch its operation parameters to them. The infrastructure costs are comparatively low and there is no need for any modification to the primary systems. It is considered the most critical component in CR networks (Sun et al., 2013; Lundén et al., 2015). Hence the increasing attention to spectrum sensing by researchers and key industry stakeholders, as well its inclusion in the IEEE 802.22, IEEE 802.11af and *long term evolution* (LTE) advanced standards (Stevenson, 2009; Shellhammer, 2008; Flores et al., 2013).

Summarising, the research in this thesis will focus on the spectrum sensing since it is the suitable approach for the realisation of a CR network.

2.3.2.1. Spectrum Sensing Challenges for CR

Spectrum sensing is believed to be the most crucial task to establish CR networks (Subhedar & Birajdar, 2011) and the very task upon which the CR operation rests (Haykin et al., 2009). However, it is challenged by several issues, since it should perform reliably and robustly even under worst case conditions (Hossain & Bhargava, 2007). These issues can be summarised as follows (Ghasemi & Sousa, 2008; Subhedar & Birajdar, 2011; Rawat et al., 2010):

a. *Channel uncertainty:* Due to channel fading or shadowing by obstacles, a low strength received signal may provide the wrong information that the PU is out of the interference range of the SU. The hidden node problem mentioned in Section 2.3.3 can also be a cause of channel uncertainty. Therefore, CR have to be sensitive enough to detect and distinguish a faded or shadowed PU signal from a white space.

b. *Noise uncertainty:* The detection sensitivity mentioned above is defined as the minimum *signal to noise ratio* (SNR) at which the primary signal can be accurately detected with a prior chosen probability (Rawat et al., 2010) and is inversely proportional to the noise power. Therefore, the calculation of the detection sensitivity requires knowledge of the noise power however this information is not available by the PU and needs to be estimated at the receiver that is the SU. Moreover the estimation is prone to calibration errors and thermal noise variations. Since a CR may not satisfy the sensitivity requirement due to an underestimate of the noise power, the detection sensitivity should be calculated with the worst case noise assumption, thereby necessitating a more sensitive detector (Tandra & Sahai, 2005).

c. *Aggregate Interference uncertainty:* The potential future deployment of CR networks, could lead to a situation where an unknown number of SU use the same licensed band. As a result, spectrum sensing will be affected by increased aggregate interference which is the combined result of the multiple SU operating over the same band. Even though the PU is out of interference range of an SU, the aggregate interference may become harmful. This uncertainty creates a need for more sensitive SU detector, as a secondary system may harmfully interfere with PU located beyond its interference range, and hence it should be able to detect them.

d. *Uncertainty due to hidden terminal:* The hidden node problem, occurs when the CR is shadowed, in severe multipath fading or inside buildings with high penetration loss, while a PU is operating in the vicinity. In such a case, a CR may not detect the presence of the signal from the operating PU and could start using an occupied channel, causing harmful interference to the PU's network.

e. *Awareness, adaptability, reliability:* The awareness capability of a CR embodies among others knowledge with respect to RF spectrum (Fette, 2004). By being aware and adapting to its environment, a CR is able to fill in the appropriate spectrum holes and reliably serve its users without causing harmful interference to the licensed user (Hossain & Bhargava, 2007). Once the PU is detected, the CR should withdraw from the spectrum, as soon as possible, to minimize the interference it may possibly incur. This is a very challenging task as the various PU will be applying different modulation strategies, data rates and transmission powers in the presence of variable propagation environments and interference generated by other SU (Ben Letaief & Zhang, 2007).

f. *High sampling rates and stringent timing requirements:* If the CR technologies are to be employed to sense frequencies assigned to the various existing wireless communications systems and network standards, the sensing bandwidth of the CR systems must range from hundreds of MHz to several GHz. This poses extra challenge to their

spectrum sensing capabilities. Very high sampling rates are required, if conventional spectrum estimation methods will be employed for spectrum sensing (Tian & Giannakis, 2007; Sun et al., 2013). Achievement of high sampling rates requires the implementation of very high-speed Analogue to Digital (ADC) converters, which is not always realistic with current technologies (Yu & Hoyos, 2009). Moreover, the high speed ADCs, are power hungry (Klumperink et al., 2007; Walden, 1999a). Meanwhile, the stringent timing requirements (Ghasemi & Sousa, 2008; Rawat et al., 2010; Bostian et al., 2016) for monitoring the dynamically changing spectrum only allow for a limited number of measurements to be collected for sensing. These measurements may not be sufficient for high-resolution signal reconstruction due to the large occupied bandwidth (Tian, 2008).

2.3.2.2. Spectrum Sensing Techniques for Cognitive Radio

There is a number of existing spectrum sensing techniques which could be classified in various ways. One of them is by dividing the techniques according to the number of CR receivers involved in the spectrum sensing process. Hence spectrum sensing techniques could be either non-cooperative or cooperative (Ben Letaief & Zhang, 2007; Bostian et al., 2016; Fette, 2009).

In non-cooperative techniques individual CR receivers operate in an autonomous manner locally performing spectrum sensing and using only their own measurements for detection of spectrum holes. On the other hand, the cooperative approach exploits the spatial diversity of the measurements of the spatially located CR receivers, which form CR network (Ian F. Akyildiz et al., 2011).

The SU users, after they have taken their own measurements, may subsequently share their information in order to make a final combined decision more accurate than the individual ones, thereby enhancing performance (Ian F. Akyildiz et al., 2011; Tomar et al., 2017).

The cooperative spectrum sensing approaches are classified according to the way the CR receivers are connected to the CR network, namely as centralized, distributed and relay-assisted (Ian F. Akyildiz et al., 2011; Lundén et al., 2015). Moreover, their performance depends among others on the autonomous performance of each of the

individual CR receivers, hence on the utilized non-cooperative spectrum sensing techniques. Therefore, the non-cooperative techniques are fundamental and affect all the other spectrum sensing techniques employed in the CR field. The non-cooperative techniques are based on the detection of the signals from the PU. Such techniques are the following (Ikuma & Pour, 2008; 3 Sun et al., 2013; Tomar et al., 2017; Bostian et al., 2016).

a. *Matched Filter:* The optimal way for the detection of any signal $x(t)$ is a matched filter (Proakis & Salehi, 2008; Ian F. Akyildiz et al., 2011), since it maximizes the SNR ratio. This implies that the SU has a priori knowledge of the PU signal. Matched filter operation is equivalent to correlation in which the unknown signal is convolved with the filter whose impulse response is matched to the shape of the signal being sought (Manolakis & Ingle, 2011). As depicted in Figure 2.2, the output of the matched filter is used for a binary decision regarding the presence or absence of the primary signal. The filter output is compared with a predefined threshold level. If the output is larger than the threshold, then the decision is H_1, otherwise the decision is H_0. Due to the coherency achieved between the input signal and the filter output, the method is computationally efficient (Ian F. Akyildiz et al., 2011). However it relies on prior knowledge of the input signal and requires synchronization and timing devices which increase hardware complexity. Moreover, the most serious drawback is the need of a matched filter dedicated to every PU signal, which is entirely not applicable and feasible for CR spectrum sensing.

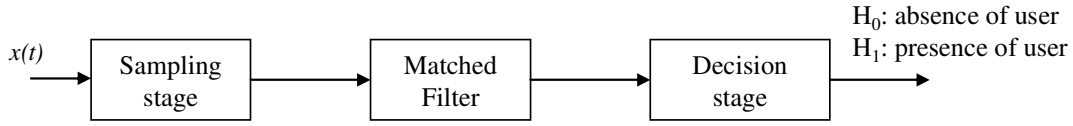

Figure 2.2: Block diagram of a Matched Filter based technique.

b. *Energy Detection:* **Energy detection** is a non coherent detection method that detects the primary signal based on the sensed energy (Malik et al.,

2010). The Energy Detector (ED) ignores the structure of the signal. Rather it estimates, in a manner analogous to what has been described in the matched filter above, the presence of the signal by comparing the energy received with a known threshold, derived from the statistics of the noise (Cabric et al., 2006). The ED is shown in Figure 2.3.(a) and consists of a low-pass filter to reject the out of band noise and adjacent signals, Nyquist sampling, square law device and integrator to compute the energy. The ED suffers from a number of drawbacks (Subhedar & Birajdar, 2011; Ghasemi & Sousa, 2008; Cabric et al., 2006): i) sensing time taken to achieve a given probability of detection may be high. ii) the detection performance is subject to the uncertainty of noise power. iii) ED cannot be used to distinguish PU from the SU signals. However, thanks to its simplicity and no requirement on a prior knowledge of PU signal, the ED is a popular spectrum sensing technique for CR purposes (Hossain & Bhargava, 2007; Cabric et al., 2006; (Doyle, 2009).

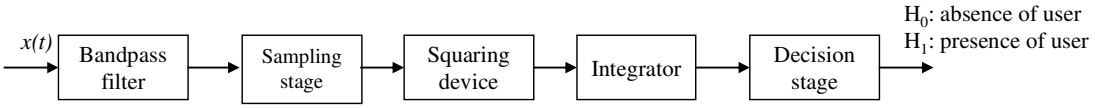

Figure 2.3: Block diagram of the Energy Detector

c. *Cyclostationarity Feature Detection:* This method takes advantage of cyclostationarity, which is an inherent property of digital modulated signals that naturally occur in the transmission of communication signals over a wireless channel (Tandra & Sahai, 2008). Generally, the transmitted signal is taken to be a stationary random process. However, when it is modulated with sinusoid carriers, cyclic prefixes as in *orthogonal frequency division multiplexing* (OFDM) and code or hoping sequences as in *code division multiple access* (CDMA), a *cyclostationarity* is induced i.e. the mean and autocorrelation of the signal show periodic behaviour. This feature is exploited in a detector, depicted in Figure 2.4. The cyclostationarity detection is accomplished by firstly calculating the cyclic autocorrelation function of the observed

signal. Then the *discrete Fourier transform* (DFT) of the autocorrelation function is computed to obtain the *spectral correlation function* (SCF), $S(f,a)$ also called cyclic spectrum, which is a two-dimensional function in terms of frequency f and cyclic frequency a. Finally, the detection is completed by searching for the *unique cyclic frequency* corresponding to the peak in the SCF plane. Again, as in the case of Matched Filter and ED, the detection is a binary decision problem. Since the spectral correlation properties of different signals are unique and are not found in stationary noise and interference (Gardner & Brown, 1987), the cyclostationary feature detection is robust to noise uncertainties and performs well in low SNR regimes. However, there are shortcomings owing to its high computational complexity and long sensing time (Tkachenko et al., 2009).

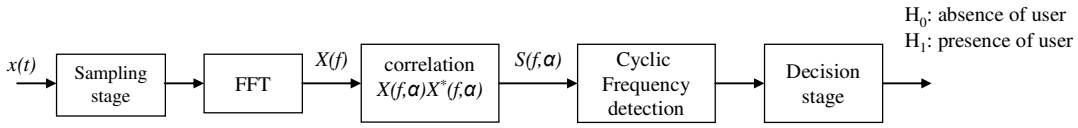

Figure 2.4: Block Diagram of a Cyclostationary feature detector.

There are also other methods proposed in the literature such as the *waveform-based* sensing where the received signal is correlated with a known copy of itself (Yucek & Arslan, 2009) and the outcome is compared with a predefined metric (Tang, 2005) and the *radio identification-based* sensing where the knowledge about the spectrum characteristics of the received signal are obtained by identifying the technologies employed by the PU (Yucek & Arslan, 2009). Both these methods require prior knowledge related to the signals transmitted by the PU. In addition, there are two methods based on the properties of covariance matrix of the received signals. The *covariance-based* detection method exploits the fact that if the signal is pure noise, then the corresponding covariance matrix is diagonal, which is not true in the presence of a PU transmission (Zeng & Liang, 2009). In the *eigenvalue-based* approach (Pillay & Hu, 2013; Wang et al., 2014), the ratio of the maximum-to-

minimum eigenvalue of the covariance matrix is compared against a threshold to determine the presence of a PU signal (Pillay & Hu, 2013; Wang et al., 2014).

It is noted that the methods described above are considered to be *narrowband* in the sense that they sense over a narrow frequency range and make a decision pertaining the whole spectrum (Sun et al., 2013), although this information is valid only for the said narrow frequency range. On the other hand, it has already been mentioned that the CR systems must be capable of sensing frequencies from the order of MHz to the order of GHz. This necessitates the application of *wideband* spectrum sensing techniques with the aim to find more spectral opportunities for the SU users. A number of these techniques are presented:

a. *FFT-based ED*: An alternative approach of the ED is proposed in (Cabric et al., 2006), where a periodogram solution is used to estimate the *power spectral density* (PSD) through square magnitude of the *Fast Fourier Transform* (FFT) of the signal. This architecture, which is depicted in Figure 2.5, provides the flexibility to process wider bandwidths and sense multiple signals simultaneously. As a consequence, an arbitrary bandwidth of the modulated signal could be processed by appropriately selecting the frequency resolution of the periodogram (Cabric et al., 2006).

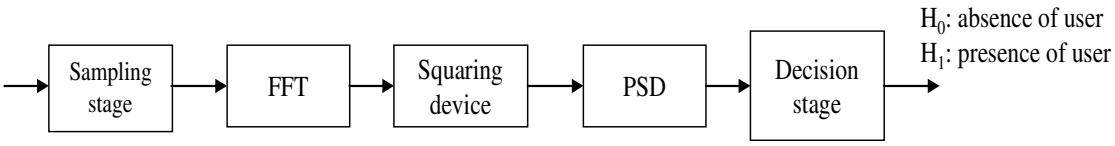

Figure 2.5: Block diagram of the FFT-based ED.

b. *Multiband joint detection*: In this method (Quan et al., 2009), shown in Figure 2.6, after the Nyquist sampling, the data are converted from one serial to a number of parallel data streams, before FFT is applied for conversion to the frequency domain. Then, the entire spectrum is divided into a series of subbands (Sun et al., 2013). Finally, decisions are taken regarding spectral opportunities for each subband. The joint detection

was found to provide better performance than in a single-band case (Quan et al., 2009; Sun et al., 2013).

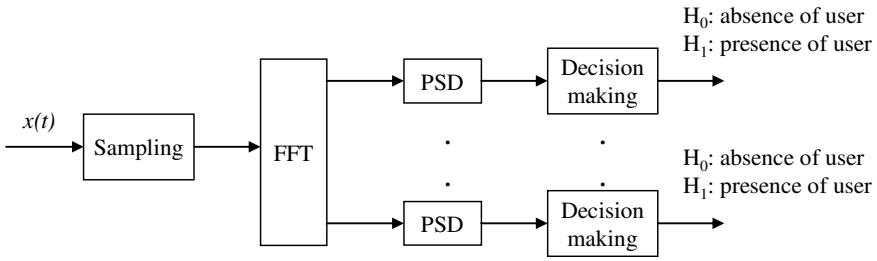

Figure 2.6: Block diagram of multiband joint detection.

c. *Wavelet based detection*: In this approach for spectrum sensing, wavelets are used for detecting edges in the Power Spectral Density (PSD) of a wideband signal (Tian & Giannakis, 2006). The signal is spectrally modelled as a train of consecutive frequency sub-bands where the power spectral characteristic is smooth within each sub-band but changes abruptly on the border of two neighbouring sub-bands (Tian & Giannakis, 2007). It is assumed that the edges (or discontinuities) in PSD are the boundaries between spectrum holes and occupied bands and hence this helps the identification of the vacant bands (Divakaran et al., 2011). By taking the multiscale product and multiscale sum of the wavelet transform of the PSD of the observed signal, the singularities (edges) of the PSD can be located and thus the vacant frequency bands can be found (Hossain & Bhargava, 2007; Yu et al., 2009; De Almeida et al., 2008). The block diagram of wavelet-based detection is shown in Figure 2.7. Wavelet based detection works well with wideband signals, but at the expense of high sampling rates required (Ben Letaief & Zhang, 2007). Moreover, this type of detector cannot detect spread spectrum signals and its computational cost is high (Ben Letaief & Zhang, 2007).

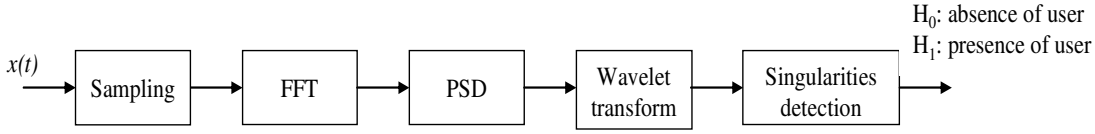

Figure 2.7: Block diagram of a Wavelet-based detector.

2.3.2.3. Spectrum Estimation Methods for Cognitive Radio

From the above discussion it is concluded that for the detection of spectrum holes boils down to a binary hypothesis-testing problem. Specifically, hypothesis H_1 refers to the presence of a PU's signal (i.e., the band under test is occupied) and hypothesis H_0 refers to the presence of ambient noise (i.e., the band is a white space). However, the radio spectrum, apart from white spaces and heavily occupied bands, includes also gray spaces (Fette, 2009; Haykin, 2005), which are partially occupied by interfering signals as well as noise. Examples of such cases include low-power interfering signals (Haykin et al., 2009), underutilized CDMA channels (Fette, 2009; Mody et al., 2007), or even mobile networks where transmissions of a PU are weak in the area where a SU user is situated (Haykin et al., 2009). If the gray spaces are not considered, they could be characterised as occupied and not as opportunities for the SU.

Moreover, the use of the FFT to compute the signal PSD refers to the traditional periodogram spectrum estimation method. It is well known that the periodogram is not a consistent estimate of the power spectrum (Manolakis et al., 2005; Proakis & Manolakis, 2006; Madisetti, 2010), due to the difficulty to satisfactorily resolve the bias-variance dilemma (Haykin, 2005; Haykin et al., 2009; Oppenheim & Schafer, 2009; Schwartz & Shaw, 1975). Given the disadvantages of the periodogram, compounded by the need for spectrum sensing to be able to provide efficient spectrum utilization and adequate spectral resolution, the drawbacks of the sensing techniques are more pronounced.

Therefore, in order to further refine and extend the scope of spectrum sensing so as to also include the possible employment of the gray spaces, and also improve the performance of the described sensing techniques, one may have to resort to sensing techniques that include spectrum estimation (Haykin et al., 2009). Given the drawbacks of the periodogram, other methods have to be investigated, as well.

Two spectrum estimation methods that have been proposed for CR are the *multitaper* (MT) spectrum estimation (Haykin, 2005; Haykin et al., 2009; Thomson, 1982) and the *filter bank* (FB) spectrum estimation (Farhang-Boroujeny, 2008a).

A filter bank is a set of band-pass filters with a common input. The input signal $x(n)$ is decomposed into a set of sub-band signals $v_k(n)$ with each sub-band signal occupying a portion of the original frequency band. Filter banks are often

implemented based on a prototype filter (Vaidyanathan, 1993). The prototype filter is a low-pass filter that is also used to realize the zeroth band of the filter bank. Other bands are realized through modulation of the prototype filter. A graphical representation of this concept with M bands is shown in Figure 2.8:

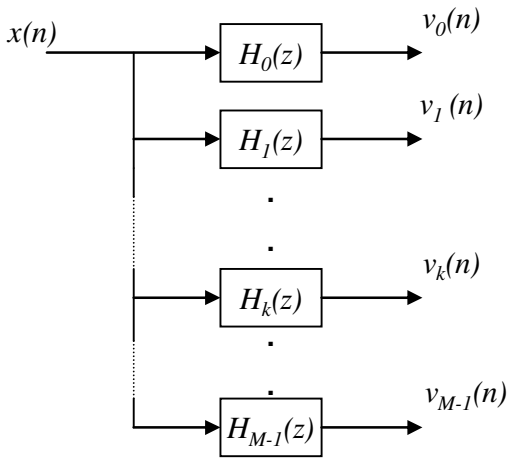

Figure 2.8: Block Diagram of an M-band filter bank.

As mentioned earlier, the frequency response of the $H_k(z)$ is obtained by modulation of the prototype (zeroth) filter $H_0(z)$, that is, by shifting its response to the right by an amount of $2\pi k / M$. The frequency responses of the prototype and the other filters are shown in Figure 2.9 (Farhang-Boroujeny, 2008b; Mitra, 2011).

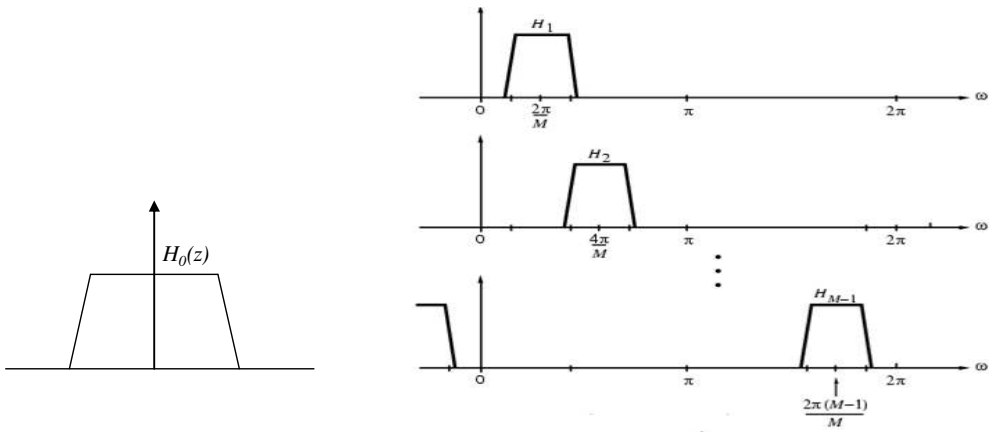

(a) (b)

Figure 2.9: Filter frequency responses: (a) Prototype filter, (b) higher order filters.

Following the discussions above, the output power of each filter is measured as an estimate of the spectral power over the associated sub-band. In other words, an estimate of PSD at the i_{th} sub-band of the filter bank is obtained as (Farhang-Boroujeny, 2008a). $P = \text{avg}[|v_i(n)|^2]$ where avg[.] denotes the time average of the argument.

The motivation for using filter banks stems from the assertion that filter bank-based multicarrier communication systems can perform very well (Farhang-Boroujeny & Kempter, 2008; Amini et al., 2006). When a filter bank multicarrier technique is exploited as the physical layer of a CR network, the same filter bank can also be used for channel sensing. Hence, in such systems, channel sensing will be done at virtually no cost (Farhang-Boroujeny & Kempter, 2008). Since in the multicarrier communication systems the optimum transmitter and receiver filters are a pair of matched root-Nyquist filters (Farhang-Boroujeny, 2008b), it turns out that the prototype filter of the relevant filter bank should be a pair of matched root-Nyquist filters (Saltzberg, 1967; Farhang-Boroujeny, 2003). However, the FB method has a number of drawbacks such as the increased computational complexity for the implementation of the prototype filter (Harris, 2004) and the trade-off between the number of RF components required and desired resolution (Sun et al., 2013; Harris, 2004).

As the name implies, the MT method applies multiple windows (tapers) to the signal data (Thomson, 1982), where the windows are *discrete prolate spheroidal* (Slepian) sequences (Slepian, 1978). The slepian sequences are the solutions to the spectral concentration problem. This seeks to find a sequence with specific length of N samples taken at sampling intervals Δt. The signal DFT has maximum energy concentration within a given bandwidth f-W to f+W centred about some frequency f, with W defined as the resolution of the bandwidth (Percival & Walden, 1993; Haykin et al., 2009). It is must be clarified that W refers to the resolution of the MT method and is not the same as the DFT resolution, also called *fundamental Fourier frequency* (the smallest nonzero Fourier frequency) (Percival & Walden, 1993). The problem leads to an eigenvalue equation with N eigenvectors as solutions, each of which is a discrete prolate spheroidal (Slepian) sequence (Percival & Walden, 1993; Thomson, 1982; Slepian, 1978). The sequences are orthogonal and each is characterised by a

distinct eigenvalue that reflects the degree of their respective spectral concentration within the bandwidth f-W to f+W. The larger the eigenvalue the greater is the energy concentration. The eigenvalues are real, positive and always <1 (Percival & Walden, 1993). They can be ordered as follows:

$$1\rangle\lambda_0(N,W)\rangle\lambda_1(N,W)\rangle...\rangle\lambda_m(N,W)\rangle...\rangle\lambda_{N-1}(\mathrm{N,W}) \qquad (2.1)$$

where the eigenvalue λ_m corresponds to the m^{th} slepian sequence.

This implies that eigenvalues and consequently their respective eigenvectors (Slepian sequences) depend on the sequence length N and the value of W. Moreover, of these eigenvalues, the first $L \le \lfloor 2N\Delta tW \rfloor$, where $\lfloor 2N\Delta tW \rfloor$ is the integer part of $2N\Delta tW$, are very close to one, while the remainder rapidly decay to zero (Percival & Walden, 1993). Therefore, for the solution of the spectral concentration problem, only the first m low-order sequences are employed. For a given time series $x(n)$ of length N and a resolution W, the MT method determines the following (Haykin et al., 2009):

a. the number L of the Slepian sequencies with $L \le \lfloor 2N\Delta tW \rfloor$

b. the actual Slepian sequencies (eigenvectors) $V^l = \left[v_0^l, v_1^l, ..., v_{N-1}^l \right]$, $l=0,1,..,L-1$

c. their corresponding eigenvalues

These Slepian sequences will be used to taper $x(n)$ and consequently a set of L Fourier transforms will be formed as follows:

$$f_k^l = \sum_{n=0}^{N} V_n^l x(n) \omega_{\mathrm{N}}^{kn} \qquad (2.2)$$

where $V^l = [v_0^l, v_1^l, ..., v_{N-1}^l]^T$ is the eigenvector representing the l^{th} Slepian sequence, $\omega_N = e^{-j2\pi/N}$ and f_k^l is the k^{th} frequency of vector f^l, with $k=0,1,..,N-1$.

Then, the MT spectral estimator is given by:

$$P_{MT} = \frac{\sum_{l=0}^{L-1} \lambda_l \left| f^l \right|^2}{\sum_{l=0}^{L-1} \lambda_l} \tag{2.3}$$

with P_{MT} the weighted averaged PSD estimation vector .

The equation above reveals the favourable properties of the MT estimation method. The Fourier transforms exhibit very low leakage within the interval $(f_k^l - W, f_k^l + W)$ due to the maximum concentration of the respective slepian tapers within the same interval. In addition, the increased leakage caused by the higher order eigenspectra is offset by the respective eigenvalues themselves which reduce the weighting of the eigenspectra (Haykin et al., 2009).

Moreover, another important feature of the MT estimator is its favourable variance properties. With increased W the number L of the slepian tapers and thus the eigenspectra contributing to the estimation increases as well. Although the leakage from the higher order eigenspectra is likewise increased, the variance of the MT estimator is steadily decreased, due to their orthogonality property (Percival & Walden, 1993). This permits the estimator to provide propitious trade-off between bias, variance and resolution and trade spectral resolution for improved spectral characteristics, that is, reduced variance of the spectral estimate without compromising the bias of the estimate (Haykin et al., 2009; Madisetti, 2010; Thomson, 1982). The MT method is consistent, that is its variance for fixed W tends to zero as $1/N$ when $N \rightarrow \infty$ (Haykin et al., 2009; Madisetti, 2010).

2.3.3. Summary

In this Section the main CR challenges, techniques and spectrum estimation methods were presented. The wideband techniques address the need to perform sensing over the whole spectrum, while more sophisticated spectrum estimation methods are required to be employed for enhanced spectrum sensing performance. However, the challenges of high sampling rates and stringent timing requirements mentioned in

2.3.2.1 remain. The next Section presents *compressive sensing* (CS) which has the potential to address these challenges.

2.4. Compressive Sensing

2.4.1. Introduction

The theoretical foundation of the modern digital revolution lies in the pioneering works of Kotelnikov, Nyquist, Shannon, and Whittaker on sampling continuous-time band-limited signals (Kotelnikov, 1933; Nyquist, 1928; Shannon, 1949; Whittaker, 1915). Their results demonstrate that signals, images, videos, and other data can be exactly recovered from a set of uniformly spaced samples taken at the so-called Nyquist rate of twice the highest frequency present in the signal of interest. Digitization has enabled the creation of sensing and processing systems that are more robust, flexible, and cheaper and consequently, more widely used than their analogue counterparts.

Unfortunately, in many important and emerging applications, the resulting Nyquist rate is so high that the result is far too many samples. Alternatively, it may simply be too costly, or even physically impossible, to build devices capable of acquiring samples at the necessary rate (Walden, 1999b). Thus, despite extraordinary advances in computational power, the acquisition and processing of signals in application areas such as telecommunications, imaging, video, medical imaging, remote surveillance, spectroscopy, and genomic data analysis, poses a tremendous challenge (Eldar & Kutyniok, 2012). This is exactly the nature of the challenge that is posed to CR in regards to spectrum sensing, which has been addressed in Section 2.3.2.1.f.

One way to address the challenges involved in dealing with such high-dimensional data, is to depend on compression, which aims at finding the most concise representation of a signal that is able to achieve an acceptance level of distortion. One of the most popular techniques for signal compression is known as transform coding, and typically relies on finding a basis or frame that provides *sparse* or compressible representations for signals in a class of interest (Bruckstein et al., 2009; DeVore,

1998; Elad, 2010). By a sparse representation, it is meant that a signal of length N, can be represented with $K << N$ nonzero coefficients; a compressible representation, means that the signal is well-approximated by another signal with only K nonzero coefficients. Both sparse and compressible signals can be represented with high precision by preserving only the values and locations of the largest coefficients of the signal, with transform coder precision dependent on the sparsity (or compressibility) of the signal encoded (Donoho et al., 1998). This process is called sparse approximation, and forms the foundation of transform coding schemes that exploit signal sparsity and compressibility, including the JPEG, JPEG2000, MPEG, and MP3 standards (Eldar & Kutyniok, 2012; Elad, 2010).

The way this works is that the full signal is acquired, and then the complete set of transform coefficients is computed. After that, the largest coefficients are encoded and the other ones are discarded (Candès, 2006). However, this process of massive data acquisition followed by compression is extremely wasteful (Shannon, 1949; Fornassier & Rauhut, 2015). One might ask that since most signals are compressible, why spend so much effort acquiring all the data when we know that most of it will be discarded. In addition another question is raised; whether there is a more sophisticated way of obtaining the compressed version of the signal more directly, by taking only a small number of measurements of the signal, so that one does not need to throw away anything. Compressive sensing (CS) also known as compressed sensing (Donoho, 2004) or compressive sampling (Candès, 2006) shows that this is indeed possible.

2.4.2. The CS Theoretical Framework

2.4.2.1. The CS Concept

The theoretical treatment of compressive sensing considers a discrete-time signal *x*, which can be viewed as an $N \times 1$ column vector in R^N with elements *x(n), n=1,2,...,N*. Any signal in R^N can be represented in terms of an orthonormal basis of $N \times 1$ vectors $\{\psi_i\}_{i=1}^{N}$ (Strang, 2016). Using the $N \times N$ basis matrix $\Psi = [\psi| \psi_1 . . . \psi_n]$ with vectors $\{\psi i\}$ as columns, a signal *x* can be expressed as:

$$x = \sum_{i=1}^{N} s_i \psi_i \qquad \text{or} \qquad x = \Psi s \qquad (2.4)$$

where s is the $N \times 1$ vector and represents the signal in the Ψ domain (Baraniuk, 2007). Both x and s are equivalent representations of the signal. Usually for radio frequency signals, x is the time domain representation and s is the frequency or Fourier domain representation. The signal x is K-*sparse* if only K s_i coefficients are nonzero and all the others are exactly zero. The signal x is compressible when only a few s_i coefficients have large values and the others are relatively small. The fact that compressible signals are well approximated by K-sparse representations forms the foundation of transform coding (Mallat, 1999). Unfortunately, the procedure under transform coding works is wasteful, as it was mentioned in 2.4.1. The number of samples N may be large even if K is much smaller. Moreover, all the N s_i coefficients have to be computed, even though only K of them is useful. Lastly, the locations of the large s_i coefficients have to be known, thus an extra burden.

Compressive sensing addresses these inefficiencies by directly acquiring a compressed signal representation without going through the intermediate stage of acquiring N samples (Candès et al., 2006a; Donoho, 2006). A linear measurement process is employed consisted of $M < N$ vectors in R^N $\{\varphi_i\}_{i=1}^{\mathrm{M}}$. Each of measurements is the inner product between x and the vector φ_i that is, $y_i = \langle x, \varphi_i \rangle = \varphi_i^{\mathrm{T}} x$, where $.^{\mathrm{T}}$ denotes transposition. If the measurements are arranged in an $M \times 1$ vector y and the measurement vectors φ_i in an $M \times N$ measurement matrix Φ, y can be expressed as $y=\Phi x$ and from equation (2.4) above it can be written as:

$$y = \Phi x = \Phi \Psi s = \Theta s \qquad (2.5)$$

where $\Theta = \Phi\Psi$ is an $M \times N$ matrix. The measurement process is not adaptive, meaning that Φ is fixed and does not depend on the signal x (Candès & Romberg, 2005; Tsaig & Donoho, 2004).

The problem now is i) to design a measurement matrix Φ so that the vital information in the K- sparse or compressible signal x is not lost by the dimensionality reduction from $x \in R^N$ to $y \in R^M$ and ii) a reconstruction algorithm to recover s (and subsequently x) from only $M < N$ measurements, since (2.5) forms an underdetermined system of linear equations and the traditional solving methods do not apply. For these two requirements to be fulfilled, the following should hold:

a. Matrix Θ must preserve the Euclidean length of all the K-sparse vectors x, a property called *Restrictive Isometry Property* (RIP) (Candès & Tao, 2005; Candès & Wakin, 2008). If this holds, then (2.5) can be solved with only $M < N$ measurements provided that $K \leq M$ (Candès & Tao, 2006; Candès et al., 2006b).

b. Matrix Φ must be largely incoherent with the basis matrix Ψ, in which the signal is K-*sparse*. Coherence measures the largest correlation between any two elements of Φ and Ψ (Donoho & Huo, 2001). The incoherence between Φ and Ψ has as result that if a signal has a dense representation in Φ, then it should have a sparse representation in Ψ (Baraniuk, 2007; Candès & Wakin, 2008). The positive effect of the incoherence between Φ and Ψ is that the larger it is the fewer measurements M are required for stable and accurate signal recovery (Donoho & Elad, 2003; Tropp et al., 2006a). In addition, it must be noted that M gets smaller as K becomes smaller as well, or in other words, signal sparsity becomes greater (Candès & Wakin, 2008), hence the CS efficiency is enhanced.

Both RIP of Θ and incoherence between Φ and Ψ can be achieved with high probability by selecting Φ as a random matrix (Baraniuk, 2007), namely, a matrix

with elements drawn from a normal, Gaussian, Bernoulli or other sub-Gaussian distributions. Such matrices obey the RIP (Candès & Wakin, 2008); Baraniuk et al., 2007) and in addition are largely incoherent with any fixed orthonormal basis Ψ (Candès & Wakin, 2008).

The random matrices have an interesting property. When Φ is random then $\Theta=\Phi\Psi$ will also be a random matrix for which the RIP holds regardless of the choice of Ψ (Baraniuk, 2007; Candès & Wakin, 2008; Baraniuk et al., 2007; Baraniuk et al., 2017), and thus (2.5) can be solved. Therefore, the focus of the problem is not on the design of the measurement matrix Φ, but the on finding a basis Ψ to which x is sparse. This property of the random matrices is called *universality* and constitutes a significant advantage to using them to construct the measurement matrices (Baraniuk et al., 2017).

An attractive property of a random matrix Φ is that the measurements it derives are *democratic*, meaning that each measurement carries roughly the same amount of information about the signal being acquired, thus rendering recovery possible by using any subset of M measurements (Davenport et al., 2009; Laska et al., 2011). Thus, one can be robust enough to the loss or corruption of a small fraction of the measurements (Baraniuk et al., 2017).

2.4.2.2. Signal Recovery

The signal reconstruction algorithm aims to find the sparsest vector s which is consistent with measurement vector $y=\Phi x$ (Fornassier & Rauhut, 2015). This naturally leads to solving the *l_0-mimization problem* (Eldar & Kutyniok, 2012):

$$min \|s\|_0 \quad \text{subject to} \quad y = \Phi x = \Phi\Psi s = \Theta s \qquad (2.6)$$

where the l_0 norm counts the number of non-zero entries in vector s. The solution of (2.6) has been proved to be NP-hard (Mallat & Zhang, 1993; Natarajan, 1995; Muthukrishnan, 2005). One way to bypass this problem is to solve the l_1-minimization problem:

$$min \|s\|_1 \quad \text{subject to} \quad y = \Phi x = \Phi\Psi s = \Theta s \qquad (2.7)$$

where the l_1 norm represents the sum of the absolute values of all the entries of s. The resulting problem, also known as basis-pursuit, is considered a convex optimization problem, is computationally feasible and can be posed as a linear programme (Donoho & Elad, 2003; Chen et al., 1998; Elad & Bruckstein, 2002; Boyd & Vanderberghe, 2004). By exploiting the signal sparsity and the RIP property of matrix Θ, the l_1-minimization approach to the solution equation 2.8 can exactly recover the signal with high probability (Candès et al., 2006a; Donoho, 2006; Candès & Romberg, 2017).

There are also other signal recovery approaches, which include greedy algorithms, such as orthogonal matching pursuit (Tropp, 2004; Davenport & Wakin, 2010; Needell & Vershynin, 2010) and iterative thresholding (Blumensath & Davies, 2009; Daubechies et al., 2004; Tropp & Needell, 2009). The greedy algorithms rely on iterative approximation of the signal coefficients and support. This is done by either iteratively identifying the support of the signal until a convergence criterion is met, or by alternatively by obtaining an improved estimate of the sparse signal at each iteration that attempts to account for the mismatch to the measured data (Eldar & Kutyniok, 2012).

2.4.2.3. Compressive vs. Classical Sampling

CS differs from classical sampling in three important respects (Eldar & Kutyniok, 2012). First, sampling theory typically considers infinite length, continuous-time signals. In contrast, CS is a mathematical theory focused on measuring finite-dimensional vectors in R^N. Second, rather than sampling the signal at specific points in time, CS systems typically acquire measurements in the form of inner products between the signal and more general test functions (measurement vectors). This is in fact in the spirit of modern sampling methods which similarly acquire signals by more general linear measurements (Walden, 1999b; Eldar & Mishali, 2009; Unser, 2000). Thirdly, the two frameworks differ in the manner in which they deal with signal recovery, i.e., the problem of recovering the original signal from the compressive

measurements. In the Nyquist-Shannon framework, signal recovery is achieved through sinc interpolation (Marks II, 1991), a linear process that requires little computation and has a simple interpretation. In CS, however, signal recovery is typically achieved using highly nonlinear methods.

2.4.3. CS Architectures

Several architectures have been implemented and/or proposed to enable compressed sampling. Examples include the *random demodulator* (RD), (Tropp et al., 2010), the compressive multiplexer (CM) (Slavinsky et al., 2011), *random filtering* (Tropp et al., 2006b), the *modulated wideband converter* (MWC) (Mishali & Eldar, 2010), *random convolution* (Romberg, 2007), and the *constraint* RD (Harms et al., 2013). The focus will be on the RD and the CM which will be described in more detail below. The RD has been implemented as hardware prototype (Ragheb et al., 2008). Due to the usefulness and applicability of its signal model to a wide range of scientific and engineering applications, it has an amazing potential impact (Tropp et al., 2010; Lexa et al., 2012). The CM has a *multi-channel* structure. Nevertheless, its hardware implementation is simpler than the RD and unlike other multi-channel architectures like the MWC it only requires one ADC rather than one per channel (Slavinsky et al., 2011).

The basic RD structure is depicted in Figure 2.10 and has three constituent components: demodulation, filtering and uniform sampling (Tropp et al., 2010). The RD assumes a class of discrete, multitone signals which are bandlimited, periodic and sparse (Tropp et al., 2010). The input signal is modulated by a square pulse train of random values {±1} generated by a *pseudorandom number* (PN) sequence. This is called the *chipping sequence* $p_c(t)$ which must alternate between values at a rate N_α at least as fast as the Nyquist frequency of the input signal. The demodulation smears the energy of the signal tones across the entire spectrum, giving each a unique spectral signature that can be discerned by the second stage which is a low-pass filter implemented as an integrator (Tropp et al., 2010). The integration time period is $1/M_a$. The final stage is an ADC which is clocked at a sampling rate of $M_\alpha < N_\alpha$. In practice, data are processed in time blocks of period T. The number of elements in the

chipping sequence is defined as $N = N_\alpha T$, while the number of measurements is defined as $M = M_\alpha T$.

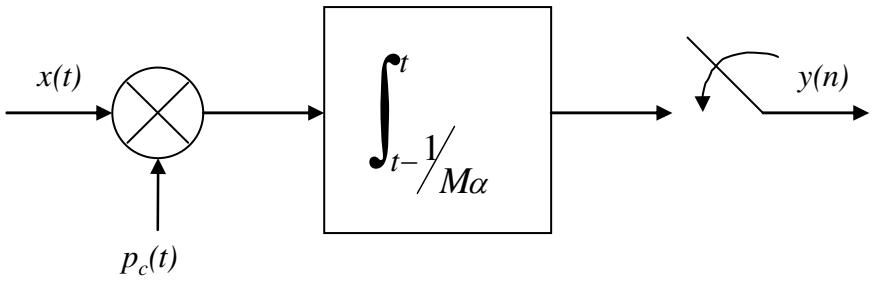

Figure 2.10: Block Diagram of the random demodulator.

As the RD directly acquires compressive measurements without firstly having to sample the continuous signal *x(t)*, this is equivalent to a system which samples *x(t)* at the Nyquist rate to yield a discrete-time vector *x*, before then applying the measurement matrix Φ to obtain the measurements (Baraniuk et al., 2017):

$$y = \Phi x \tag{2.8}$$

The measurement process is the dot product of *x* with the random sequence $p_c(t)$ for each sequential block of *N/M* coefficients (Baraniuk et al., 2017). Considering also (2.4), the output *y(n)* from the RD can be considered as a linear transformation of the discrete vector *s*. This transformation is expressed as $\Theta = \Phi\Psi$ with the signals being sparse in the Ψ domain. As for matrix Φ, it is a $M \times N$ banded matrix containing *N/M* randomly generated ±1 values per row, so for example, with *N=9* and *M=3*, Φ will be:

$$\Phi = \begin{bmatrix} +1 & -1 & +1 & 0 & 0 & 0 & 0 & 0 & 0 \\ 0 & 0 & 0 & +1 & +1 & -1 & 0 & 0 & 0 \\ 0 & 0 & 0 & 0 & 0 & 0 & -1 & -1 & +1 \end{bmatrix} \tag{2.9}$$

If the sparsity basis is the DFT matrix F, then by employing l_1-minimization, the RD can recover the Fourier representation α of $x(t)$, by solving the following equation:

$$y = \Phi x = \Phi F^{-1} s = G\alpha \qquad (2.10)$$

with $G = \Phi F^{-1}$ being the recovery matrix of the RD architecture. It is empirically shown that recovery is feasible under the condition $M \geq 1.7K \log(N/K + 1)$ (Tropp et al., 2010) with K being the sparsity of $x(t)$.

The major advantage of the RD is that it bypasses the need for a high-rate ADC. Demodulation is typically much easier to implement than sampling, yet it allows the use of a low-rate ADC. As a result, the system can be constructed from robust, low-power, readily available components even while it can acquire higher band limit signals than traditional sampling hardware (Tropp et al., 2010).

Since its introduction, various enhancements to the original RD have been proposed. From a CR network viewpoint, to improve spectrum sensing performance, the RD has been employed in parallel segmented CS architectures (Yu & Hoyos, 2009; Taheri & Vorobyov, 2011) and while effective in terms of the sampling rate requirements and spectrum recovery, it increases complexity due to the inherent parallel structure. In (Y. Lu et al., 2011), multiple RD signal acquisition architectures are utilised before spectrum sensing to lower the sampling rate, but the infrastructure complexity is increased due to the windowing and synchronization issues between SU. The RD in (Zhao et al., 2011) integrates the MT spectral estimation method, in combination with *singular value decomposition* (SVD). A series of RD architectures are employed, each one incorporating both MT and SVD. This incurs considerable hardware and computational overheads. Other RD-based solutions address limitations relating to the non-ideal chipping sequences (Harms et al., 2013; Mangia et al., 2011), but these mandate *a priori* knowledge of the input signal to improve performance, which is not always feasible in wireless communications.

The basic CM structure, which is shown in Figure 2.11, is a parallel architecture. It acquires J independent signal channels, each with bandwidth BHz, and all being sampled at the Nyquist rate $2B$Hz (Slavinsky et al., 2011). As in the RD, each

channel $x_j(t)$ is modulated by a pseudorandom chipping sequence $p_j(t)$ with ± 1 values and chipping frequency at least the Nyquist rate. The channel outputs are then summed and sampled once per chip by an analog-to-digital converter (ADC) operating at the Nyquist rate. It is noted that the summation occurs across the channels and not over time as in the RD and the MWC (Slavinsky et al., 2011). As in the case of the RD, the essential requirement for subsequent signal acquisition is sparsity, which for the CM means the signals are jointly sparse over the combined bandwidth, so recovery of multiple signals with a total bandwidth of $2JB$Hz is feasible at a sampling rate of $2B$ Hz (Slavinsky et al., 2011).

It is noted that the operation of the CM can be viewed as first $x_j(t)$ are sampled to give the corresponding time series $x_j(n)$, before the summation takes place (Slavinsky et al., 2011). Hence, the output of the CM can be expressed as:

$$y(n) = \sum_{j=1}^{J} x_j(n)\, p_j(n) \tag{2.11}$$

Considering N samples for $x_j(n)$, (2.11) can be written in vector form as:

$$y = \sum_{j=1}^{J} \Phi_j x_j \tag{2.12}$$

where Φ_j is a $N \times N$ diagonal matrix with the main diagonal being populated by independent identically distributed (i.i.d.) entries from a random distribution, which in (Slavinsky et al., 2011) is chosen to be the Rademacher, since it can only take ± 1 values.

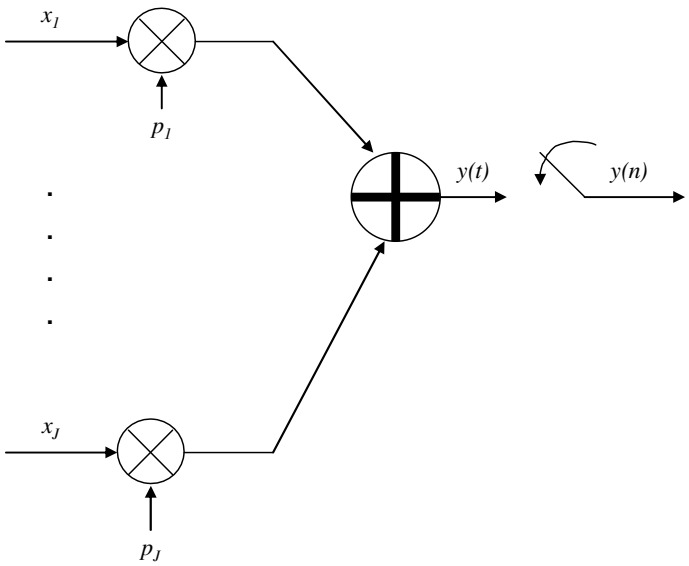

Figure 2.11: Block Diagram of the compressive multiplexer.

Assuming that signals $x_j(t)$ are sparse in the frequency domain, (2.4) is valid for each of them

$$x_j = F^{-1} f_j \tag{2.13}$$

where now the sparsity basis is the DFT matrix F and vector f_j is the representation of vector x_j in the frequency domain. Consequently (2.12) can be written as:

$$y = \sum_{j=1}^{J} \Phi_j x_j = [\Phi_1, \Phi_2, .., \Phi_J] \begin{bmatrix} x_1 \\ x_2 \\ . \\ . \\ x_J \end{bmatrix} = [\Phi_1, \Phi_2, .., \Phi_J] \begin{bmatrix} F^{-1} f_1 \\ F^{-1} f_2 \\ . \\ . \\ F^{-1} f_J \end{bmatrix} =$$

$$= [\Phi_1, \Phi_2, .., \Phi_J] \begin{bmatrix} F^{-1} & & & & \\ & F^{-1} & & & \\ & & . & & \\ & & & . & \\ & & & & F^{-1} \end{bmatrix} \begin{bmatrix} f_1 \\ f_2 \\ . \\ . \\ f_J \end{bmatrix} = [\Phi_1 F^{-1}, \Phi_2 F^{-1}, .., \Phi_J F^{-1}] \begin{bmatrix} f_1 \\ f_2 \\ . \\ . \\ f_J \end{bmatrix} =$$

$$y = \sum_{j=1}^{J} \Phi_j x_j = [\Phi_1, \Phi_2, .., \Phi_J] \begin{bmatrix} x_1 \\ x_2 \\ . \\ . \\ x_J \end{bmatrix} = [\Phi_1, \Phi_2, .., \Phi_J] \begin{bmatrix} F^{-1} f_1 \\ F^{-1} f_2 \\ . \\ . \\ F^{-1} f_J \end{bmatrix} =$$

$$= [\Phi_1, \Phi_2, .., \Phi_J] \begin{bmatrix} F^{-1} & & & & \\ & F^{-1} & & & \\ & & . & & \\ & & & . & \\ & & & & F^{-1} \end{bmatrix} \begin{bmatrix} f_1 \\ f_2 \\ . \\ . \\ f_J \end{bmatrix} = [\Phi_1 F^{-1}, \Phi_2 F^{-1}, .., \Phi_J F^{-1}] \begin{bmatrix} f_1 \\ f_2 \\ . \\ . \\ f_J \end{bmatrix} =$$

$$= G^{CM} \begin{bmatrix} f_1 \\ f_2 \\ . \\ . \\ f_J \end{bmatrix} \qquad (2.14)$$

where G^{CM} is the recovery matrix, being the result of concatenating matrices $\Phi_j F^{-1}$. The sparsity basis for the CM model is not the Fourier matrix, but a $JN \times JN$ block diagonal matrix with $N \times N$ Fourier bases F along the diagonal (Slavinsky et al., 2011). This is due to the fact that the CM has multiple signals as input and consequently the CM derives a vector q, which is the combined representation of these signals $x_1, x_2, .., x_J$ in the Fourier domain. Since G^{CM} satisfies the RIP (Romberg, 2009), the CS problem for a CM architecture is thus the recovery of q, solving the following equation by applying CS techniques (Candès & Romberg, 2017):

$$y = G^{CM} q \qquad (2.15)$$

According to (Romberg, 2009) G^{CM} satisfies the RIP, therefore (2.15) can be solved by applying CS recovery algorithms, as in (2.7).

In all the CS architectures discussed, performance degrades, albeit gracefully, with increasing levels of noise (Tropp et al, 2010; Eldar & Kutyniok, 2012). Increasing

noise inevitably results in more significant frequency components appearing in a signal spectrum, leading to a corresponding decrease in sparsity and hence CS performance. Moreover, sparsity has been exploited in digital signal processing for denoising applications (Donoho, 1995), which are shown to be more effective with enhanced signal sparsity (Mallat, 1999). Thus, the concepts of sparsity and noise are inexorably linked, where the enhancement of the former resulting in a reduction in the latter. In this thesis, the focus will primarily be upon signal sparsity, because this is the fundamental premise underlying the CS theoretical framework (Candès & Wakin, 2008).

2.5. Discussion

This Chapter has firstly presented a brief historical background and developments that lead to CR and discussed the most well-known techniques and spectrum estimation methods suitable for CR spectral sensing. Referring to the challenges that CR faces, it stressed the need for wideband spectrum sensing and highlighted the potential of CS to address the major challenges of high sampling rates and stringent timing requirements. A background to the CS framework and a description of the RD and CM architectures has been given, with the key synergistic relationship between signal sparsity and noise levels highlighted.

From this detailed literature review, the following critical observations have been made:

a. The RD model inherently assumes a multitone signal structure, or narrowband modulation types [15 of Journal]. However, in wireless applications where multiband signals with continuous spectra are often encountered, the RD may require a larger number of tones to attain a suitable signal approximation (Eldar & Kutyniok, 2012), with a consequent impact on the computational cost for both the signal sampling and recovery stages.

b. Spectrum estimation techniques are not incorporated into the existing CS architectures, so they are constrained by the innate limitations of the periodogram spectral estimator highlighted in Section 2.3.2.3. When more sophisticated spectral estimation techniques e.g. MT estimator, than the periodogram are considered (Zhao et al., 2011), any possible advantages are negated by the higher computational overheads.

c. Existing CR spectrum sensing techniques apply the binary hypothesis test in order to assign an occupancy status to a frequency/spectral band. They do not consider the existence of possible gray states, which can have a notable impact upon CR spectrum sensing performance.

d. The aforementioned RD variants all either incur increased complexity or require *a priori* knowledge of the input signals. They are also not designed to exploit potentially favourable signal characteristics that can enhance sparsity and thereby CS performance.

e. Existing CS architectures all exploit signal sparsity in the frequency domain. With the potential improvement of spectrum utilization, the sparsity level of the wireless networks signals will be reduced, thereby impacting CS performance. Hence, is necessary to examine how CS architectures can operate so that they are able to exploit possible signal sparsity in alternative domains, other than Fourier.

These observations confirm that existing CS architectures like the RD and CM have a number of limitations to be resolved in order for them to be efficaciously applied in spectrum sensing applications for CR purposes. This provided the motivation for the technical contributions that will be presented in subsequent chapters, but firstly the research methodology adopted will be presented.

Chapter 3

Research Methodology

3.1 Introduction

This Chapter presents the research methodology adopted in order to design, develop, test and critically evaluate both the new generic CS framework and its individual components. Due to the nature of this project, although the quantitative approach is mostly employed, the qualitative one is also used for evaluation purposes. The quantitative approach is classified to inferential, experimental and simulation (Kothari, 2004). The first is not considered further since mostly used in surveys where characteristics of a studied population sample are inferred to the entire population and also does not provide great control over the research environment (Kothari, 2004).

Ideally it would have been better to employ the experimental approach that is the hardware implementation and testing of the generic CS framework in a real wireless communications environment. However this is not a practical decision. The wireless communication systems are very complex in nature due to the architectures and the environments in which they are deployed and operate. This is also true for the CS architectures. There is a great variety of the wireless standards and signal types involved, the hardware components to be put together and the parameters that have to be controlled, while the CS-based signal recovery is a complex process. Random processes are also involved, such as the noise present in every communication signal, or the sampling stage in a CS architecture. The aforementioned complexity and variable environments make the hardware implementation difficult, costly and time consuming. Moreover, hardware imperfections pertaining to elements and functions not considered in this research could affect the simulation results and consequently deflect the relevant conclusions to wrong directions.

On the other hand the simulation approach which has become widely adopted (Kasch et al., 2009), is a realistic approach. The complex environments like the

wireless communication systems cannot be easily analysed without resorting to simulation-based techniques (Tranter et al., 2003). Moreover, much greater control of the simulation environment and its parameters is permitted, thereby permitting better observation of the system behaviour (Kothari, 2004), before the undertaking of any unnecessary, costly and time consuming hardware implementation.

An overview of the research process is presented followed by a more detailed discussion of the simulation environment in the next two sections.

3.2 Overview of the Research Process

The various actions and steps of the research process are illustrated in Figure 3.1:

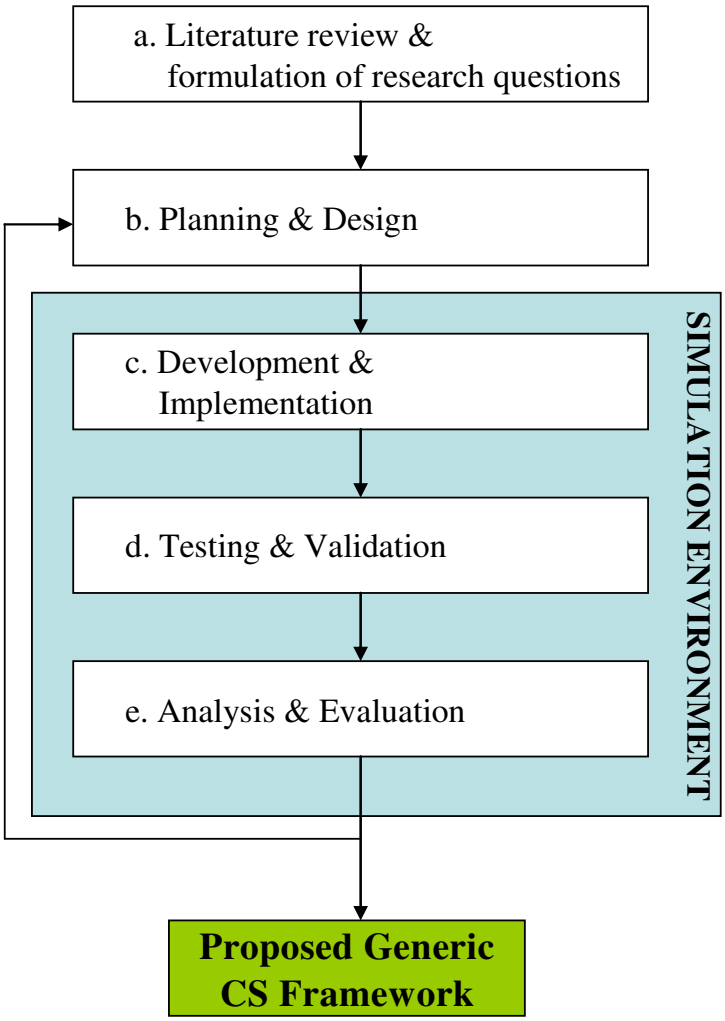

Figure 3.1: Block Diagram of the Research Process and its various steps.

a. Critical and extensive review of wireless communications literature, in particular that relating to CR technology, the CS paradigm and existing architectures and their potential to address spectrum sensing for CR applications. Identification of key technical limitations pertaining to existing architectures and the subsequent formulation of the overarching research question and the associated objectives.

b. Planning of the various phases of the research, definition of the requirements and design of the simulation environment within which the research will be conducted.

c. Development and implementation of the algorithms pertaining to the generic CS framework and its various components.

d. Testing and validation of the CS framework and its various components under various scenarios using correctness checks and rigorous functionality tests.

e. The performance of the generic CS framework and its constituent components is evaluated and analysed using the data derived from the previous step. The steps 3-6 are reiterated until all scenarios are considered and the models are developed and tested to the satisfactory fulfilment of the research objectives underpinning the research question of this thesis.

The final outcome of the research process described above is the proposed generic CS framework.

3.3 The Simulation Environment

In this Section, an overview of the simulation environment will be given followed by a description of the simulation software platform, the simulation parameters and the basic simulation blocks.

3.3.1 Overview

The environment which is simulated concerns CS architectures being part of a CR receiver, namely an SU receiver in a CR network, as depicted in Figure 3.2. The CS architectures are able to process signals from multiple PU, whose structure and modulation are encountered in wireless communication systems. Subsequently the CS architectures sub-sample and recover the signal, thereby providing the necessary information for the performace evaluation of the proposed CS models.

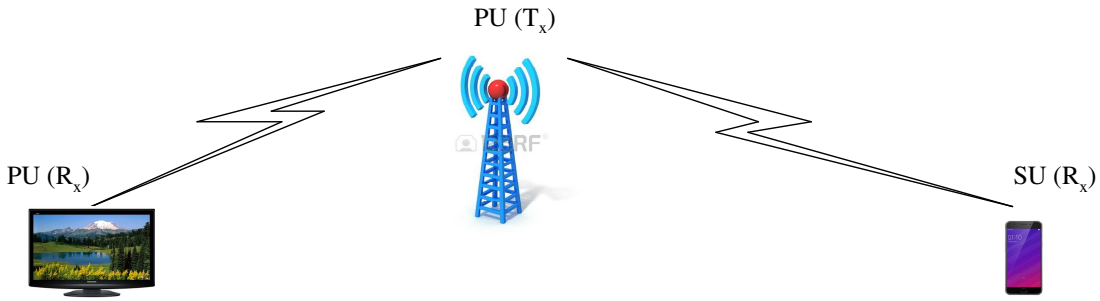

Figure 3.2: Simplified diagram of a CR network.

The signals employed are either test signals employing various digital or analog modulation types, or others with structure and basic parameters congruent with standards proposed in wireless networks, such as the 802.11af and LTE (Keysight Technologies, 2012; 3GPP, 2017; Flores et al., 2013).

There are two basic assumptions in this simulation environment: The first is the signal enters the CR receiver without having been affected by any of the impairments and uncertainties appertaining to a telecommunications channel such as the hidden node problem mentioned in Section 2.3.2. Only varying levels of *additive white gaussian noise* (AWGN) are considered as the principal source of interference. The

second assumption is that hardware imperfections are not taken into account. These assumptions are made in order to ensure that the results derived and the subsequent conclusions are only dependent on the input signals, the nature of the classical CS architectures and the improvements achieved by the new framework proposed in this thesis.

Finally, it is emphasised that a key research aim is not exact signal recovery after CS, but instead accurate spectrum/channel sensing for CR applications. This means the focus is not on the actual measurement of signal sparsity levels *per se*, but upon developing novel strategies which enhance and better exploit sparsity for a range of wireless communications related signals which are commonly associated with CR based networks.

3.3.2 Simulation Platform

There is a variety of software packages that have been developed over the years and are widely used in the simulation of communication systems. There are for example general-purpose programming languages such as C++, Java and FORTRAN, or modeling languages like SIMULINK (Mathworks, 2017) and OPNET (Riverbed, 2017). Languages like C++ are compiler based, which can be time consuming. The modeling languages like SIMULINK provide relatively simple block diagram of the model without the need to write code, however they do not offer more detailed information about the functionality of each block, so they are not controllable by the user.

An alternative to the above is MATLAB (Mathworks, 2017) command language which is widely accepted by the community for a number of reasons. It especially designed for computationally intensive problems and numerical and mathematical analysis, while it offers user-friendly graphical capabilities. Moreover, it contains an extensive array of built-in functions and toolboxes especially developed for communications and signal processing. In addition, it has an understandable error reporting and a very comprehensive command structure, which allows expressing algorithms and simulating environments with relatively few lines. MATLAB is interpreter based language, hence it exhibits slower execution times; however this drawback can be easily compensated by a more powerful personal computer (PC).

Therefore it was chosen as the modelling tool for the research presented in this thesis. The MATLAB version and the specifications of the PC used are summarized in Table 3.1.

Table 3.1: Simulation Platform and PC Specifications.

Software Platform	PC Specifications	
MATLAB 11.1/R2011b	Processor	Intel®Core™ i5 2430M (2.4GHz, Bus Speed 5GT/s DMI, 3MB SmartCache)
	RAM	4GB, DDR3 1066MHz
	Hard Disk	600GB, 8MB Buffer Size, 5400rpm
	OS	Windows 7 Home Premium

3.3.3 Simulation Parameters

This sub-section further describes the simulation environment by specifying its parameters, which are given in Table 3.2. They are related to the features of the signals employed and the operation characteristics of the CS architectures.

The digital modulation schemes chosen for the test signals, namely BPSK, QPSK, 16/64QAM, reflect those typically used in CR and other wireless standards (DeNardis, 2011; Task Group 4, 2017; Flores et al., 2013; Mody & Chouinard, 2010; 3GPP, 2010; Rakesh et al., 2010). The analog modulation types employed, that is AM and chirp, which are again widely used in wireless networks and other applications like Radar and geophysics (Tropp et al., 2010; Task Group 4, 2017; De Nardis & Di Benedetto, 2007).

The OFDMA access scheme is chosen because it is widely used in modern wireless communications, such as the 4G mobile networks (LTE) which are continuously deployed worldwide (3GPP, 2016). Moreover, OFDMA is considered a candidate in combination with other OFDM-like formats for 5G systems (Banelli et al., 2014).

The CDMA access scheme is also widely employed being the preferred option in 3G wireless standards like IS-95, CDMA2000 and UMTS (Ipatov, 2005), whereas

signal processing, namely channelization, scrambling and modulation type employed, is takes place according to the said standards.

For the input signals and the relevant PSD, a length (duration) t and N=2048/4096 samples and FFT points respectively is considered, pursuant to the requirements of wireless standards such as LTE and IEEE 802.22 (3GPP, 2016; Jain, 2014). The use of FFT length being a power of 2 is widely adopted due to its greater computational efficiency (Schwartz & Shaw, 1975). The length N corresponds to a Nyquist sampling rate $f_S = 1/\Delta t$ being at least equal to twice the available signal bandwidth B, according to the Nyquist theorem (Schwartz & Shaw, 1975), with Δt being the sampling interval (Percival & Walden, 1993). There is an obvious interdependency between the signal parameters. The frequency resolution (or equivalently the fundamental frequency) Δf of the signal PSD depends on the Nyquist rate f_S and the FFT length N, according to equation (3.1). Certainly, the higher the value of N, the better the resolution, but this comes at the expense of CS processing time at the recovery stage. In general, B, f_S, t, and N are determined to the design requirements. In this case of the test signals for instance, the signal length N could be set first according to the rationale discussed above. Then the bandwidth B is arbitrarily determined and consequently the other parameters according to (3.1). Furthermore, the number of active carriers is always chosen so the signal being considered will exhibit sparsity within the bandwidth B, which is a requirement discussed in Section 2.4.

$$\Delta f = \frac{2B}{N} \leq \frac{f_S}{N} = \frac{f_S}{f_S t} = \frac{1}{t} = \frac{1}{N\Delta t} \qquad (3.1)$$

Concerning the OFDM based signals, where in each channel (symbol) there is a superposition of closely spaced digitally modulated signals, the parameter values are taken according to (Keysight Technologies, 2012; 3GPP, 2017; Flores et al., 2013), in which the wireless network standards IEEE 802.11af and LTE that employ OFDM are presented.

In regards to the CS features, the sensing matrices are populated from i.i.d. entries of the Rademacher distribution, whose respective variable is the simplest probabilistic object (Tropp et al., 2010; Slavinsky et al., 2011), while the sparse bases are the DFT

Table 3.2: Simulation Parameters and their values or characterization

Parameters	**Value/Characterization**	
Test signals		
Modulation Schemes	QPSK, BPSK, 16QAM, 64QAM, AM, chirp	
Signal length/FFT length (samples)	2048	
Signal duration t (ms)	300	
Available bandwidth B (kHz)	≈3.4	
Bandwidth b per carrier (Hz)	≈430 (digital modulation), ≈40 (analog modulation)	
Number of carriers	1, 2, 4 (digital modulation), 1, 4 (analog modulation)	
PSD resolution Δf (Hz)	≈3.35	
Nyquist rate f_S (kHz)	1.01x2B (2048 samples)	
Input *signal-to-noise-ratio* (SNR) (dB)	AWGN (4dB to 8.1dB) as per IEEE 802.22. Down to 3dB and -3dB for AM and chirp signals	
OFDM signals		
	LTE	**802.11af**
Modulation Schemes	QPSK	
OFDM channel bandwidth (MHz)	3	6
Number of sub-carriers per channel	181	144
Sub-carrier spacing Δf_{sub} (Hz)	16575	2x20833
OFDM symbol (channel) duration (s)	1/16575	1/2x20833
Signal length (samples)	4096	
Input SNR (dB)	AWGN (0dB to 15dB)	
Signal bandwidth B (MHz)	≈34	≈42.67
Number of active channels within B	2	

Resolution Δf (Hz)	16584	20845
CDMA test signals		
Signal length before encoding (samples)	64	
Signal length after channelization (samples)	2048	
Maximum number of CDMA channels	32	
Scrambling codes	PN sequences	
Modulation type of baseband data	QPSK	
CS architectures		
Compressed sampling rates (%Nyquist)	50.5, 25.25, 12.625, 6.3125, 3.15625	
Number of CS measurements M	1024, 512, 256, 128, 64	
Distribution of sensing matrix entries	Rademacher	
Sparsities	Fourier (frequency), WH (sequency)	
Recovery algorithm	l_1-norm minimization	
Number of channels	1, 2 or 4	

and WHT matrices for frequency and sequency sparse signals respectively. The dimensions of the sensing matrices are $M \times N$ with M being the number of CS measurements and N the signal length. The recovery algorithm is based on l_1-norm minimization (Eldar & Kutyniok, 2012; Candès & Romberg, 2017) signal sub-sampling by the CS architectures, results in proportionally lower number of measurements, as it is shown at the CS features in Table 3.2. Due to the banded nature of the sensing matrices employed, it is not practically feasible to use intermediate sampling rates.

3.3.4 Simulation Blocks

The simulation environment consists of a number of functional software blocks shown in Figure 3.3. They have been specifically designed and developed so to reflect the operation of the generic framework and its individual novel CS models.

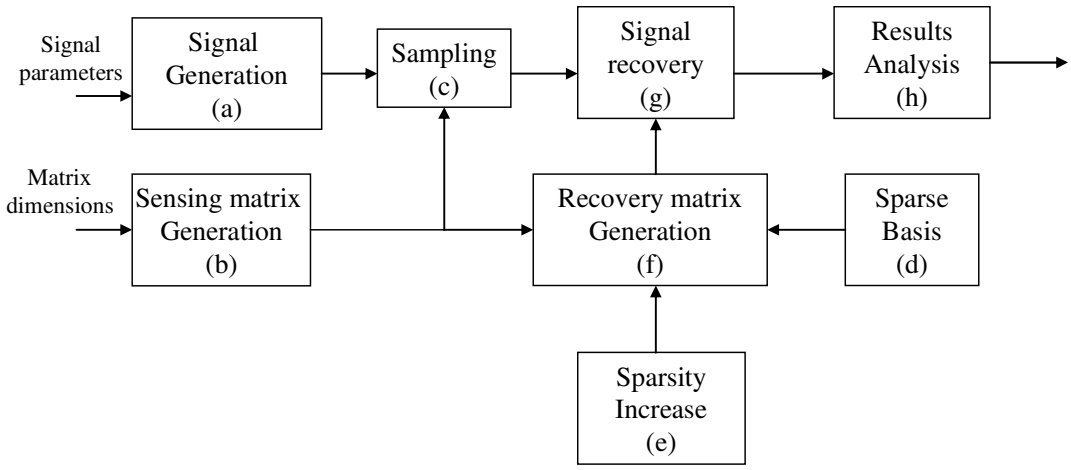

Figure 3.3: Overview of the simulation process.

A description of the blocks follows:

a. The signal generation block uses the parameters defined in the Table 3.2. MATLAB objects, built-in functions and libraries taken from the communications and statistical toolboxes in order to generate the various signals are employed. These include random number generators, modulation objects and libraries, pulse shaping and built-in mathematical functions.

b. The sensing matrix block generates the measurement matrices employed in the CS architectures, namely the block diagonal matrix employed in the RD based architectures, and the diagonal matrix utilized by the CM based architectures. It employs MATLAB matrix operations, random number generators and built-in mathematical functions.

c. The sampling block multiplies the sensing matrices and the signal to derive the CS measurements.

d. The sparse domain block generates the bases to which the signals employed are sparse. It utilises MATLAB functions taken from the signal processing and communications toolboxes as well as built-in mathematical functions.

e. The sparsity increase block generates suitable matrices that modify the sparse bases so that the signal sparsity is increased in these modified bases. Matrix and mathematical functions are employed, along with functions from the signal processing toolbox. The latter include filtering, AR parametric modelling and signal tapering.

f. The recovery matrix block generates the matrices employed for the signal recovery in the sparse domain. It is the result of the multiplication of the matrices generated at blocks d. and e.

g. The recovery block utilizes a CS recovery algorithm to recover the signal. It employs the recovery matrix and the output of the sampling block.

h. The results analysis block uses the output from the recovery block to present and analyse the results of the simulation process. MATLAB mathematical, control flow and plot functions are employed in this block.

3.4. Performance Evaluation and Metrics

For the critical performance evaluation of the new CS framework, two baseline comparators were considered; the classical RD and CM architectures. The rationale is that the research contributions pertain to enhancements of these classical CS architectures concerning their ability to reliably and accurately identify the occupied frequencies/channels as being part of a CR receiver that performs spectrum sensing.

Consequently the selected performance metrics employed for critical evaluation need to reflect the aforementioned capability to some extent. One such performance metric is *spectral leakage*, which is defined as the signal energy that leaks from one frequency resolution Δf, to another (Manolakis et al., 2005). It is measured as the percentage of the energy/power lying outside the occupied frequencies, as shown in equation (3.2). Spectral leakage is related with favourable bias-variance PSD properties, that is low spectral leakage leads to low bias hence to reliable and accurate

spectral estimation (Manolakis et al., 2005; Manolakis & Ingle, 2011; Madisetti, 2010). Moreover, low spectral leakage means greater signal sparsity since fewer active frequency components are present and more efficient CS performance can be achieved (see Section 2.4.2.1).

$$spectral\ leakage = \frac{P_{occ}}{P_{total}} \cdot 100\% \qquad (3.2)$$

where P_{occ} represents the power within the occupied frequencies and P_{total} the total signal power.

The spectral leakage is measured against different sub-Nyquist sampling rates in order to evaluate the efficiency of each of the enhanced CS architectures compared with the respective original design. Since a telecommunications environment is being considered, the noise robustness of the CS architectures must also be evaluated. Hence the PSD spectral leakage is measured across a range of input SNR values, so the evaluation assessment criteria are that a CS architecture must be efficient and robust to be able to perform at both sub-Nyquist sampling rates and low SNR values, yet be capable of performing accurate and reliable CR spectrum sensing.

A complementary approach to numerically evaluating spectral leakage performance is a *qualitative assessment* of the relevant PSD graphs, where the spectral signal characteristics are visually compared (Proakis & Manolakis, 2006). In this thesis, PSD graphs pertaining to the recovered signals are perceptually compared to showcase the ability of the various CS architectures to effectively identify bands and channels.

In regards to spectral classification, the *Euclidean distance* or l_2*-norm* (Strang, 2016; Rafael & Woods, 2017; Petrou & Petrou, 2010) between vectors is employed, where the vectors contain the occupancy status information derived by the CS model under evaluation. A *reference vector* v_{ref} is introduced which contains the real occupancy status information. According to the discussion in Section 2.2.2.3, three possible occupancy states for each frequency resolution are considered: *1* for an occupied frequency, *0* for vacant and ½ for partially occupied (gray). The vector v_{cs} associated with each CS architecture is then compared with the reference vector v_{cs}

and the lower their respective Euclidean distance, the greater their *similarity* and hence spectral classification capability. This similarity metric is defined as:

$$similarity = \frac{1}{\left\| \mathrm{v}_{CS} - \mathrm{v}_{ref} \right\|_2} \tag{3.3}$$

with $\left\| v_{cs} - v_{ref} \right\|_2$ being the l_2-norm of the vectors. The rationale behind using a metric from the image processing field (Rafael & Woods, 2017; Petrou & Petrou, 2010) is that bandwidth, frequency resolution and occupancy states can be respectively treated in the same way as image, pixels and brightness levels. In image processing two images can be viewed as vectors where the vector entries represent image pixels with the values assigned being the brightness levels of the pixels. The images are compared by the Euclidean distance between the vectors. Likewise, the bandwidths can be viewed as vectors where the vector entries are frequency resolutions and the values the entries are represent the respective occupancy states.

Another performance metric used to validate all the algorithms in the new CS framework is the level of signal sparsity achieved. As noted in Chapter 2, signal sparsity is central to CS theory, since CS performance improves with increased sparsity. Sparsity level is determined by the number of the active frequency components present in a given signal, where a frequency is considered active if it exceeds the predefined threshold defined in (Karampoulas et al., 2015).

The final assessment metric employed for the new CS framework is the SNR (Laska et al., 2007) which is defined by equation (3.4):

$$SNR_{system} = 10\log\left(\frac{\left\| P_{Nyq} \right\|_2}{\left\| P_{Nyq} - P_{CS} \right\|_2} \right) \tag{3.4}$$

where P_{Nyq} is the vector form of the signal power derived at or above the Nyquist rate and P_{CS} is the power of signal recovered by the CS architectures. The system SNR shows how close is the recovered version of the signal in the sparse domain to the original one. The metric specifically measures the quality reconstruction of a CS architecture (Tropp et al., 2010), regardless of the sparsity bases employed. Therefore

it is used in Chapter 6 of this thesis to compare the performance of CS architectures under different sparsity bases.

3.5 Software Validation

Verification and validation techniques were applied throughout the design, development and implementation of the generic CS framework. In a MATLAB interactive environment, the design was refined through iterations and verification cycles. Verification activities included static analysis techniques such as code reading and inspection, code reviewing, control flow, data use, check of proper definition of variables and failure analysis (Schaefer et al., 2014; Braione et al., 2012; Mathworks, 2017).

In order to rigorously validate the constituent software blocks shown in Figure 3.3, the baseline comparators and the algorithms of the generic CS framework dynamic tests were separately implemented, for which the outcome concerning success/failure was known *a priori*. First the simulation blocks were validated with data sets specifically designed according to the function of each block. For the signal block the data sets were employed to ensure that the signals with the appropriated characteristics are generated. Similarly, suitable predesigned data sets were used to test the matrix blocks for the generation of matrices with the appropriate structure. Moreover, the baseline comparators and the framework algorithms were validated under verifiable scenarios with known outcomes. Test signals with a priori known input and output characteristics and structure were employed in order to ensure the correct and expected operation of the comparators and the framework. For example, in order to validate the classical RD, a simple signal consisting of a few tones with known positions was employed as input and was compared with the recovered output.

The data results for every simulation scenario were also tested for being statistically significant and fit to the respective CS model. In order to do this and since the simulation environment has random processes involved, the Monte Carlo approach has been adopted (Papoulis, 1991; Mathworks, 2017). For each of the simulation scenarios considered in this CS framework, 500 experiments were performed and the values of the variables of interest are averaged across the

corresponding observed values from each experiment. It is noted that in regards to the number of experiments, the larger the number the closer the observed values to the true values of the variables. The data significance and their fitness to the model (Leon-Garcia, 1994), or in other words the association between the model and the output data, are tested with the significance level set to 5% (Leon-Garcia, 1994). Thus, for the given novel CS model and from the 500 observations, it is expected that at least 475 times the model fits to the output data. This means that the observed enhancements revealed by the data are due to the model.

3.6 Summary

This Chapter has detailed the methodology adopted for the simulation work undertaken in this thesis. A simulation environment has been developed in the MATLAB to implement various classical CS architectures, as well as a proposed generic CS model and its individual components. A detailed description of this environment and the constituent simulation blocks, parameter settings and the various metrics used for critical performance evaluation have been specified along with a description of the software verification and validation techniques employed. The next Chapter will present the first contribution of this thesis, namely the AR-based CS model.

Chapter 4

An Autoregressive-based Compressive Sensing Model for Spectrum Sensing

4.1 Introduction

As discussed in *Chapter 2*, the wideband nature of the typical signals found in CR networks dictates the employment of high sampling rates for spectrum sensing purposes, which is a major challenge. However, although CS has the potential to address such a challenge, there is a need for performance improvement of the CS architectures, as discussed in Section 2.5.

Several CS architecture enhancements were discussed, in particular concerning the RD and MWC. These enhancements however, are achieved at the cost of increased complexity or require system calibration (Israeli et al., 2014). Furthermore, CS architectures such as the RD, only perform efficiently for specific types of signals that are sparse bandlimited, periodic and approximated by a sum of multitones (Tropp et al., 2010). In the case of multiband, digitally modulated signals frequently encountered in CR applications, the RD performance depends on the number of tones required for their approximation (Tropp et al., 2010; Eldar & Kutyniok, 2012). This can have a significant impact on the computational overhead of the RD if the number is large (Eldar & Kutyniok, 2012). A high number of tones indicate low frequency sparsity, which in turn negatively affects the CS performance of the architecture.

This provided the motivation to investigate ways to improve performance by not only modifying the existing CS architectures, but exploiting favourable signal features to increase sparsity and thereby enhance CS performance. To this end, a new *autoregressive* (AR)-based CS model is presented which achieves effective signal sparsity increase by precolouring the signal using an AR filter (Marple, 1987; Manolakis et al., 2005). Precolouring has the effect of enhancing signal sparsity by

sharpening dominant frequencies while attenuating the weaker ones. In other words as highlighted in Chapter 2, precolouring reduces the signal noise level. It is also important to stress the new model is applicable to both RD and CM structures.

The new AR-based CS model along with a brief discussion about precolouring and the AR filter are presented in *Section 4.2*, before the simulation setup and critical results discussion are presented in *Sections 4.3* and *4.4* respectively. Finally a summary of the key findings from this model are provided in *Section 4.5*.

4.2 The AR-based CS Model

One of the fundamental premises of CS performance improvement is the concept of sparsity, that is the greater the signal sparsity the better the performance. Hence, for a specific signal in question, one option to enhance CS performance is to investigate ways to increase signal sparsity prior to its application to a CS architecture. This is not an option when the aim is exact signal recovery, since a change in sparsity level changes the frequency content of the signal. In this thesis, the aim is not exact signal recovery but instead the derivation of a PSD estimate for spectrum sensing for CR applications. Thus the signal modification due to increased sparsity is permissible provided the derived PSD can still identify the status of the spectral bands.

The AR filter provides a way to enhance signal sparsity and thereby reduce the signal noise level by precolouring (Manolakis et al., 2005), by emphasising dominant frequency components of the input signal, while attenuating weaker ones.

Besides its potential to increase signal sparsity, the choice of the AR filter is attractive for two reasons: i) the computational burden to estimate the AR parameters is much lower than other models of the same linear parametric family (Marple, 1987) and ii) the AR process is more appropriate for representing spectra which have relatively few narrow peaks (Marple, 1987; Proakis & Manolakis, 2006), which importantly is the case most often encountered in wireless networks, where signals are inherently frequency sparse. Both the precolouring process and the AR filter design will now be discussed.

4.2.1 The AR Filter and Precolouring Integration in the RD Architecture

AR is a special case of the linear parametric *Autoregressive Moving Average* (ARMA) model which assumes the signal is generated by an appropriate time-series model driven by white noise source. It is formally described by (Marple, 1987; Manolakis et al., 2005):

$$x(n) = \sum_{k=1}^{p} a_k x(n-k) + w(n) \qquad (4.1)$$

where $w(n)$ is the input white noise process, $x(n)$ the output of the signal at time n, the model parameters and p the number of the parameters also known as the model order.

The model is considered stable in order to generate finite values for the signal $x(n)$, therefore it has a finite frequency response $H(f)$ and consequently the frequency domain equivalent of (4.1) is (Manolakis & Ingle, 2011; Oppenheim & Schafer, 2009):

$$P(f) = \left|X(f)\right|^2 = \left|H(f)\right|^2 \left|X_w(f)\right|^2 \qquad (4.2)$$

where $P(f)$ and $X(f)$ are respectively the *power spectral density* (PSD) and Fourier Transform of x, and $X_w(f)$ the Fourier transform of w.

Since the input driving process $w(n)$ is white noise, it exhibits a flat power spectrum equal to its variance σ_w^2 (Proakis & Manolakis, 2006), so (4.2) can also be written as:

$$P(f) = \left|X(f)\right|^2 = \sigma_w^2 \left|H(f)\right|^2 \qquad (4.3)$$

Introducing the a_k parameters and the model order p, (4.3) can be expressed as (Madisetti, 2010; Manolakis & Ingle, 2011; Percival & Walden, 1993):

$$P(f) = \frac{\sigma_w^2}{\left|1 + \sum_{k=1}^{p} a_k e^{-j2\pi fk}\right|^2} \tag{4.4}$$

Hence, the AR model can be viewed as an all-pole filter with coefficients a_k, which generates the signal $x(n)$ when it is excited by input white noise $w(n)$. Figure 4.1 depicts a simplified block diagram of an AR filter.

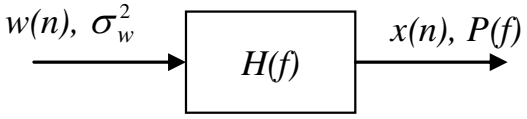

Figure 4.1: Simplified block diagram of an AR filter.

The next step is the calculation of the parameters a_k and the selection of the model order p. From the various methods proposed to estimate the a_k parameters of an AR process, the *modified covariance* method (Ulrich & Clayton, 1976; Nutall, 1976), yields a stable, low-biased spectral estimate, and so is used to select p for the AR filter throughout the thesis.

Regarding the selection of the filter order p, it is determined according to one of several criteria that have been proposed, such as the *final prediction error* (FPE) criterion (Akaike, 1970) the *Akaike information criterion* (AIC) (Akaike, 1974), the *criterion autoregressive transfer* (CAT) (Parzen, 1974) and the *minimum description length* (MDL) criterion (Rissanen, 1983). The underlying premise is minimizing some function of p relevant to the selected criterion. This takes into account that while increasing p reduces the modelling error which equals the white noise variance σ_w^2, it comes at the expense of complexity (Manolakis et al., 2005). For the AR model used in this thesis, the MDL criterion was selected, since it is an improved variant of FPE, AIC and CAT (Marple, 1987) and is also statistically consistent (Manolakis et al.,

2005; Rissanen, 1983), so the probability of choosing the most appropriate filter order tends to 1 as the signal length *N* tends to infinity. The MDL is given by:

$$MDL(p) = N\ln(\sigma_w^2) + p\ln(N) \qquad (4.5)$$

with N being the number of signal samples (signal length).

Since *w(n)* has a flat spectrum and a PSD equal to σ_w^2 at all frequencies, it is apparent from (4.3) that the Fourier transform *X(f)* and PSD *P(f)* of *x(n)* are completely determined by the AR filter frequency response *H(f)*, scaled by the white noise variance. Since the input is white noise, where all frequencies are equally present, and the output a signal with a relatively small number of dominant frequencies, the AR filter acts as a colouring filter to the signal.

Most importantly, the colouring effect of the AR filter enhances frequency sparsity. A white noise signal does not exhibit any sparsity as all frequencies are equally present in terms of their energy content. Conversely, *x(n)* exhibits reduced noise level due to the energy concentration in a relatively small number of frequencies, so when the AR filter is excited with noise *w(n)* to produce *x(n)* at its output, it increases sparsity from zero to that of *x(n)*. This means dominant frequencies of *x(n)* are emphasised while weak frequencies are attenuated, thereby rendering them easier to be identified as occupied in CR applications.

This specific AR filter exhibits the same behaviour independently of the input, but for an input *x(n)*, the filter further enhances strong frequencies while attenuating or eliminating weaker ones, thereby increasing the output dynamic range and lowering spectral leakage. This means the AR filter enhances sparsity when it is driven by *x(n)*. This can formally be expressed as:

$$x_C(n) = x(n) + \sum_{k=1}^{p} a_k x_C(n-k) \qquad (4.6)$$

So by increasing sparsity, the performance of the corresponding CS architectures can be improved by precolouring the input signal. This is depicted in Figure 4.2 that

shows the AR-RD architecture, where the AR filter processes the input signal before being applied to the RD architecture.

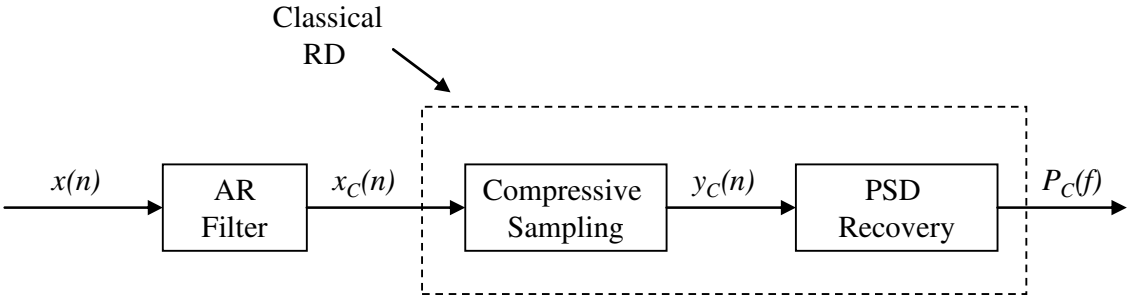

Figure 4.2: Block diagram of the AR-RD architecture. The dotted lines block represents the classical RD structure.

The input is first precoloured by AR filter according to (4.6) before being processed by the classical RD, in the manner described in Section 2.4.3. Firstly $x_C(n)$ is sub-sampled to give $y_C=Ax_C$ before the corresponding frequency vector $f_C=Fx_C$ is recovered by solving:

$$y_C = Ax_C = AF^{-1}f_C = Gf_C \tag{4.7}$$

for f_C using a recovery algorithm (Candès & Romberg, 2017), where it is assumed the signal lengths of both x and x_C is N samples and $M<N$. Matrix A is the measurement matrix with dimensions $M \times N$, while F and $G=AF^{-1}$ are the DFT and recovery matrices respectively, each with dimensions $N \times N$. By processing the sparsity enhanced precoloured version of $x(n)$, the RD provides improved performance because the output PSD emphasises the dominant bands while attenuating the weak ones.

The corresponding pseudo code for the AR-RD is given in the Algorithm 4.1.

Algorithm 4.1: Pseudo code for the AR-RD

Inputs: signal $x(n)$ of length N samples.

Variables: M - number of measurements or equivalently the length of output $y(n)$ of sub-Nyquist sampling, p - the AR filter order, F – the $N \times N$ DFT matrix, A - the $M \times N$ measurement matrix.

Outputs: P_C of $x(n)$

1: ***Initialise*** M, F, p.

2: ***Calculate*** AR filter coefficients α_k from $x(n)$, p.

3: ***Calculate*** $x_C(n)$ using (4.6).

4: ***Construct*** A.

5: ***Calculate*** $y_C = Ax_C$.

6: ***Calculate*** $G = AF^{-1}$.

7: ***Apply*** l_1 minimisation algorithm to solve $y_C = Gf_C$ for f_C.

8: ***Calculate*** $P_C = |f_C|^2$.

9: **END**

There are however, two key constraints in the precolouring RD architecture arrangement in Figure 4.2:

a. Precolouring cannot be applied at the transmission end prior to the input signal being sub-sampled by the RD, as this imposes a computational cost on any licensed user i.e., PU, which is not an acceptable design scenario.

b. Precolouring alters the input signal information content before CS, which is undesirable for the PU since it may affect the QoS provided.

This provided the motivation to investigate alternative novel RD solutions whereby the benefits of increased sparsity and noise reduction are still exploited, but

the overheads on the PU are minimised by transferring the precolouring process to the receiver. The only cost would then be ensuring the availability of the AR filter coefficients at the receiver, which is currently the situation with existing telecommunication providers who do this for speech coding purposes (Karampoulas et al., 2014; Rakesh et al., 2010; 3GPP, 2010). The design aim is thus to seamlessly integrate the AR coefficients and subsequent precolouring process into the RD architecture in Fig. 4.2. This is achieved as follows:

Considering that both $x(n)$ and $x_C(n)$ comprise N samples, (4.6) can be viewed as a set of equations, with each calculating the value of $x_C(n)$ with $n \in [1, N]$:

$$x_c(1) = a_1 x_c(0) + a_2 x(-1) + ... + a_p x_c(1-p) + x(1) = x(1) + 0x(2) + 0x(3) + .. + 0x(N)$$
$$x_c(2) = a_1 x_c(1) + a_2 x_c(0) + ... + a_p x_c(2-p) + x(2) = c_1 x(1) + x(2) + 0x(3) + .. + 0x(N)$$
.
.
$$x_c(N) = a_1 x_c(N) + a_2 x_c(N-1) + .. + a_p x_c(N-p) = c_{N-1} x(1) + c_{N-2} x(2) + ... + x(N)$$

or in matrix form as:

$$x_c = Cx \tag{4.8}$$

where x_C and x are $N \times 1$ vector expressions of $x_C(n)$ and $x(n)$ respectively, while C is termed the *precolouring matrix* (PM) which has dimensions $N \times N$ and the form:

$$C = \begin{bmatrix} 1 & 0 & 0 & . & . & . & 0 \\ c_1 & 1 & 0 & . & . & . & 0 \\ c_2 & c_1 & 1 & . & . & . & 0 \\ . & . & . & . & . & . & . \\ . & . & . & . & . & . & . \\ c_{N-1} & c_{N-2} & . & . & . & . & 1 \end{bmatrix} \tag{4.9}$$

This is a lower triangular Toeplitz matrix so it is always invertible and the main diagonal elements are all equal to unity. C is completely defined by its first column, the elements of which can be derived by the following recursive equation:

$$c_n = \sum_{k=1}^{p} \alpha_k c_{n-k} \qquad k = 1,2,..,p \qquad n = 1,2..,N-1 \qquad (4.10)$$

where it is assumed that $c_0=1$ and $c_k=0$ for $k<0$.

So incorporating precolouring into the RD has been achieved by means of the PM which can be implemented by applying C in either the sampling or recovery stages i.e., respectively applied to either matrices A or G, as will now be discussed.

PM in the sampling stage: Referring to Figure 4.2, the PM is applied so the output of the RD is a coloured version $y_C(n)$. There is no longer an input AR filter, so taking into consideration (4.8), (4.7) can be written as:

$$y_C = Ax_C = ACx = A_C x \qquad (4.11)$$

This equation reveals that it is possible for the RD sampling process to derive $y_C(n)$ if the measurement matrix A is modified to $A_C=AC$. However, A_C is not a banded matrix anymore and consequently it cannot express the functions of the RD described in Section 2.4.3.

When PM is applied in the recovery stage, the measurement matrix A remains unchanged and PM modifies matrix G. In the recovery stage of the RD architecture in Figure 4.2, PM is applied in such a way that the f_C is recovered with the output of the sampling stage being $y(n)$ instead of $y_C(n)$. The RD sampling process in this case is then expressed as:

$$y = Ax \qquad (4.12)$$

The PM now modifies G since according to the CS theory (Section 2.4.2), the recovery matrix is dependent on the sparsity basis, so the modification of G also alters the Fourier basis. The modified basis has to link x and f_C in the same manner the Fourier basis F links x and f. It can be concluded from (4.8) that:

$$Fx_C = FCx = f_C \rightarrow f_C = F_C x \rightarrow x = F_C^{-1} f_C \tag{4.13}$$

which means the new sparsity basis is matrix F_C=FC, which is always invertible, since C is invertible. Thus (4.12) can be written as:

$$y = AC^{-1}F^{-1} f_C = G_C \, f_C \tag{4.14}$$

So f_C and subsequently the PSD $P_C(f)$ are recovered from the measurements y with $G_C = AC^{-1}F^{-1} = AF_C^{-1}$ now being the recovery matrix instead of G.

This theoretical derivation confirms the RD architecture can undertake precolouring without the need of the input AR filter in Figure 4.2, by using matrix C which is formed from the a_k filter coefficients. The increased sparsity introduced by precolouring, is now accomplished by the modified recovery matrix G_C, which is determined by the PM. In other words, signal x exhibits enhanced sparsity in basis F_C compared to the Fourier matrix F. It is evident that both precolouring approaches i.e., either applying an AR filter before the RD or integrating the PM in the recovery stage are equivalent as exactly the same frequency vector f_C is obtained, so the same CS performance is achieved. The resulting RD-based architecture which from now will be termed *i*PM-RD (Karampoulas et al., 2014), is shown in Figure 4.3 with $p_c(t)$ being the chipping sequence which modulates x as shown in Figure 2.10.

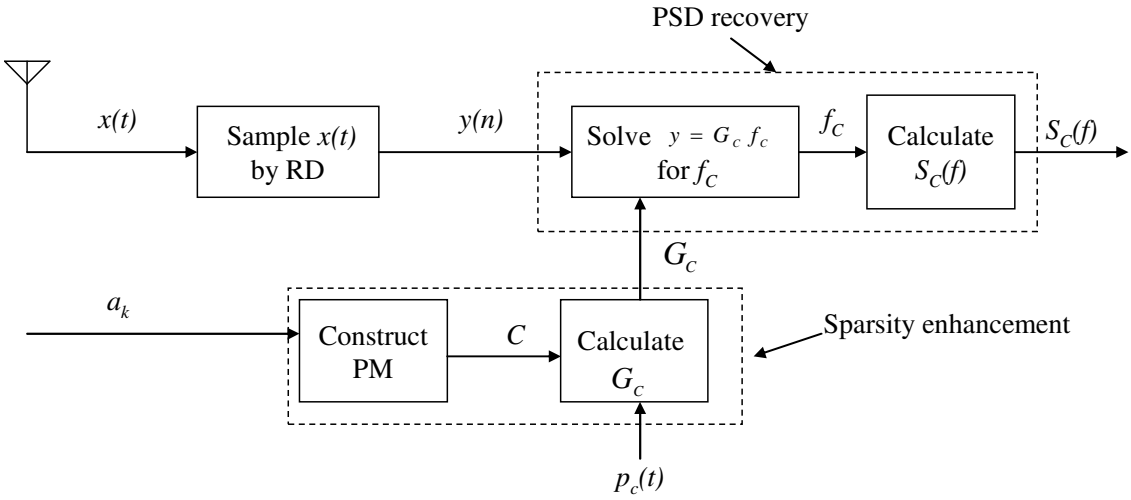

Figure 4.3: Block diagram of the *i*PM-RD architecture.

The corresponding pseudo code for the *i*PM-RD is given in the Algorithm 4.2.

Algorithm 4.2: Pseudo code for the *i*PM-RD

Inputs: signal $x(n)$ of length N samples.

Variables: M - number of measurements or equivalently length of $y(n)$ output of sub-Nyquist sampling, p- the AR filter order, F- the $N \times N$ DFT matrix, A- the $M \times N$ measurement matrix.

Outputs: P_C of $x(n)$

1: ***Initialise*** M, F, p.

2: ***Calculate*** AR filter coefficients α_k from $x(n)$, p.

3: ***Construct*** A.

4: ***Calculate*** $y=Ax$.

5: ***Construct*** C from (4.10) .

6: ***Calculate*** $G_C=AC^{-1}F^{-1}$.

7: ***Apply*** l_1 minimisation algorithm to solve $y=G_C f_C$ for f_C.

8: ***Calculate*** $P_C=|f_C|^2$.

9: **END**

Both the *i*PM-RD and classical RD are single-channel architectures since only one input signal is considered. It is assumed that they acquire transmissions from different PU across the entire bandwidth of interest, so the resulting incoming signal will have a spectral width greater than each of the individual transmissions, hence it exhibits less sparsity. For *i*PM-RD in particular, there is an additional matter appertaining to the choice of AR filter coefficients. Since this model is parametric, each individual PU signal will be characterised by its own set of coefficients and to accommodate all these sets, a multi-channel structure is required.

In (Yu & Hoyos, 2009; Yu et al., 2008) a multi-channel version of the RD has been presented, where the input signal is applied to each of the parallel branches. Based on this, the concept of the parallel structure can be employed under a different approach. Instead of considering a single channel where different signals from the PU are input, multiple channels, each one corresponding to a PU, are considered. Each channel in the parallel structure receives and processes a single PU signal using its own AR filter coefficients. This relaxes the sampling rate requirements and renders feasible the application of the precolouring process in the case of existence of more than one PU. Figures 4.4a and 4.4b depict the block diagrams for the multi-channel RD and *i*PM-RD architectures respectively. The individual architectures are defined by the corresponding sampling and recovery matrices. The individual PSD are then summed to form a combined PSD of all incoming signals, so for J input channels:

$$P = \sum_{j=1}^{J} P_j \tag{4.15}$$

in the case of the multi-channel RD and,

$$P_c = \sum_{j=1}^{J} P_c^j \tag{4.16}$$

For the multi-channel *i*PM-RD, where P_j and $P_c^{\,j}$ are the PSDs derived by the j^{th} branch of the RD and *i*PM-RD multi-channel architectures respectively.

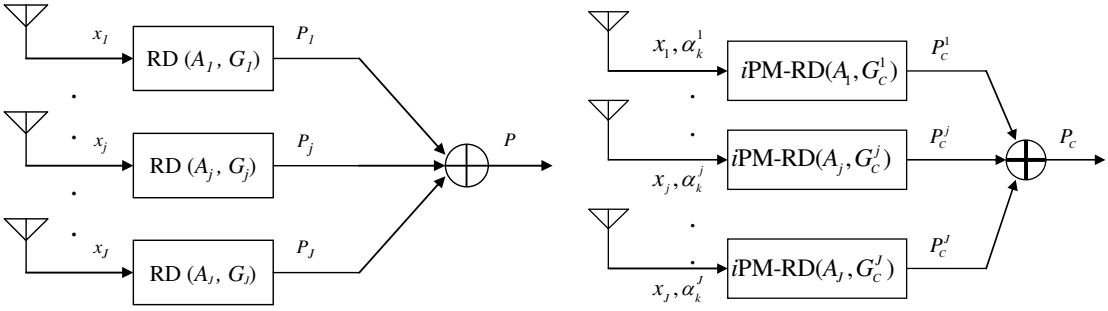

(a) (b)

Figure 4.4: Block diagram of the multi-channel (a) RD and (b) *i*PM-RD.

4.2.2 The CM version of the AR-based CS Model

In the previous Section, the integration of precolouring into the CS process has been achieved for the RD, via the new *i*PM-RD architecture, where precolouring is accomplished by embedding a PM in the recovery stage. In this Section, the integration of precolouring into the *Compressive Multiplexer* (CM) architecture will be presented.

The CM was described in Section 2.4.3. It is an alternative parallel CS architecture with J independent, jointly sparse input signals, each of bandwidth B Hz (Slavinsky et al., 2011). As in the RD, each channel $x_j(t)$ is modulated by a pseudorandom chipping sequence $p_j(t)$ with ± 1 values and chipping frequency at least the Nyquist rate $2B$ of the individual signal. In contrast the CM has no integrator before sampling. The channel outputs are firstly summed and then sampled by an ADC operating at a rate equal to $2B$, to give output $y(n)$. The CS results because the sampling rate is $2B$, while the combined Nyquist sampling rate is $2JB$. The n^{th} output is given by:

$$y(n) = \sum_{j=1}^{J} x_j(n)\, p_j(n) \qquad (4.15)$$

With N samples for each signal, (4.15) can be written in vector form as:

$$y = \sum_{j=1}^{J} \Phi_j x_j \tag{4.16}$$

where Φ_j is a NxN diagonal matrix, with the main diagonal populated by *independent identically distributed* (iid) entries from a random distribution, which for the CM is the Rademacher distribution (Slavinsky et al., 2011).

As discussed in Chapter 2, the vector form representation of (4.16) is given by:

$$y = \sum_{j=1}^{J} \Phi_j x_j = [\Phi_1, \Phi_2, .., \Phi_J] \begin{bmatrix} x_1 \\ x_2 \\ . \\ . \\ x_J \end{bmatrix} = [\Phi_1, \Phi_2, .., \Phi_J] \begin{bmatrix} F^{-1} f_1 \\ F^{-1} f_2 \\ . \\ . \\ F^{-1} f_J \end{bmatrix} =$$

$$= [\Phi_1, \Phi_2, .., \Phi_J] \begin{bmatrix} F^{-1} & & & & \\ & F^{-1} & & & \\ & & . & & \\ & & & . & \\ & & & & F^{-1} \end{bmatrix} \begin{bmatrix} f_1 \\ f_2 \\ . \\ . \\ f_J \end{bmatrix} = [\Phi_1 F^{-1}, \Phi_2 F^{-1}, .., \Phi_J F^{-1}] \begin{bmatrix} f_1 \\ f_2 \\ . \\ . \\ f_J \end{bmatrix} =$$

$$= G^{CM} \begin{bmatrix} f_1 \\ f_2 \\ . \\ . \\ f_J \end{bmatrix} \tag{4.17}$$

where G^{CM} is the result of concatenating matrices $\Phi_j F^1$ and f_j the frequency vector for each respective x_j. The sparsity basis for the CM architecture is not the Fourier matrix, but a $JN \times JN$ block diagonal matrix with $N \times N$ Fourier bases F along the diagonal (Slavinsky et al., 2011). This is due to the fact that the CM has multiple signals as input and consequently the CM derives a vector q, which is the combined representation of these signals $x_1, x_2, .., x_J$ in the Fourier domain. Since G^{CM} satisfies the RIP (Romberg, 2009), the CS problem for a CM architecture is thus the recovery

of q, solving the following equation by applying CS techniques (Candès & Romberg, 2017):

$$y = G^{CM} q \tag{4.18}$$

The integration of precolouring into the CM is accomplished in an analogous manner to that of the RD. For each signal x_j the corresponding PM matrices C_j are calculated from the corresponding a_k^j coefficients. Then applying (4.13) to each of the signals x_j, a coloured version of the corresponding Fourier transform can be derived:

$$f_{Cj} = Fx_{Cj} = FCx_j = FC_j x_j \rightarrow x_j = C^{-1} F^{-1} f_{C_j} \tag{4.19}$$

From (4.19), (4.17) can be expressed in vector form as:

$$y = \sum_{j=1}^{J} \Phi_j x_j = [\Phi_1, \Phi_2, .., \Phi_J] \begin{bmatrix} x_1 \\ x_2 \\ . \\ . \\ x_J \end{bmatrix} = [\Phi_1, \Phi_2, .., \Phi_J] \begin{bmatrix} C_1^{-1} F^{-1} f_{C_1} \\ C_2 F^{-1} f_{C_2} \\ . \\ . \\ C_J^{-1} F^{-1} f_{C_J} \end{bmatrix} =$$

$$= [\Phi_1, \Phi_2, .., \Phi_J] \begin{bmatrix} C_1^{-1} F^{-1} & & & & \\ & C_2^{-1} F^{-1} & & & \\ & & . & & \\ & & & . & \\ & & & & C_J^{-1} F^{-1} \end{bmatrix} \begin{bmatrix} f_{C_1} \\ f_{C_2} \\ . \\ . \\ f_{C_J} \end{bmatrix} =$$

$$= [\Phi_1 C_1^{-1} F^{-1}, \Phi_2 C_2^{-1} F^{-1}, .., \Phi_J C_J^{-1} F^{-1}] \begin{bmatrix} f_{C_1} \\ f_{C2} \\ . \\ . \\ f_{CJ} \end{bmatrix} = G_{C_{CM}} \begin{bmatrix} f_{C_1} \\ f_{C_2} \\ . \\ . \\ f_{C_J} \end{bmatrix} \tag{4.20}$$

where G_c^{CM} is now the result of concatenating matrices $\Phi_j C_j^{-1} F^{-1}$, the sparsity basis is the $JN \times JN$ block diagonal matrix with $N \times N$ bases FC_j along the diagonal. The CS recovery algorithms reconstruct the combined coloured representation q_C and the PSD $P_C(f)$ of the signals $x_1, x_2, .., x_J$ in the frequency domain from:

$$y = G_C^{CM} q_C \tag{4.21}$$

The block diagram of the CM-based architecture, which is termed *i*PM-CM, is shown in Figure 4.5.

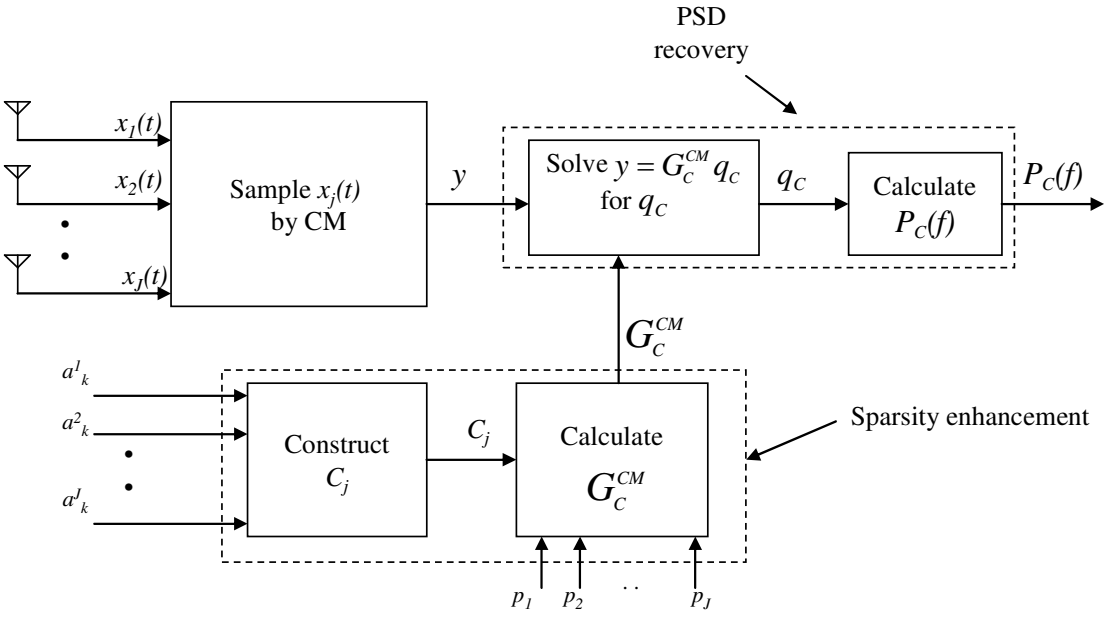

Figure 4.5: Block diagram of the *i*PM-CM.

The corresponding pseudo code for the *i*PM-CM is given in the Algorithm 4.3.

Algorithm 4.3: Pseudo code for the *i*PM-CM

Inputs: signals $x_j(n)$ of length N samples, $j=1,..,J$.

Variables: p- the AR filter order, F- the $N \times N$ DFT matrix, Φ_j - the $N \times N$ measurement matrices, $j=1,..,J$.

Outputs: Combined P_C of $x_j(n)$, $j=1,..,J$

1: ***Initialise*** F, p.

2: ***Calculate*** AR filter coefficients a_k^j from $x_j(n)$, p, $j=1,..,J$.

3: ***Construct*** Φ_j, $j=1,..,J$.

4: ***Calculate*** $y = \sum_{j=1}^{J} \Phi_j x_j$.

5: ***Construct*** C_j from (4.10) for $j=1,..,J$.

6: ***Calculate*** matrices $\Phi_j C_j^{-1} F^{-1}$, $j=1,..,J$.

7: ***Construct*** G_C^{CM} by ***concatenating*** matrices $\Phi_j C_j^{-1} F^{-1}$, $j=1,..,J$.

$y = G_c^{CM} q_C$

8: ***Apply*** l_1 minimisation algorithm to solve for q_C.

9: ***Calculate*** $P_C=|q_C|^2$.

10: **END**

In this Section, the AR-based CS model has been presented as both a single and multi-channel version, where precolouring has been seamlessly integrated into both the RD and CM architectures. A sparsity enhancement element is constructed by the AR filter coefficients, which modifies both the sparsity basis and recovery matrix. The block diagram of the AR-based CS model with its main functions is shown in Figure 4.6.

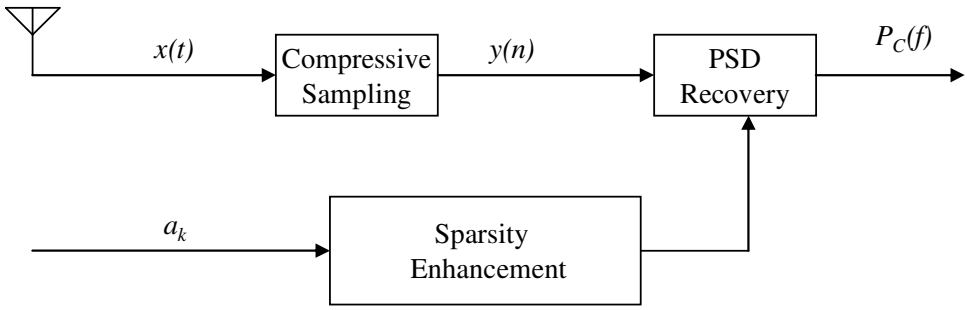

Figure 4.6: Block diagram of the generic AR-based CS model.

The next section presents the simulation setup for both versions of the AR-based CS model, with Section 4.4 then critically analysing their respective performances.

4.3 Simulation Setup

Initially, a series of simulations were conducted to determine the best model order for the precolouring AR filters to be employed in RD and CM, using the *MDL* criterion described in Section 4.2. Test signals are considered, with the relevant parameters shown in Table 3.2, though analogous experiments can also be performed with signals having different parameter values. It is noted that each of these signals are assumed to be the inputs to either a single-channel architecture or to one of the branches of the multi-channel counterpart. For each modulation type analysed, the corresponding *MDL* values are calculated using (4.5) to determine the most appropriate AR filter order.

The performance of both AR-based CS models will now be critically evaluated in comparison with the traditional RD and CM architectures. Firstly, the functions of the single-channel RD and *i*PM-RD architectures are simulated; namely signal sampling, the formation of matrices G and G_C respectively and the recovery of the respective Fourier spectra and PSDs. For the *i*PM-RD in particular, the PM matrix is formed prior to G_C. Digitally modulated test signals are generated, reflecting the typically used signal modulation types in CR together with other wireless standards (DeNardis, 2011; Task Group 4, 2017; Flores et al., 2013; Mody & Chouinard, 2010; 3GPP, 2010; Rakesh et al., 2010), including QPSK, BPSK, 16QAM and 64 QAM. The signal parameters are shown in Table 3.2. All signals are generated by the MATLAB simulation platform, with random sequences modulated by appropriate modulation alphabets (Ipatov, 2005; Proakis & Manolakis, 2006), before frequency up-conversion by the carrier frequencies. The signal carriers lie within a bandwidth from 0 to B, however their positions are unknown. Furthermore, AWGN is added to the signals to give different input SNR in accordance with the aforementioned wireless standards.

Experiments were undertaken at various sub-sampling (below Nyquist) rates using the CS performance metrics defined in Section 3.4, namely PSD spectral leakage against sampling rate and input SNR, while the algorithms 4.2, 4.3 for the *i*PM-RD and *i*PM-CM respectively are validated using the sparsity metric. For the spectral leakage performance, the input SNR was set to 8.1dB as per IEEE 802.22 standard, while for the SNR robustness the sampling rate was arbitrarily chosen to around 25.25% of Nyquist, though other sub-Nyquist rates are equally applicable.

The performance is also visually assessed by comparing the PSD graphs derived from the RD and *i*PM-RD architectures respectively, with input SNR set at 8.1 dB and sampling rates at 25.25% and 3.15625% of Nyquist. As mentioned in Section 3.3.3, the objective is not exact signal PSD recovery, but efficient identification of occupied spectral bands, which is a key CR requirement. This holds for both RD and CM architectures, with the focus being not to explicitly measure the level of sparsity, but to critically analyse how precolouring can be effectively applied to enhance sparsity and secure improved CS performance in the respective architectures.

The second series of simulations pertain to the multi-channel RD and *i*PM-RD architectures. It is assumed each channel is assigned to a specific PU who transmits over a specified band; therefore each signal has one carrier and is sparse over the bandwidth B. As in the single-channel architecture, PSD spectral leakage is measured against sampling rate and input SNR using the same range of sub-sampling rates.

In an analogous manner, the same main functions of the *i*PM-CM are simulated. Since the CM is a parallel architecture, the sampling is performed after summation of the input signals, while G_C^{CM} results from the concatenation of the separate PM matrices C_j corresponding to signals x_j respectively. The modulations schemes and signal parameters of the signals employed are the same as in the case of the *i*PM-RD, though since the sampling rate is always fixed at the Nyquist rate in the CM architecture, the respective performances at different sampling rates are not relevant. In this CS setup, each individual signal has only one carrier and a 4-channel CM architecture is considered, so the combined signal be frequency sparse.

4.4 Simulation Results Discussion

Before critically evaluating the results, the order p of the AR filter and the coefficients to generate both the PM and subsequent recovery matrices are chosen for $p=4$ for the series of experiments in this Chapter. In Figure 4.7, where the MDL values are plotted against p for four different modulations types, it is observed that for all schemes the minimum MDL is attained at $p=8$. It is also clear that there is an abrupt fall in MDL when $p=4$. Since the aim is not to find a best fit to the signal

model but the derivation of a PSD suitable for identification of active bands, intuitively a further comparison between $p=4$ and $p=8$ is merited, since an increase of the value of p has impact on system complexity. To this end, Table 4.1 shows the MDL values for both $p=4$ and $p=8$, together with the corresponding time delays (TDL) for each modulation scheme. The TDL appertains to the processing time required for the calculation of the relevant AR filter coefficients that is filter latency. The MDL results for $p=4$ and $p=8$ show that the MDL is lower by 6.5%, 6.95%, 2.77%, and 1.55% at QPSK, BPSK, 16QAM and 64 QAM respectively, giving an average improvement of approximately 4.45%. However, this comes with increased filter latency of 44%, 45%, 36% and 27% for QPSK, BPSK, 16QAM and 64QAM respectively, with the average being around 38%. Therefore the design of an AR filter with $p=4$, provides a pragmatic trade-off between best-fit order and latency compared with the $p=8$ option (Karampoulas et al., 2013b).

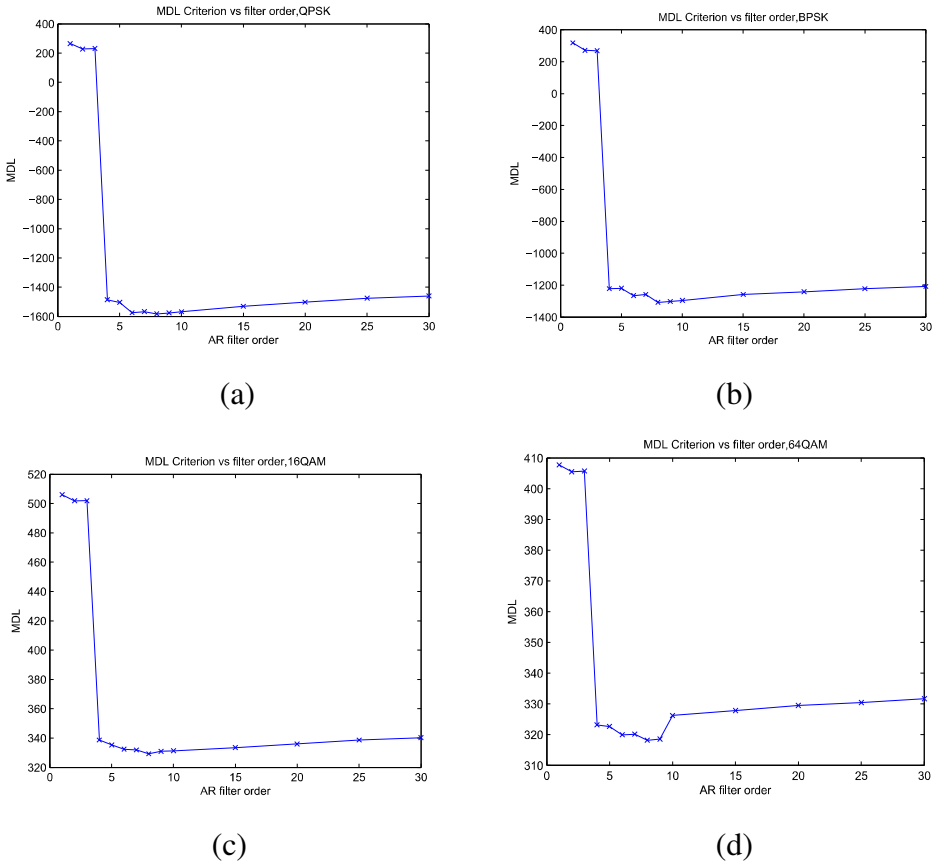

Figure 4.7: Variations in AR filter order using MDL for (a) QPSK, (b) BPSK, (c) 16QAM and (d) 64QAM.

Table 4.1: MDL values and corresponding AR filter latencies

p	MDL QPSK	TDL QPSK (msec)	MDL BPSK	TDL BPSK (msec)	MDL 16QAM	TDL 16QAM (msec)	MDL 64QAM	TDL 64QAM (msec)
4	-1468.1	127	-1222.3	136	338.63	130	323.2	189
8	-1583.1	183	-1307.3	197	329.25	176	318.19	240

Next follows the validation of the algorithm 4.2 which corresponds to *i*PM-RD. Figure 4.8 shows the effect of precolouring on sparsity for QPSK modulation, at a sampling rate 25.25% of Nyquist and across a range of input SNR. The active frequency threshold was set to 20dB relative to the maximum energy value, though an arbitrary threshold value is equally valid (Karampoulas et al., 2015). The curves show that precolouring reduces the number of the signal active frequency components, thereby enhancing sparsity. More specifically, CS increases the number of active frequency components and thereby reduces sparsity when no precolouring is applied, as the green and red curves reveal. This is due to the performance degradation incurred by CS, since the sampling rate is below Nyquist (Laska et al., 2007). When precolouring is applied however, the signal sparsity is enhanced significantly, thus validating the performance of algorithm 4.2. Thus based on the discussion in Chapter 2, the signal noise is reduced which in turn improves CS performance.

This section analyses the effect of precolouring upon the single-channel RD. To this end, the single-channel *i*PM-RD architecture is compared with the classical RD. The comparative PSD spectral leakage performance is then critically evaluated for different sub-Nyquist sampling rates and for QPSK, BPSK and 16/64QAM modulation types, with results displayed in Figure 4.9.

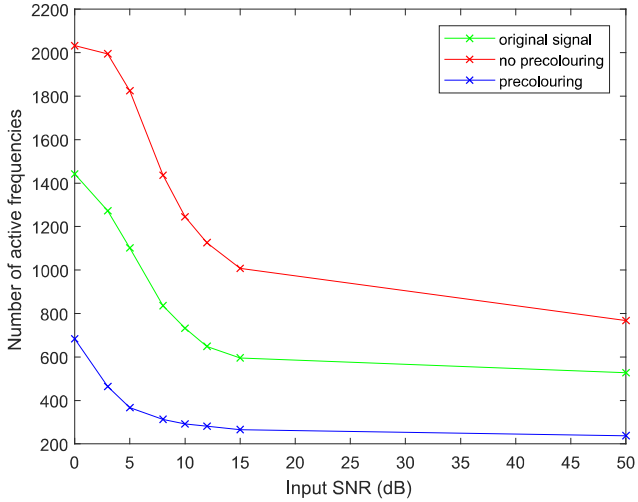

Figure 4.8. The effect of precolouring on sparsity of a QPSK signal using algorithm 4.2.

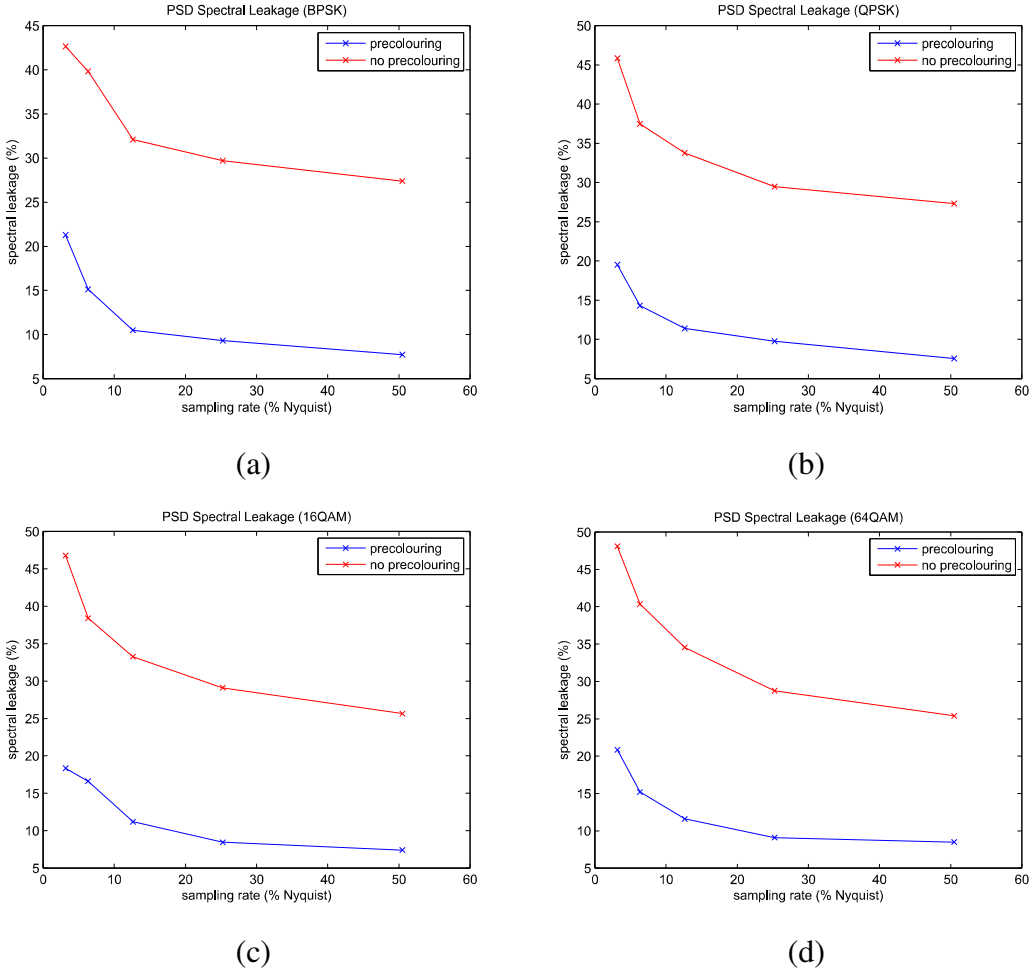

Figure 4.9: PSD spectral leakage vs sampling rate for classical RD (no precolouring) *i*PM-RD (precolouring) architectures, with 2 carrier signals for (a) BPSK, (b)QPSK, (c) 16QAM and (d) 64QAM.

The resulting PSD spectral leakage for *i*PM-RD is consistently lower across the range of sampling rates for all analysed modulation types, with it providing an overall average spectral leakage improvement approximately 40% compared with the classical RD, where the average spectral leakage is always above 25%, while it is always lower than 25% for *i*PM-RD. This results in increased sparsity in the PSD. In the precolouring case, even when the sampling frequency falls to just 20% of the Nyquist rate, the spectral leakage is only approximately 10%, while it is constantly over 30% when precolouring is not applied. This superior spectral leakage performance highlights the key benefit of using the PM in the CS architecture in amplifying dominant frequencies i.e., occupied bands, while concomitantly attenuating weaker components, i.e. those outside the occupied bands.

To appraise the robustness of the *i*PM-RD architecture, results are presented in Figure 4.10, where the PSD spectral leakage is measured at different input SNR levels. The spectral leakage behaviour to noise of *i*PM-RD is analogous to that witnessed in Figure 4.9, with an average improvement of more than 35%. In the case of no precolouring, the leakage never falls below 30%, while it is consistently below 25% when precolouring is employed. As noise increases, so does the energy outside the occupied bands and hence the spectral leakage. However, when precolouring is applied, only frequencies within the occupied bands are amplified, while those outside are attenuated so leading to lower leakage and enhanced spectral sparsity.

The reason for the similar behaviour of signals with different digital modulation types observed is attributed to the fact that in reality both BPSK and QPSK are special cases of QAM modulation (Proakis & Salehi, 2008).

To verify the theoretical framework of the *i*PM-RD architecture, a comparative analysis with the AR-RD is presented in Table 4.2 for the QPSK modulation, though the findings are equally applicable to other modulation types. For completeness the results for the original RD are also included. It is evident that the shifting of the precolouring process to the recovery stage leads to exactly the same CS performance so corroborating the theory in Section 2.4.2.

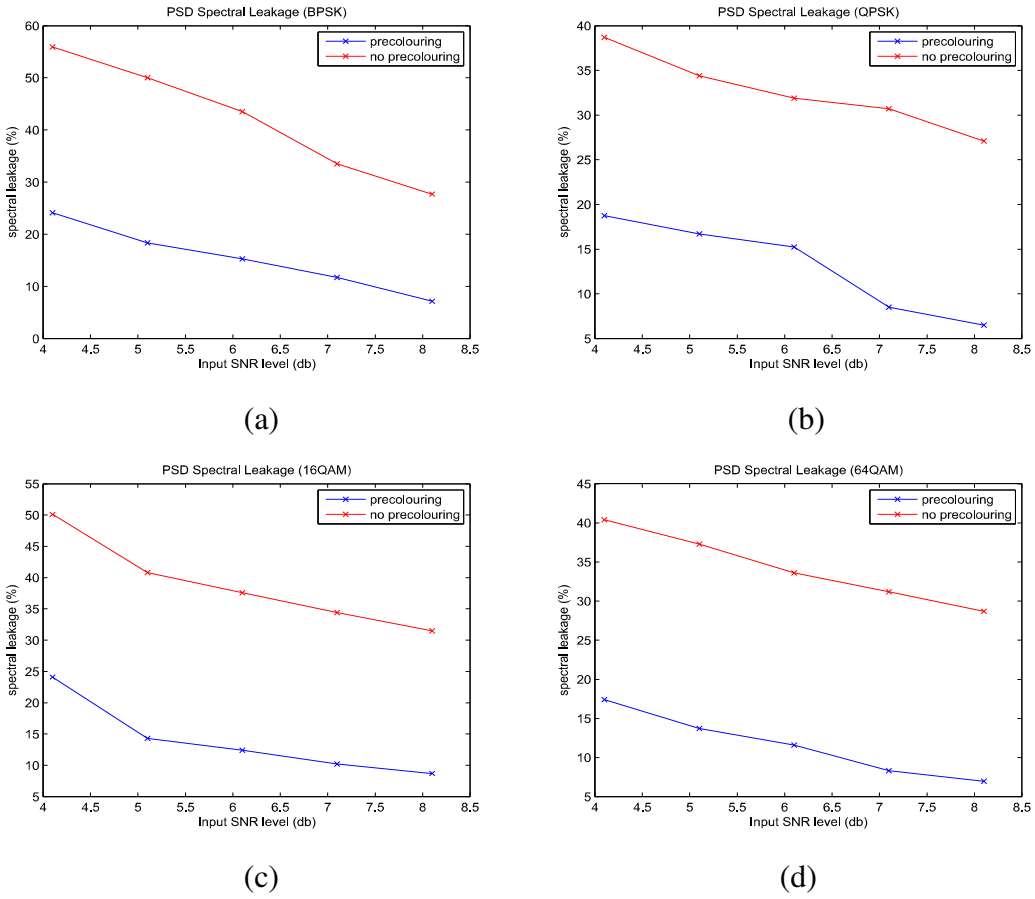

Figure 4.10: The effect of precolouring on PSD spectral leakage derived by RD-based architectures for (a) QPSK, (b) BPSK, (c) 16QAM and (d) 64QAM test signals for various input SNR values.

Table 4.2: PSD spectral leakage comparison for AR-RD, *i*PM-RD and RD architectures

Sampling Rate (% Nyquist)	PSD spectral leakage (%) AR-RD	PSD spectral leakage (%) *i*PM-RD	PSD spectral leakage (%) original RD
3.15625	19.5	19.5	45.83
6.3125	14.3	14.3	37.47
12.625	11.4	11.4	33.75
25.25	9.78	9.78	29.5
50.5	7.56	7.56	27.3

The improved performance of the *i*PM-RD compared with the classical RD is also evident from a visual inspection of the respective PSD graphs depicted in Figures 4.11

and 4.12. It is assumed that within bandwidth *B* there are two occupied spectral bands for which the locations of the respective carrier frequencies are unknown. Figure 4.11 shows the normalised PSD graphs for the different modulation schemes with the sampling rate is set to 50.5% Nyquist corresponding to 1024 signal samples, whereas Figure 4.12 shows the normalised PSD graphs derived at sampling rate of 3.1525%, that is with 64 signal samples. Both QPSK and 64QAM signals are considered, though BPSK and 16QAM could be equally applicable for the reason discussed above. Spectral leakage is evidently less pronounced for *i*PM-RD, even at the lowest sampling rate of 3.15625% of Nyquist frequency. While exact PSD recovery does not take place, from a CR viewpoint this is an encouraging outcome as it means occupied bands can still be identified in the precolouring case at high CS levels, in contrast to when no signal precolouring is used, where such decisions cannot be successfully made.

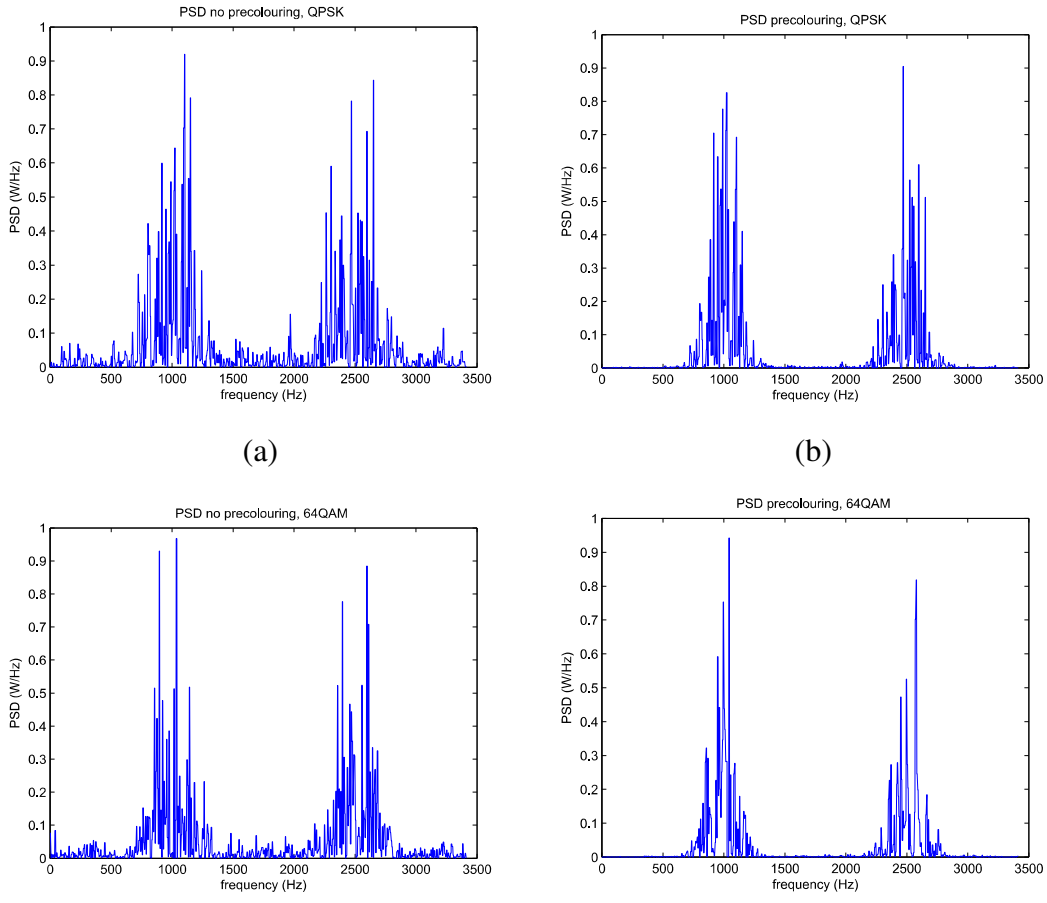

Figure 4.11: Recovered normalised PSD for QPSK (a), (b) and 64QAM (c), (d) modulations, at a sampling rate 50.5% Nyquist.

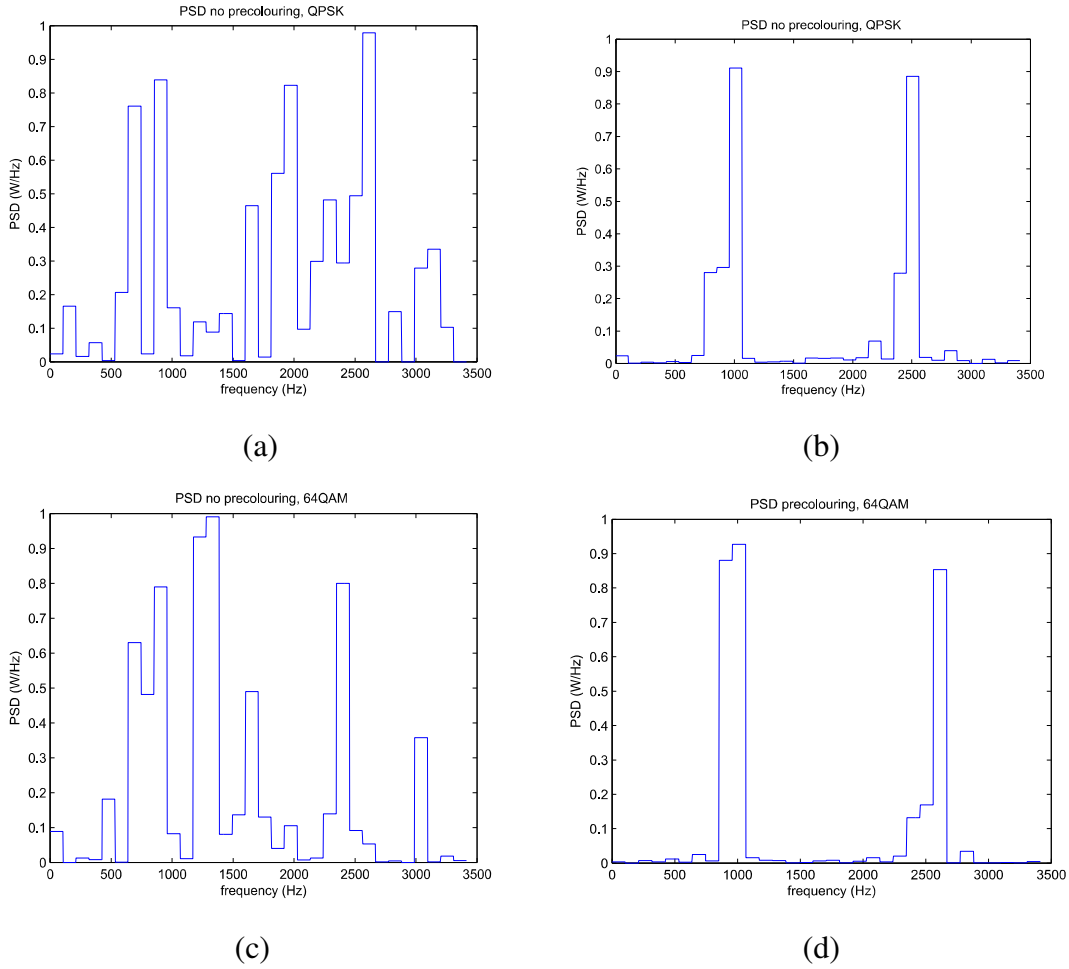

Figure 4.12: Recovered normalised PSD derived from RD-based architectures for QPSK (a), (b) and 64QAM (c), (d) modulations, at a sampling rate 3.15625% of Nyquist.

The next series of experiments considered the respective multi-channel RD-based architectures, and are similarly comparative metrics as their single-channel counterparts. Firstly, the PSD spectral leakage performance for different sub-Nyquist sampling rates and for the QPSK, BPSK and 16/64QAM modulation types is plotted in Figure 4.13. It is apparent PSD spectral leakage is consistently lower across the range of sampling rates and for all modulation types for the *i*PM-RD structure, being always higher than 20% in the classical RD (no precolouring), while it is lower than 20% in the case of precolouring (*i*PM-RD), even with sampling rates as low as 10% of Nyquist. Overall, *i*PM-RD provides an average improvement in PSD spectral leakage of at least 40% compared with the classical RD architecture.

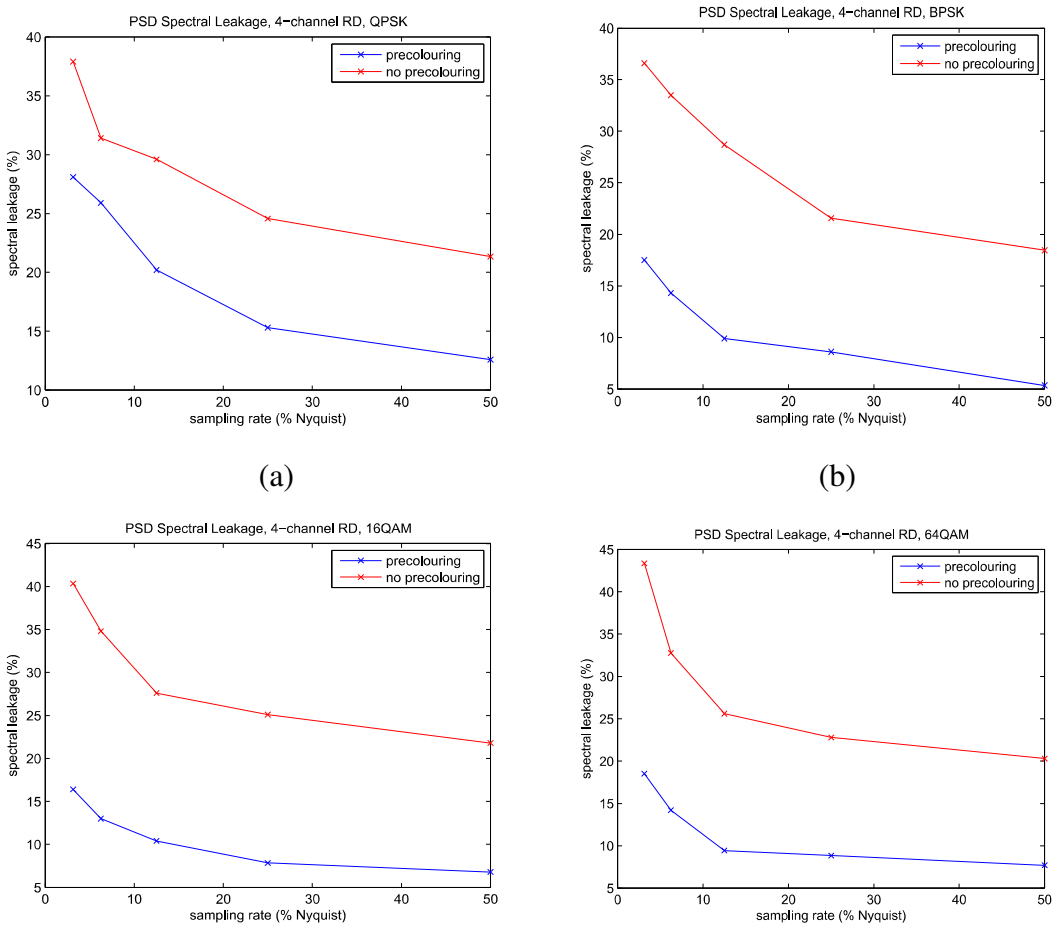

Figure 4.13: PSD spectral leakage vs sampling rate for multi-channel classical RD (no precolouring) and multi-channel *i*PM-RD (precolouring) architectures.

A similar trend is observed in Figure 4.14, when the PSD spectral leakage is analysed at different input SNR levels. It is always lower than 25% in the case of precolouring, while it never falls below 20% when no precolouring is applied, with the overall improvement for *i*PM-RD being on average more than 50% compared to the classical RD. These improvements are also extendible to multi-channel CS structures like the multi-channel *i*PM-RD and the CM.

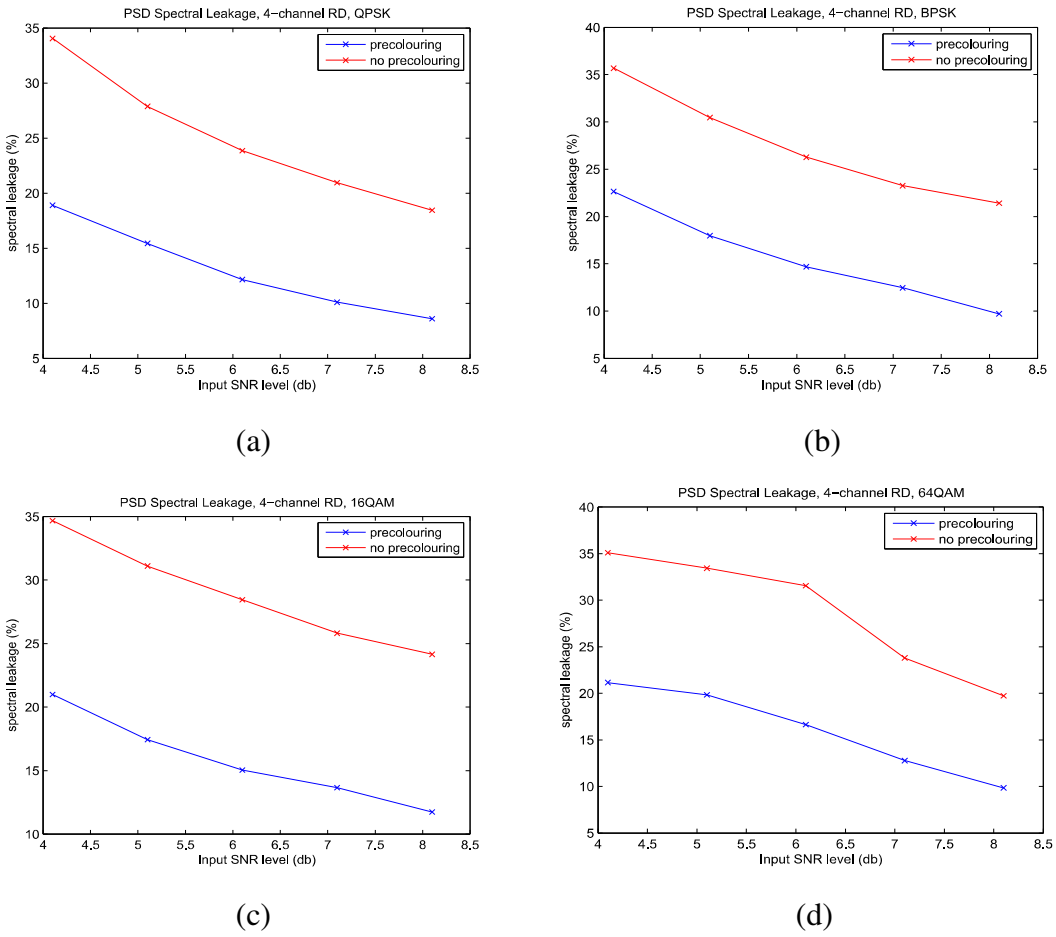

Figure 4.14: The effect of precolouring on PSD spectral leakage derived by multichannel RD-based architectures for (a) QPSK, (b) BPSK, (c) 16QAM and (d) 64QAM test signals for various input SNR values.

The multi-channel *i*PM-RD is better able to distinguish occupied bands/ frequencies than the classical RD. Figures 4.15a and 4.15b, show the combined PSD derived from the classical RD and the *i*PM-RD respectively. The carriers are situated 500Hz apart from each other and QPSK is used, though other modulation schemes can be used. With the sampling rate at 50.5% of Nyquist, the results reveal the resolution capability of the *i*PM-RD permits the carriers to be detected while the classical RD cannot distinguish them.

Even when the sampling rate falls to approximately 25% of Nyquist (Figure 4.15c) the *i*PM-RD is still able to distinguish the carriers and only when the sampling rate drops to approximately 12.5% of Nyquist (Figure 4.15d), is carrier detection not feasible. This is important since from a CR perspective, it is vital for a SU to accurately identify vacant and occupied carriers and bands. When a SU performs

spectrum sensing with the classical RD, the information that the entire spectrum from 250Hz to 2250Hz is occupied is inaccurate as confirmed in the respective PSD graphs for *i*PM-RD. So by applying precolouring the *i*PM-RD model exhibits consistently better spectrum sensing performance by virtue of its superior carrier identification capability.

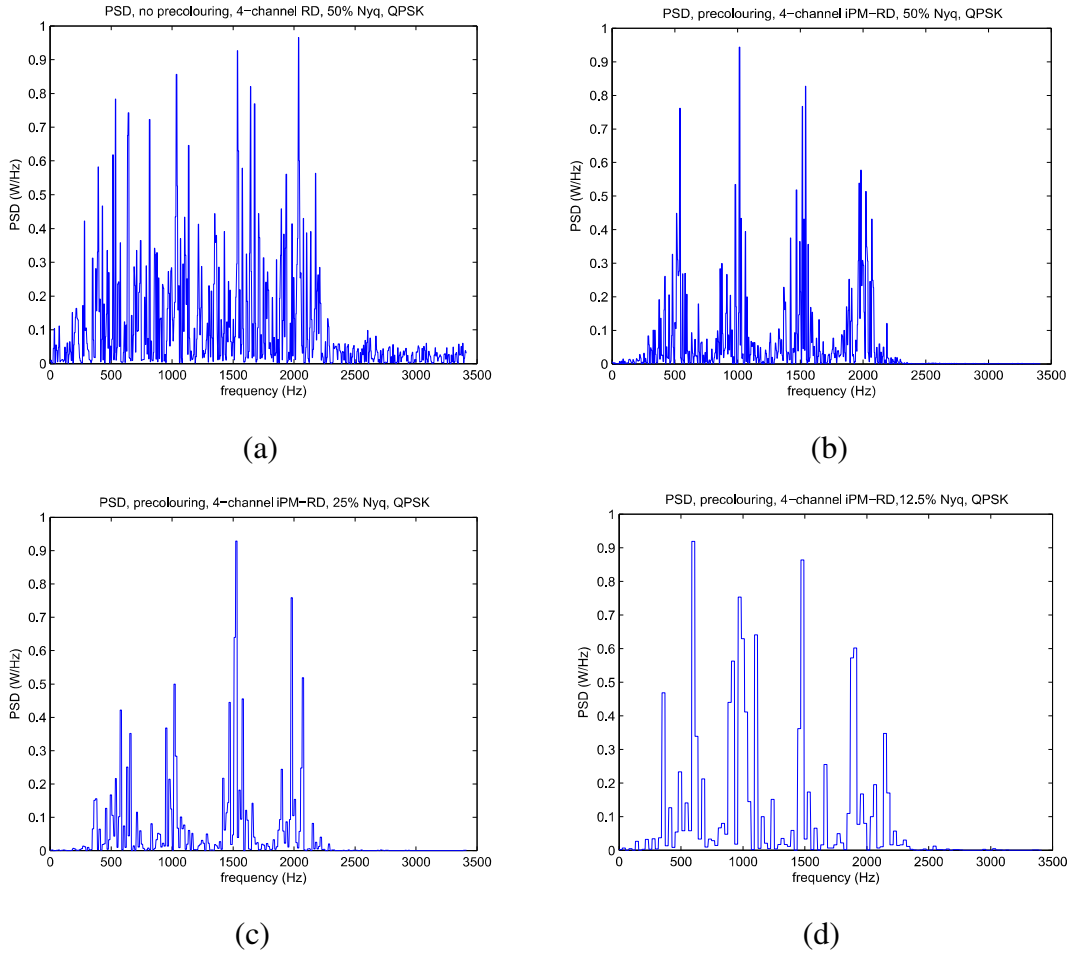

Figure 4.15: Recovered normalised PSD derived from (a) 4-channel RD, (b), (c), (d), 4-channel *i*PM-RD.

The next series of simulations appertain to the CM-based *i*PM-CM architecture. First the relevant algorithm 4.3 is validated in a similar manner to algorithm 4.2. A 2-channel CM is considered and QPSK signals are employed at channel inputs. The results are shown in Figure 4.16 and again reveal increased sparsity when precolouring is applied to the QPSK signals.

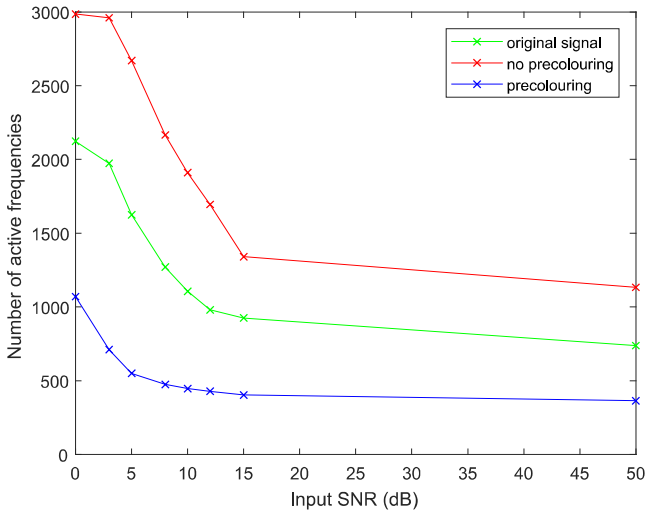

Figure 4.16. The effect of precolouring on sparsity of QPSK signals using algorithm 4.3.

Figure 4.17 shows the corresponding performance of the classical CM and *i*PM-CM against input SNR. A similar improvement trend is observed as in the RD case, namely that embedding precolouring into the CS architecture enhances overall noise robustness. PSD spectral leakage is at least 15% lower in the precolouring case across the range of input SNR levels, while the corresponding average spectral leakage reduction is ≈60%. It never acquires values below 20% when no precolouring is applied, while it is always lower than 20% with precolouring.

Figures 4.18a and 4.18b respectively present the normalised PSD derived from the classical CM and *i*PM-CM architectures. As with the RD-based architecture, the resolution capability of the *i*PM-CM permits the carriers to be distinguished, while the classical CM is unable to distinguish them. The only information the classical CM is able to provide is that the spectrum is completely occupied and no carrier identification is possible. From a CR perspective, the spectrum sensing performance of a SU is enhanced by the utilisation of the *i*PM-CM architecture with its superior carrier identification capabilities.

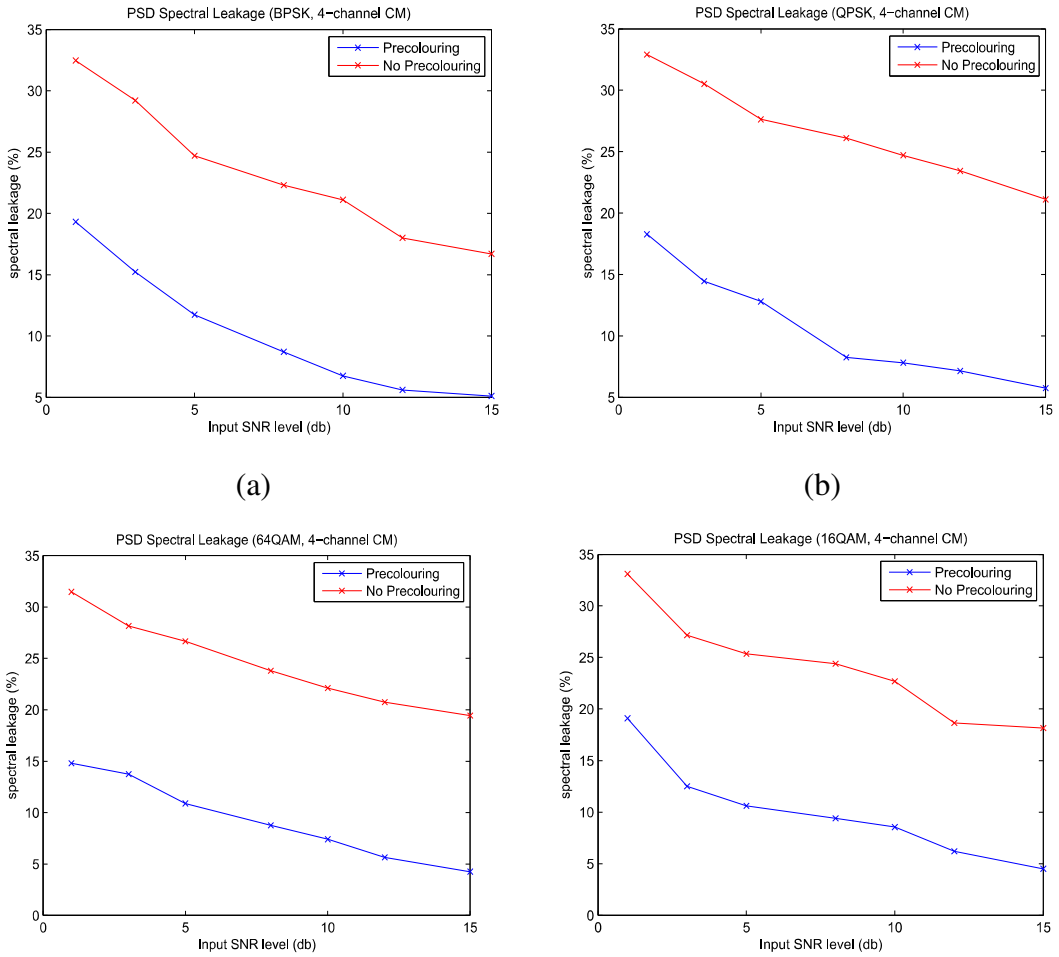

Figure 4.17: Effect of precolouring on PSD spectral leakage derived by the classical CM and *i*PM-CM architectures for (a) QPSK, (b) BPSK, (c) 16QAM and (d) 64QAM test signals.

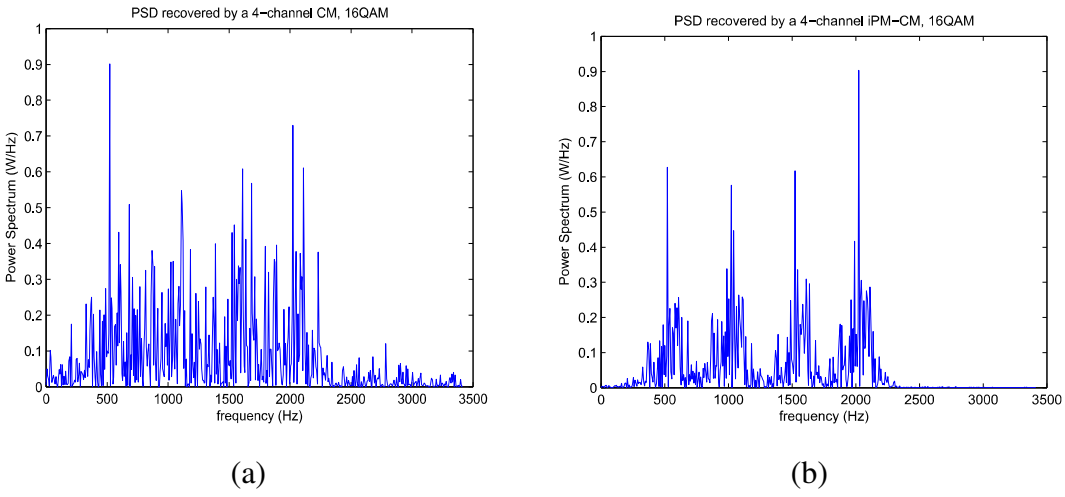

Figure 4.18: Recovered normalised PSD derived (a) from classical CM and (b) from the *i*PM-CM for 16QAM modulation scheme.

While the AR method enhances CS performance, it is also evident this improvement depends on *a priori* knowledge of the input signals, namely the set of filter coefficients. In CR applications, although such knowledge could be provided by the telecommunications providers, i.e., PU, however this reliance undermines the autonomy of CR receivers. Furthermore, the derivation of the PSD is based on the Fourier periodogram, which is an inconsistent spectral estimator, as discussed in Section 2.3.2.3. This provided the motivation for the application of non-parametric and sophisticated spectrum estimation methods to the CS architectures and the subsequent investigation and critical analysis of their performance. This is the subject of the Chapter 5 that follows.

4.5 Summary

This chapter has presented the novel AR-based single-channel and multi-channel compressive spectrum models. It employs AR filtering to precolour the signal, so to increase frequency sparsity and consequently enhance CS performance. The precolouring process is seamlessly integrated to the model and does not require major burden from the PU who can provide the respective AR filter coefficients. The model is applicable to both RD and CM compressive sensing architectures, therefore two novel separate architectures were presented, namely the *i*PM-RD along with its multi-channel counterpart and the *i*PM-CM. Both were found to provide enhanced performance against their classical counterparts in regards PSD spectral leakage against sub-Nyquist sampling rates. They have also exhibit enhanced robustness against input noise.

While this chapter has exploited underlying signal structures in applying parametric methods to enhance CS performance of existing architectures, the next chapter will investigate and critically analyse the performance of these CS architectures when non-parametric spectrum estimation methods are incorporated.

Chapter 5

A Multitaper-based Compressive Sensing Model for Spectrum Sensing

5.1 Introduction

The classical RD and CM architectures and their respective versions of the AR-CS model presented in the previous Chapter employed the DFT based periodogram spectrum estimator, which has a number of drawbacks. The finite length of the signals processed by the periodogram causes sidelobe leakage which leads to a biased spectral estimate (Manolakis et al., 2005; Madisetti, 2010). The periodogram also has inherent variance limitations because it does not decrease as the signal length increases (Manolakis et al., 2005; Madisetti, 2010), so it is not a consistent spectrum estimator. On the other hand, as discussed in Section 2.3, the transition of spectrum sensing for CR from a mere binary-type detection of spectrum holes to a more efficient and accurate spectral classification, requires the application of a more sophisticated spectrum estimation technique than the periodogram.

It has also been noted that the MT spectral estimation method affords a favourable trade-off between spectral bias, variance and spectral resolution (Haykin, 2005; Haykin et al., 2009; Manolakis et al., 2005; Thomson, 1982) and exhibits a maximal energy concentration within a given bandwidth, centred about a particular frequency. It is therefore able to produce more accurate and reliable spectral estimates and has been proposed for spectrum sensing in CR (Haykin et al., 2009). Moreover, as in the precolouring case and from a CS perspective, the spectral leakage reduction can be viewed as increase in signal sparsity and noise reduction, which is a key to enhanced CS performance. Finally, the MT method is non-parametric, thus signal independent, so no extra burden is imposed on signal providers (PU), which from a CR system perspective is advantageous (Karampoulas et al., 2015). These combined favourable

features of improved spectral estimation, increased sparsity and no burden to PU, provided the motivation to investigate ways to integrate the MT method in existing CS architectures in order to improve their performance.

This Chapter presents a novel *MT-based compressive sensing model*, which seamlessly integrates the MT spectral estimator into the signal recovery CS stage. The favourable properties of the MT method enhance signal sparsity, thereby improving CS performance, with as in the previous Chapter, the model being applicable to both RD and CM architectures. The new model along with a brief discussion of the MT method will now be presented.

5.2 The MT-based CS Model

A major problem in spectrum estimation is the trade-off between bias, variance and resolution when trying to improve spectral estimates of a time series. Due to the finite signal length to be processed, the theoretically infinite signal length is truncated, so the spectral estimate is already biased and spectral leakage present (Madisetti, 2010), while concomitantly the variance of the periodogram can take unacceptable values (Schwartz & Shaw, 1975; Manolakis et al., 2005). Both bias and variance can be mitigated by tapering (windowing) the signal (Proakis & Manolakis, 2006) instead of truncating i.e., essentially applying a rectangular window. Due to the nature of the windows employed however, when attempting to control bias and spectral leakage, this reduces the resolution (Marple, 1987). Similarly, any decrease in variance of the periodogram comes at the expense of bias and resolution (Madisetti, 2010; Manolakis et al., 2005). These drawbacks are inherent to the existing CS architectures, because they use the DFT based periodogram in the recovery process.

In the MT spectral estimation method (Thomson, 1982), rather than use a single taper, multiple tapers are applied to the same signal data to produce multiple modified Fourier transforms and periodograms. The tapers are the discrete prolate spheroidal (Slepian) sequences (Slepian, 1978; Percival & Walden, 1993) that have some favourable properties: they are orthogonal and their Fourier transforms have maximal energy concentration within a given bandwidth. The orthogonality of the tapers makes the corresponding periodogram-based spectral estimates independent, so the

averaging reduces the variance. This property, coupled with the maximal energy concentration within the aforementioned bandwidth, permits the MT method more favourable exchanges between spectral resolution, bias and variance (Hossain & Bhargava, 2007).

Besides the above mentioned favourable features, the reduced spectral leakage that is induced increases the number of the frequency components which are equal or close to zero. This results in increase of signal sparsity, which is beneficial from the CS perspective. Next the MT method and its integration to the RD and CM architectures will be presented.

5.2.1 The MT Method and the RD-based MT-RD Architecture

The sequences (tapers) employed by the MT method are solutions to the spectral concentration problem discussed in 2.3.2.3. This seeks to find a sequence with specific length of N samples in the time domain whose DFT has maximum energy concentration within a given bandwidth f-W to f+W centred about some frequency f, with W defined as the resolution of the MT estimator (Slepian, 1978; Percival & Walden, 1993; Haykin et al., 2009), which is not the same as the fundamental Fourier frequency Δf, as also discussed in 2.3.2.3. The problem leads to an eigenvalue equation with N eigenvectors as solutions, each of which is a discrete prolate spheroidal (Slepian) sequence (Percival & Walden, 1993; Slepian, 1978; Thomson, 1982). The sequences are orthogonal and characterised by distinct eigenvalues that reflect the degree of their respective spectral concentration within the bandwidth f-W to f+W. The larger the eigenvalue the greater is the energy concentration.

As discussed in 2.3.2.3, these Slepian sequences taper a time series $x(n)$ and consequently a set of L Fourier transforms will be formed as follows:

$$f_k^l = \sum_{n=0}^{N} V_n^l x(n) \omega_N^{kn} \qquad (5.1)$$

where $V^l = [v_0^l, v_1^l, ..., v_{N-1}^l]^T$ is the eigenvector representing the l^{th} Slepian sequence, $\omega_N = e^{-j2\pi/N}$ and f_k^l is the k^{th} frequency of vector f^l, with $k=0,1,..,N-1$.

From (5.1), f^l can be written in matrix form as:

$$f^l = \begin{bmatrix} \omega_N^{0\cdot 0} & \omega_N^{0\cdot 1} & . & . & \omega_N^{0\cdot (N-1)} \\ . & . & . & . & . \\ \omega_N^{k\cdot 0} & \omega_N^{k\cdot 1} & . & . & \omega_N^{k\cdot (N-1)} \\ . & . & . & . & . \\ \omega_N^{(N-1)\cdot 0} & \omega_N^{(N-10\cdot 0} & . & . & \omega_N^{(N-1)\cdot (N-1)} \end{bmatrix} \begin{bmatrix} v_0^l & 0 & . & . & 0 \\ 0 & v_1^l & 0 & . & 0 \\ 0 & 0 & v_2^l & . & 0 \\ . & . & . & . & 0 \\ 0 & 0 & 0 & . & v_{N-1}^l \end{bmatrix} \begin{bmatrix} x_0 \\ . \\ x_n \\ . \\ x_{N-1} \end{bmatrix} =$$

$$= FU^l x \qquad (5.2)$$

where F is the $N \times N$ DFT matrix, x the vector form of the time series $x(n)$ and $U^l = diag(V^l)$ the $N \times N$ diagonal matrix whose main diagonal is populated by the elements of the V^l eigenvector.

Since there are L Slepian sequences, a weighted average MT-based Fourier transform f_{MT} can be formed from (5.1), as follows:

$$f_{MT} = \frac{\sum_{l=0}^{L-1} \lambda_l f^l}{\sum_{l=0}^{L-1} \lambda_l} \qquad (5.3)$$

where the frequency vector f^l is weighted by its associated eigenvalue λ_l.

This weighted average Fourier transform in (5.3) reveals the favourable leakage and variance properties of the MT method in the same way (2.3) does in 2.3.2.3.

Based on (5.2), (5.3) can be written in matrix form as:

$$f_{MT} = \frac{\sum_{l=0}^{L-1} \lambda_l f^l}{\sum_{l=0}^{L-1} \lambda_l} = \frac{\sum_{l=0}^{L-1} \lambda_l F U^l x}{\sum_{l=0}^{L-1} \lambda_l} = \frac{F}{\sum_{l=0}^{L-1} \lambda_l} (\lambda_0 U^0 + \lambda_1 U^1 + .. + \lambda_{L-1} U^{L-1}) x =$$

$$= \frac{F}{\sum_{l=0}^{L-1} \lambda_l} [\lambda_0 diag(V^0) + \lambda_1 diag(V^1) + .. + \lambda_{L-1} diag(V^{L-1})] x =$$

$$= \frac{F}{\sum_{l=1}^{L-1} \lambda_l} \begin{bmatrix} \sum_{l=0}^{L-1} \lambda_l v_0^l & 0 & . & . & 0 \\ 0 & \sum_{l=0}^{L-1} \lambda_l v_1^l & 0 & . & 0 \\ . & 0 & . & . & 0 \\ . & . & . & . & 0 \\ 0 & 0 & . & . & \sum_{l=0}^{L-1} \lambda_l v_{N-1}^l \end{bmatrix} x = FSx \qquad (5.4)$$

with S being a $N \times N$ diagonal MT matrix, where the elements s_{kk} of the main diagonal are given by:

$$s_{kk} = \frac{\sum_{l=0}^{L-1} \lambda_l v_k^l}{\sum_{l=0}^{L-1} \lambda_l} \qquad k=0,1,..N-1 \qquad (5.5)$$

The values of s_{kk} depend upon the Slepian sequences and their associated eigenvalues, and so are signal independent, which is a natural consequence of the fact that the MT method is non-parametric.

The next design step is to integrate the MT method into the classical RD, thereby introducing a new MT-RD architecture. The recovery stage output of this architecture will be the combined averaged Fourier transform f_{MT} (see 5.4). The integration can be achieved in a manner analogous to that witnessed for precolouring discussed in Chapter 4. The key difference is that matrix S will now be used for the integration of the MT method instead of the precolouring matrix C.

(5.4) can also be expressed as:

$$f_{MT} = (FS)x = F_{MT}x \rightarrow x = F_{MT}^{-1} f_{MT} = S^{-1}F^{-1} f_{MT} \qquad (5.6)$$

where $F_{MT} = FS$ is a modified $N \times N$ DFT matrix windowed by S (Karampoulas et al., 2015). Specifically, the elements of the k^{th} column of F are weighted by the s_{kk} elements of S, and since S is diagonal it is always invertible, so (5.6) will always be

valid. Recalling the equation (2.8) for the classical RD function and considering (5.6) it follows that:

$$y = \Phi x = \Phi S^{-1} F^{-1} f_{MT} = G_{MT} f_{MT} \qquad (5.7)$$

So f_{MT} can be recovered if the recovery matrix $G_{MT}=\Phi S^{-1}F^{-1}$ is used instead of $G=\Phi F^{-1}$ which is the case in the classical RD. This change in the recovery matrix results from the change of the sparsity basis, which is now F_{MT} instead of F. The modified basis links between x and f_{MT} in the same manner as the Fourier basis F links x and α in the case of the classical RD discussed in Section 2.4.3.

While the integration of S described above takes place in the recovery stage, it is also possible to implement the integration in the sampling stage by rewriting (5.6) as (Karampoulas et al., 2015):

$$f_{MT} = F(Sx) = Fx_{MT} \qquad (5.8)$$

where $x_{MT} = Sx$ is signal x windowed by S, namely the k^{th} element of x is weighted by the s_{kk} element of S. Using the classical RD equation (2.8), (5.8) can be expressed as:

$$y_{MT} = \Phi x_{MT} = \Phi F^{-1} f_{MT} = G f_{MT} \qquad (5.9a)$$

This reveals that f_{MT} can be recovered if the output of the sampling process is the measurement vector y_{MT} or alternatively, the input to the RD is x_{MT}. This is equivalent to having x as the RD input and using $\Phi_{MT} = \Phi S$ as the measurement matrix, as confirms the following equation:

$$y_{MT} = \Phi x_{MT} = \Phi S x = (\Phi S) x = \Phi_{MT} x \qquad (5.9b)$$

Therefore, f_{MT} could be recovered if the measurement matrix is Φ_{MT} instead of Φ, while the recovery matrix remains $G=\Phi F^{-1}$. Since S is a diagonal matrix, the banded structure of Φ is retained to Φ_{MT}, with the elements of the k^{th} column of the latter being weighted by the s_{kk} element of S. Thus Φ_{MT} can express the functions of the RD. Furthermore, the diagonal structure of S retains the randomness and consequently does not affect the low coherence of Φ, which is requirement for effective CS performance (Baraniuk et al., 2017).

It has been shown there are two approaches to implement the MT-RD architecture both of which exploit the enhanced MT properties via S, which scales either Φ or F. In regards to Φ, the diagonal structure of S does not affect its low coherence which is requirement for effective CS performance (Baraniuk et al., 2017). By modifying F, S creates a basis in which signals exhibit greater sparsity so improving the potential CS performance.

However, the approach pertaining to the modification of the measurement matrix Φ has a drawback. It requires both $\Phi_{MT}=\Phi S$ and Φ matrices, the first for the sampling function and the second for the formation of a recovery matrix $G=\Phi F^{-1}$. This is an additional and unnecessary overhead compared to the modification of the Fourier basis, where only matrices A for sampling and $F_{MT}=FS$ for the recovery matrix $G_{MT}=\Phi S^{-1}F^{-1}$ are required. Furthermore, the values of the S matrix elements, as parameters of the MT-RD architecture, once calculated, can be embedded into G_{MT}, the elements of which can be stored for future use (Ragheb et al., 2008), so the overall MT-RD architecture complexity is not augmented. The complete MT-RD architecture is depicted in Figure 5.1, and will be used from now in the thesis.

The corresponding pseudo code for the new MT-RD algorithm is given in the Algorithm 5.1. It is important to stress that due to the non-parametric nature of the MT method, it is not imperative to employ a multi-channel version as was the case in the AR-RD architecture presented in Chapter 4. It is assumed the spectral environment is sensed by either a single or multiple antenna and all signals are summed to form the input $x(t)$ to the CS architecture.

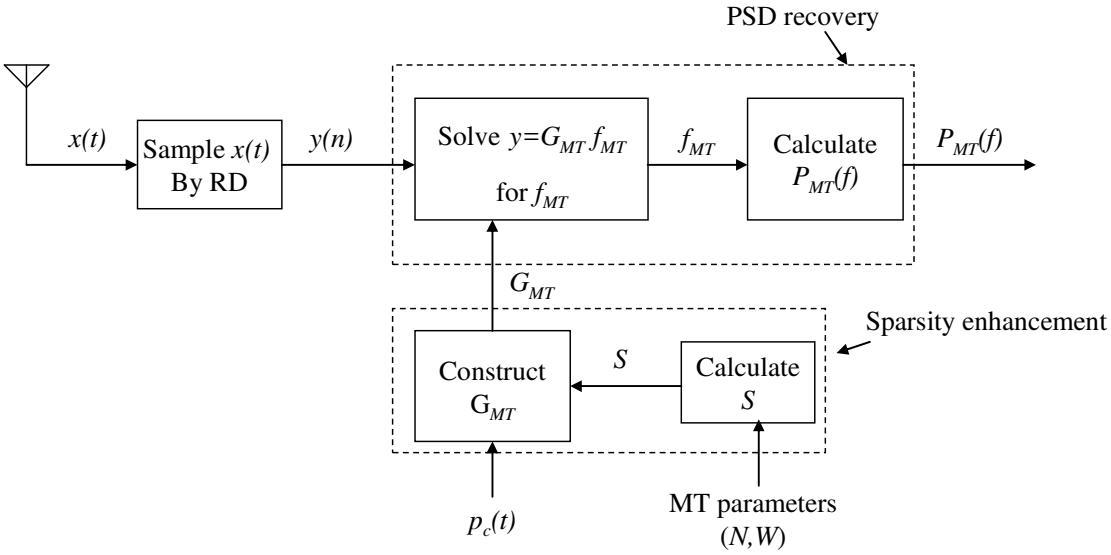

Figure 5.1: Block diagram of the MT-RD architecture.

Algorithm 5.1: Pseudo code for the MT-RD

Inputs: signal $x(n)$ of length N samples

Variables: M - number of measurements or equivalently length of $y(n)$ output of sub-Nyquist sampling, F- the NxN DFT matrix, Φ- the $M \times N$ measurement matrix, W- the resolution of the MT estimator.

Outputs: P_{MT} of $x(n)$

1: ***Initialise*** M, F, W.

2: ***Calculate*** eigenvectors V^l and eigenvalues λ_l of the MT for $l=0,1..,L-1$.

3: ***Calculate*** elements s_{kk} of S using (5.5), $k=0,1,..N-1$.

4: ***Construct*** Φ.

5: ***Calculate*** $y=\Phi x$.

6: ***Calculate*** $G_{MT}=\Phi S^{-1}F^{-1}$.

7: ***Use*** l_1 minimisation algorithm to solve $y=G_{MT}f_{MT}$ for f_{MT}.

8: ***Calculate*** $P_{MT} = \left| f_{MT} \right|^2$

9: **END**

5.2.2 The CM-based MT-CM Architecture

In the previous Section, the integration of the MT method was shown to be applicable to the RD architecture, with matrix S included in the recovery stage of the classical RD. The integration of the MT method to the *Compressive Multiplexer* (CM) architecture will now be presented.

The CM architecture described in 2.4.3, is a parallel CS architecture with J independent, jointly sparse input signals, each of bandwidth B Hz (Slavinsky et al., 2011). As in the RD, each channel $x_j(t)$ is modulated by a pseudorandom chipping sequence $p_j(t)$ with ± 1 values and chipping frequency at least the Nyquist rate $2B$ of the individual signal. However, in contrast CM has no integration before sampling. Subsequently, the channel outputs are firstly summed and then sampled by an ADC operating at a fixed rate is equal to $2B$, to give the output $y(n)$. The CS results because the sampling rate is $2B$, while the combined Nyquist sampling rate is $2JB$. Recalling (2.12), output $y(n)$ is given by the equation:

$$y = \sum_{j=1}^{J} \Phi_j x_j \tag{5.10}$$

with Φ_j being a $N \times N$ diagonal matrix, with the main diagonal being populated by iid entries from a Rademacher distribution (Slavinsky et al., 2011).

Again, recalling equation (2.14), (5.10) can be written as:

$$y = G^{CM} q \tag{5.11}$$

where G^{CM} the result of concatenating matrices $\Phi_j F^{-1}$ and vector q is the combined representation of these signals $x_1, x_2, .., x_J$ in the Fourier domain. CS recovery algorithms can be applied to solve (5.11) for q.

The integration of the MT method into the CM is accomplished in an analogous manner to that of the integration of precolouring to the subject architecture. The crucial difference is that now S is applied to all channels, instead of multiple PM

matrices. Applying (5.8) to the j^{th} channel, the corresponding MT-based Fourier transform is:

$$f_{MT_j} = FSx_j \rightarrow x_j = S^{-1}F^{-1}f_{MT_j} \qquad (5.12)$$

Using (5.12), (5.10) can be written as:

$$y = \sum_{j=1}^{J} \Phi_j x_j = [\Phi_1, \Phi_2, .., \Phi_J] \begin{bmatrix} x_1 \\ x_2 \\ . \\ . \\ x_J \end{bmatrix} = [\Phi_1, \Phi_2, .., \Phi_J] \begin{bmatrix} S^{-1}F^{-1}f_{MT_1} \\ S^{-1}F^{-1}f_{MT_2} \\ . \\ . \\ S^{-1}F^{-1}f_{MT_J} \end{bmatrix} =$$

$$= [\Phi_1, \Phi_2, .., \Phi_J] \begin{bmatrix} S^{-1}F^{-1} & & & & \\ & S^{-1}F^{-1} & & & \\ & & . & & \\ & & & . & \\ & & & & S^{-1}F^{-1} \end{bmatrix} \begin{bmatrix} f_{MT_1} \\ f_{MT_2} \\ . \\ . \\ f_{MT_J} \end{bmatrix} =$$

$$[\Phi_1 S^{-1}F^{-1}, \Phi_2 S^{-1}F^{-1}, .., \Phi_J S^{-1}F^{-1}] \begin{bmatrix} f_{MT_1} \\ f_{MT_2} \\ . \\ . \\ f_{MT_J} \end{bmatrix} = G_{MT}^{CM} \begin{bmatrix} f_{MT_1} \\ f_{MT_2} \\ . \\ . \\ f_{MT_J} \end{bmatrix}$$

$$G_{MT}^{CM} \begin{bmatrix} f_{MT_1} \\ f_{MT_2} \\ . \\ . \\ f_{MT_J} \end{bmatrix} \qquad (5.13)$$

where G_{MT}^{CM} is now the result of concatenating matrices $\Phi_j S^{-1} F^{-1}$ and the sparsity basis is a $JN \times JN$ block diagonal matrix with $N \times N$ bases FS along the diagonal. The CS recovery algorithm reconstructs the combined MT representation q_{MT} and the PSD $P_{MT}(f)$ of the signals $x_1, x_2, .., x_J$ in the frequency domain from:

$$y = G_{MT}^{CM} q_{MT} \tag{5.14}$$

The block diagram of the CM-based MT-CM architecture is shown in Figure 5.2, where $p_1, p_2, .., p_J$ modulate the signals $x_1, x_2, .., x_J$ respectively (see Figure 2.11).

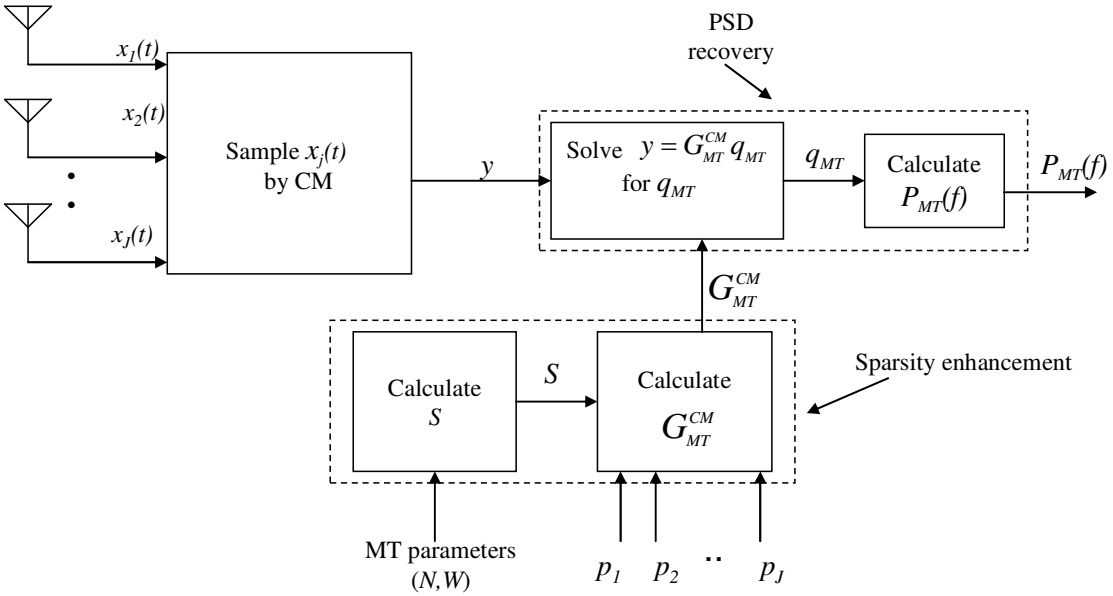

Figure 5.2: Block diagram of the MT-CM architecture.

The corresponding pseudo code for the MT-CM algorithm is given in the Algorithm 5.2.

Algorithm 5.2: Pseudo code for the MT-CM architecture

Inputs: $x_j(n)$ of length N samples, $j=1,..,J$.

Variables: F- the $N \times N$ DFT matrix, Φ_j- the $N \times N$ measurement matrices, $j=1,..,J$, W- the resolution of the MT estimator.

Outputs: Combined P_{MT} of $x_j(n)$, $j=1,..,J$

1: ***Initialise*** F, W.

2: ***Calculate*** elements s_{kk} of S using (5.5) for $k=0,1,..N-1$.

3: ***Construct*** Φ_j, $j=1,..,J$.

4: ***Calculate*** $y = \sum_{j=1}^{J} \Phi_j x_j$.

5: ***Calculate*** matrices $\Phi_j S^{-1} F^{-1}$, $j=1,..,J$.

6: ***Construct*** G_{MT}^{CM} by ***concatenating*** matrices $\Phi_j S^{-1} F^{-1}$, , $j=1,..,J$.

7: ***Use*** l_1 minimisation algorithm to solve $y = G_{MT}^{CM} q_{MT}$ for q_{MT}.

8: ***Calculate*** $P_{MT} = \left| q_{MT} \right|^2$.

9: **END**

This section has presented a new MT-based CS model, where a specific matrix is constructed from various MT parameters and then seamlessly integrated into both RD and CM architectures. This matrix enhances sparsity through the modification of the sparsity basis and the recovery matrix. The block diagram of the MT-based CS model with its main constituent blocks is shown in Figure 5.3.

The next Section presents the simulation setup for the two versions of the MT-based CS model, while Section 5.4 critically analyses their respective CS performances.

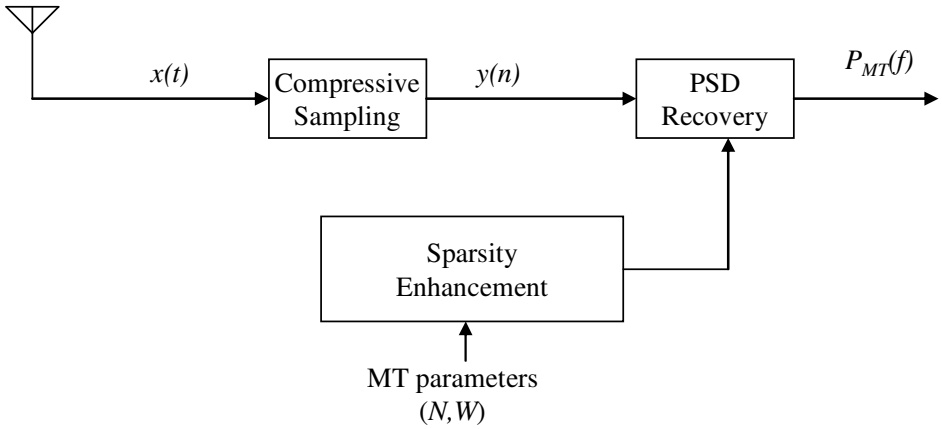

Figure 5.3: Block diagram of the generic MT-based CS model.

5.3 Simulation Setup

The performance of both versions of the MT-based CS model is critically evaluated against the traditional RD and CM architectures respectively. Since the MT method is non-parametric, only the input signals will be available.

As in Chapter 4, the simulation setup will first simulate the classical RD and the MT-RD, with the crucial difference now matrix S containing the MT parameters is formed instead of the PM. Three test signals will be considered:

a. A signal composed of a series of sinusoids (tones) which is amplitude modulated so it exhibits the structure of a narrowband communication signal.

b. A slowly varying linear chirp signal, as these are widely encountered in telecommunications, with a chirp spread spectrum (CSS) technique being employed in the physical layer of the IEEE 802.15.4 standard (Task Group 4, 2017).

c. As in Chapter 4, a QPSK test signal to investigate the performance upon wideband digitally modulated signals.

Table 3.2 details the parameters for the signals employed in this simulation. For the AM signals, first the tones and their spacing are created before their summation and subsequent frequency up-conversion by the carrier frequency. For the chirp signals the start and end frequencies are selected, which along with the time length determines the rate of frequency change at 135Hz. The value of the number of the Slepian sequencies L was set to $L=10$ according to (Haykin et al., 2009). The rationale for this is that the resolution W of the MT method is typically taken to be a small multiple of the frequency resolution (fundamental frequency) Δf (Percival & Walden, 1993). If W is chosen to be a multiple of 5, the value of L becomes equal to 10.

The performance is analyzed at various sub-sampled (below Nyquist) rates and corresponding samples shown in Table 3.2. As mentioned in Chapter 3 the performance metrics are the PSD spectral leakage against sampling rate and input SNR. For the spectral leakage performance, the input SNR was set to 8.1dB as per IEEE802.22 standard, while for the SNR robustness the sampling rate was arbitrarily chosen to 25.25% of Nyquist, though other sub-Nyquist rates are equally applicable.

The performance is also assessed visually by the comparison of the signal PSD graphs which are derived by the RD and MT-RD architectures respectively, with input SNR set at 8.1 dB and sampling rate at 25.25% of Nyquist. In order to corroborate the robustness of the MT-RD architecture, for the AM and chirp signals the input SNR was set to just 3dB and even -3dB rather than 8.1dB.

It is noted that the aim is not the exact recovery of the signal PSD, but the efficient identification of the occupied spectral bands, which is a key objective in CR. It is also noted that the aim is not to measure sparsity levels, but to investigate and critically analyse the role the MT method plays in sparsity enhancement and the subsequent performance improvement of the CS architectures.

In regards the simulation of the MT-CM architecture, the signals are the same as the case of the MT-RD. The sampling rate is always fixed at the Nyquist rate and 4-channel CM and MT-CM architectures are considered, so the combined signal to be frequency sparse.

5.4 Simulation Results Discussion

Firstly, the MT-RD architecture algorithm 5.1 is validated in the same way as algorithm 4.2in Chapter 4. An AM signal is employed with the sampling rate again set at 25.25% of Nyquist and the active frequency 20dB relative to the maximum energy value. Figure 5.4 shows the effect of the MT method on sparsity for AM modulation across a range of input SNR. While the application of CS without the MT reduces sparsity as the green and red curves reveal, the application of algorithm 5.1 to the RD architecture provides sparsity enhancement.

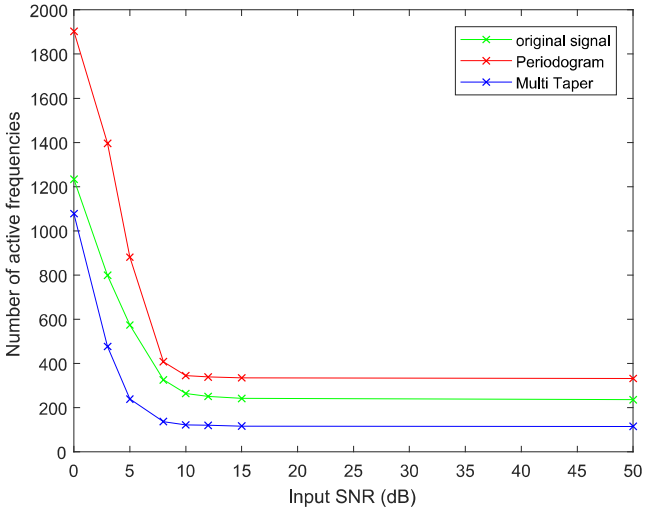

Figure 5.4. The effect of the MT method on sparsity of an AM signal using algorithm 5.1.

Next the results pertaining to the effect of embedding the MT method in the new MT-RD architecture are analysed and compared with the original RD. The PSD spectral leakage performance for the AM and chirp signals are plotted in Figure 5.5 for different sub-Nyquist sampling rates. It is evident the PSD spectral leakage is consistently lower across the range of sampling rates for both signal types, with an overall average spectral leakage improvement of ≈20% and ≈18% for the AM and chirp signals respectively. This reflects the key maximal energy concentration property of the Slepian sequences that underpin the MT-RD architecture. Applying the MT method to narrowband signals like AM and chirp signal can be considered as a means of enhancing sparsity, because the reduction in spectral leakage results in fewer significant frequency components, so the respective frequency vectors of the signals are sparser. This leads to improved CS performance, which along with the favourable properties of the MT method gives a more accurate spectral estimate.

Figure 5.5 confirms that the MT method consistently provides lower spectral leakage of more than 40% compared to the periodogram for both AM and chirp signals and only at sampling rates below 10% of Nyquist rate both the periodogram and MT tend to converge to large amounts of spectral leakage, since the rates are too low to facilitate accurate PSD recovery.

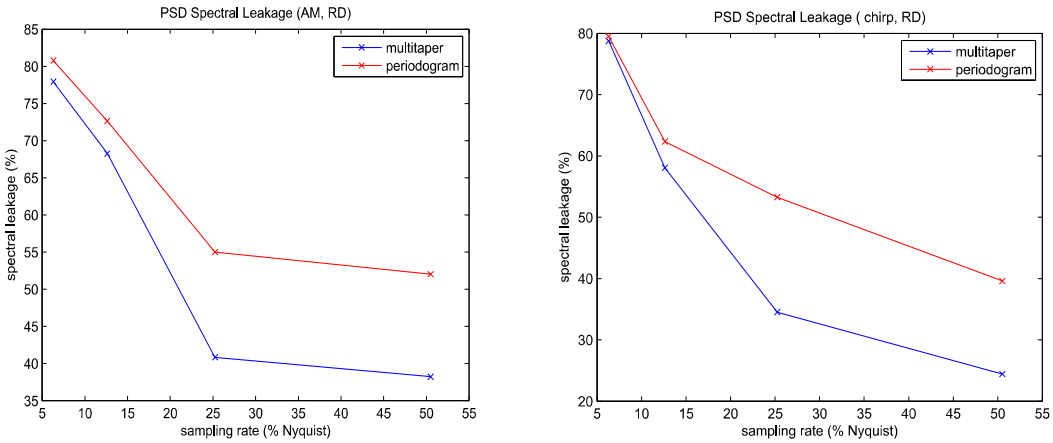

(a) (b)

Figure 5.5: PSD spectral leakage vs sampling rate for classical RD (periodogram based) and MT-RD architectures with (a) AM and (b) chirp signals.

The superior noise robustness of the MT-RD architecture is revealed in Figure 5.6, where the spectral leakage is plotted for different input SNR levels. Again there is an overall average spectral leakage improvement of ≈21% and 34% for AM and chirp respectively for the new MT-RD architecture, with the leakage being consistently below 50% when the MT method is employed, while it never falls below 40% in the case of the periodogram case for both AM and chirp signals.

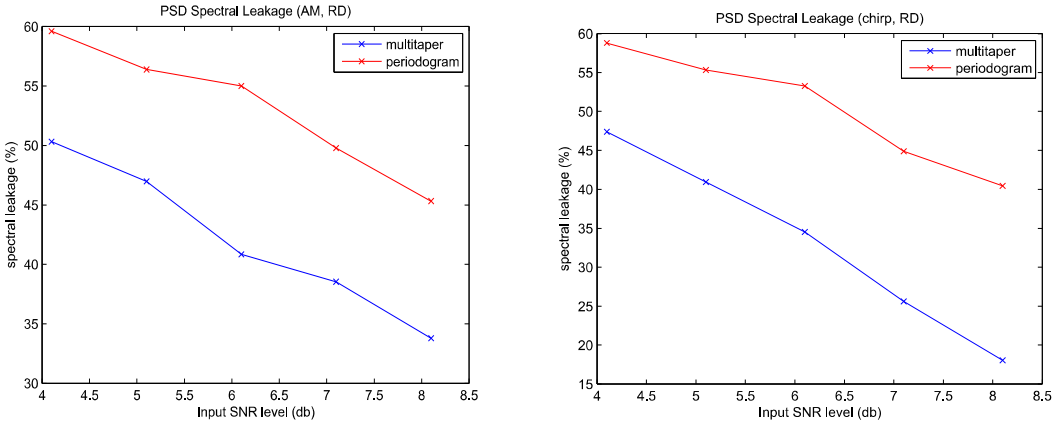

(a) (b)

Figure 5.6: PSD spectral leakage vs input SNR for classical RD (periodogram based) and MT-RD architectures with (a) AM and (b) chirp signals.

These results emphasise the beneficial role the MT method plays in not only ensuring improved CS performance for narrowband signals by reducing leakage, but

also in attenuating noise by reducing its variance (Percival & Walden, 1993), so the noise component energy is reduced thereby rendering the corresponding frequency components less significant and the AM and/or chirp signals more sparse.

The effect of the MT and the superior performance of the MT-RD is also substantiated in Figures 5.7 (a) and (b), where the normalised PSD graphs for both AM and chirp signals are respectively depicted. The spectral leakage is much less pronounced in the case of the MT-RD for both signal types, which confirms the MT-RD theory presented in Section 5.2 and even at low SNR levels e.g., -3dB, the Slepian sequences of the MT method are able to reduce leakage and variance related to the real signal and noise component respectively.

The superiority of the MT-RD is also apparent when the classical RD and MT-RD architectures are tested in more strict conditions in regards to the number of occupied frequencies and level of noise. Figure 5.8 shows the PSD graphs for an AM signal with 4 carriers, the first at 800Hz and the others located 600Hz from each other, hence the occupied frequencies are located around 600, 1000, 1200, 1600, 1800, 2200, 2400 and 2800Hz. The input SNR is set at -3dB, while the sampling rate at 25.25% of Nyquist. It is evident that in the case of the classical RD the occupied frequencies are not distinguishable due to the spectral leakage of the periodogram however the corresponding PSD from the MT-RD facilitates successful identification of dominant frequency components, despite the high noise environment.

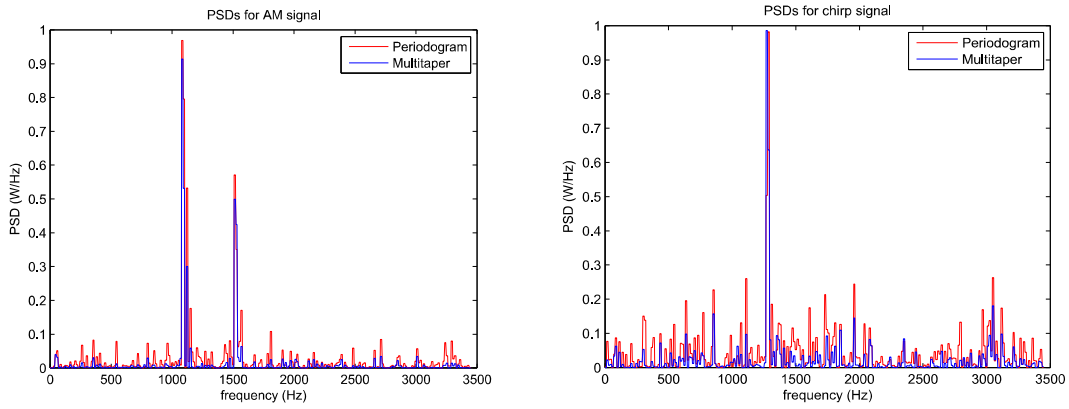

(a) (b)

Figure 5.7: Recovered normalised MT-RD and periodogram-based PSD for (a) AM and (b) chirp signals at 25.25% Nyquist rate and -3dB input SNR.

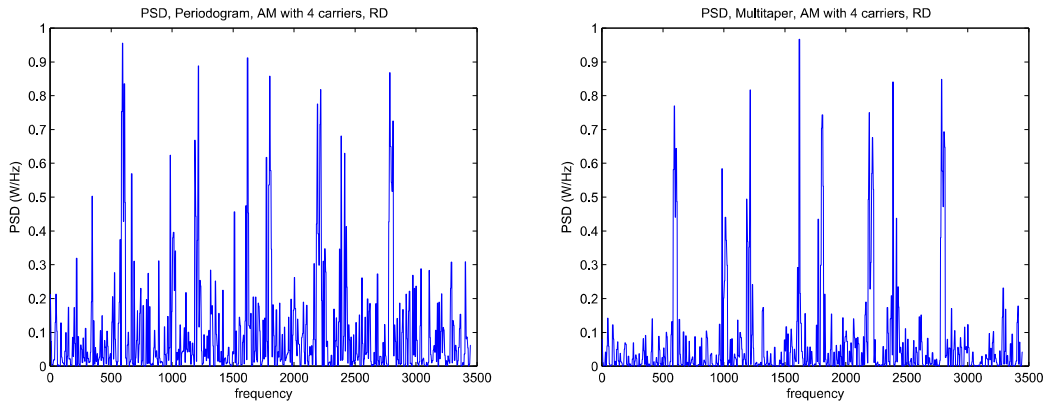

(a) (b)

Figure 5.8: Recovered normalised PSD for (a) classical RD and (b) MT-RD at 25% Nyquist rate and -3dB input SNR.

The next series of simulations appertain to the CM-based MT-CM architecture. First the relevant algorithm 5.2 is validated the same way as algorithm 5.1. A 2-channel CM and AM signals as channel inputs are considered. The results are shown in Figure 5.9 and as with algorithm 5.1 they reveal the sparsity increase when MT method is applied to the AM signals.

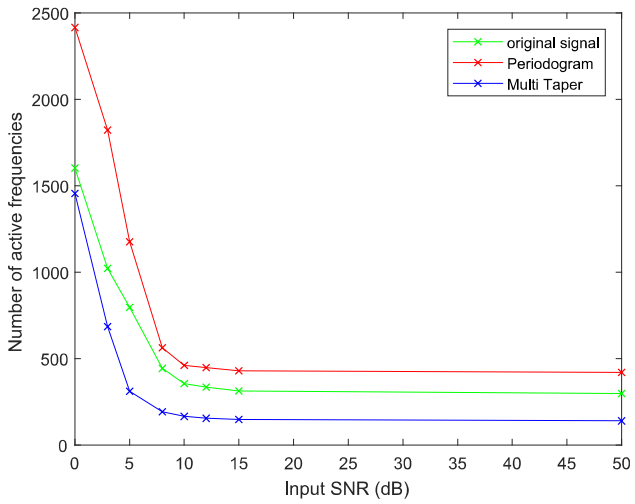

Figure 5.9. The effect of the MT method on sparsity of AM signals using algorithm 5.2.

The next series of experiments relate to the new MT-CM architecture, which like its RD counterpart, also exhibits enhanced CS performance, compared with the classical CM. Figure 5.10 shows the results of the spectral leakage measurement against input SNR with AM and chirp signals for both the classical CM and MT-CM

architectures, with the overall average improvements being approximately 18% and 21% respectively.

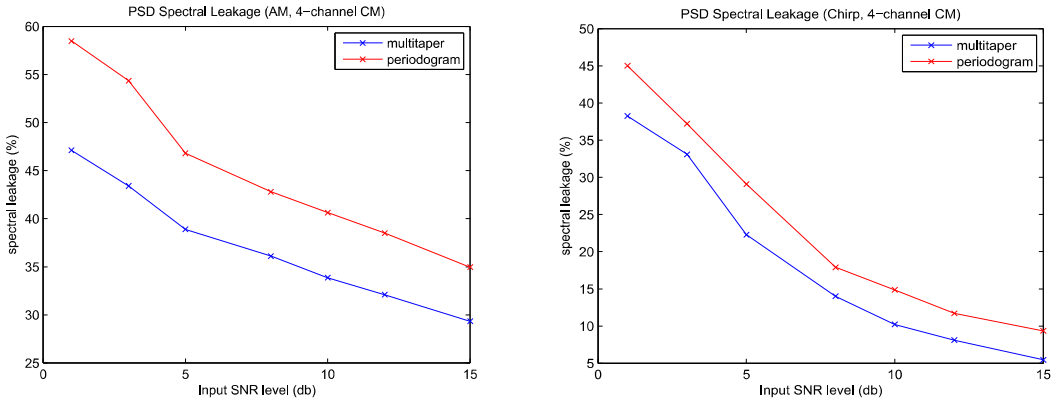

(a) (b)

Figure 5.10: PSD spectral leakage vs input SNR for classical CM (periodogram based) and MT-CM architectures with (a) AM and (b) chirp signals.

This superior performance is also evident in Figures 5.11 and 5.12, where the normalised PSD graphs at 8dB and 3dB SNR are respectively depicted, for AM and chirp signals. The resulting spectral leakage is much less pronounced for both signal types, especially for the low 3dB level, because the Slepian sequences of the MT method act upon both the actual signal and noise components, in the same way as in the MT-RD architecture.

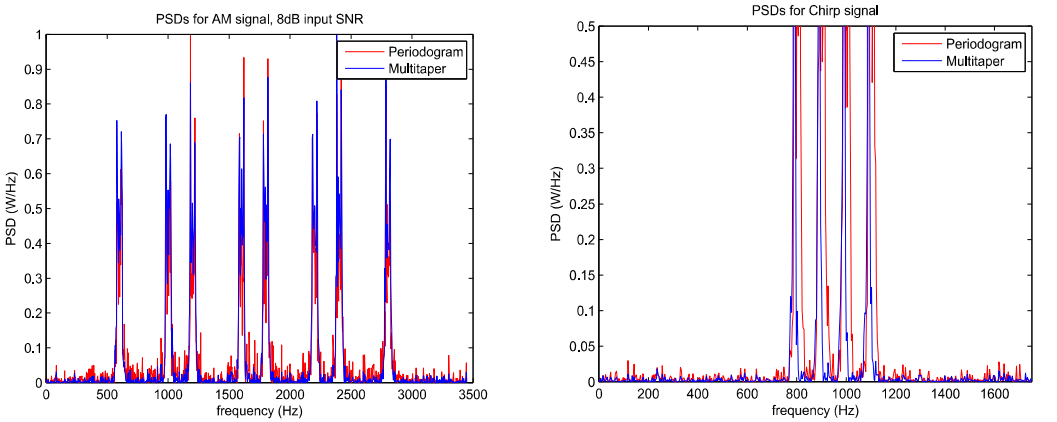

(a) (b)

Figure 5.11: Recovered normalised PSD derived from CM (periodogram-based) and MT-CM architectures for (a) AM and (b) chirp signals at 8.1dB input SNR.

The robustness of the MT-CM architecture is further substantiated even when the input SNR is set as low as -3 dB. As it is apparent in Figure 5.13, the MT-CM related PSD keeps the noise level sufficiently low for the active frequencies to be distinguished, while the periodogram-based PSD derived by the classical CM is too noisy across the whole spectrum to distinguish the active frequencies of an AM signal.

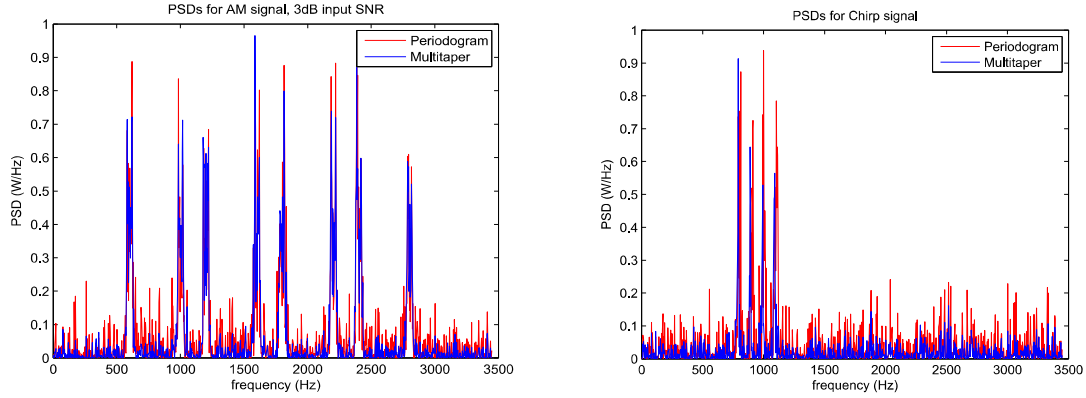

(a) (b)

Figure 5.12: Recovered normalised PSD derived from CM (periodogram-based) and MT-CM architectures for (a) AM and (b) chirp signals at 3dB input SNR.

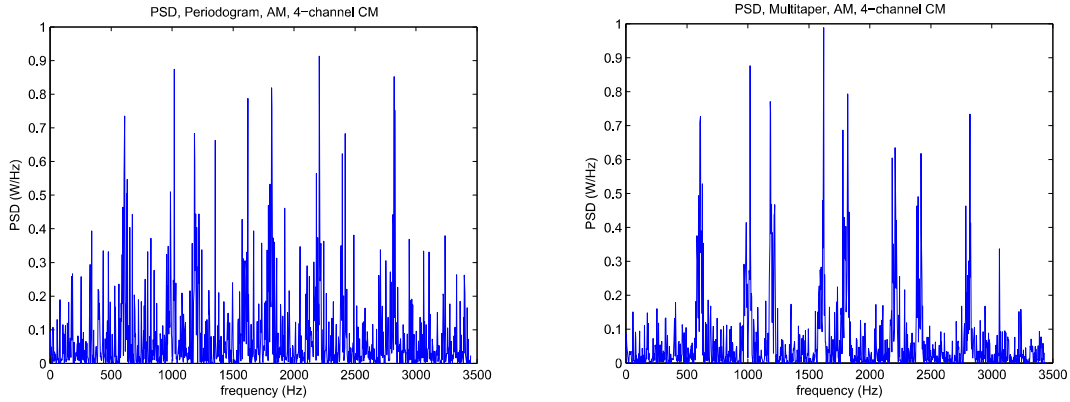

(a) (b)

Figure 5.13: Recovered normalised PSD for (a) classical CM and (b) MT-CM at -3dB input SNR.

While the MT method enhances the CS performance for narrowband signals like AM and chirps, the corresponding results for wideband digitally modulated signals such as QPSK, are not as encouraging. Figures 5.14a and 5.14b plot the spectral leakage against sampling rate and input SNR respectively for the RD based architectures, while Figure 5.15 plots spectral leakage against input SNR for the CM

based architectures. There is no discernible improvement in the MT-RD and MT-CM cases compared with their respective classical counterparts, with minor differences attributable to the random nature of both the CS process (randomness of the measurement matrix) and noise component of the QPSK signal.

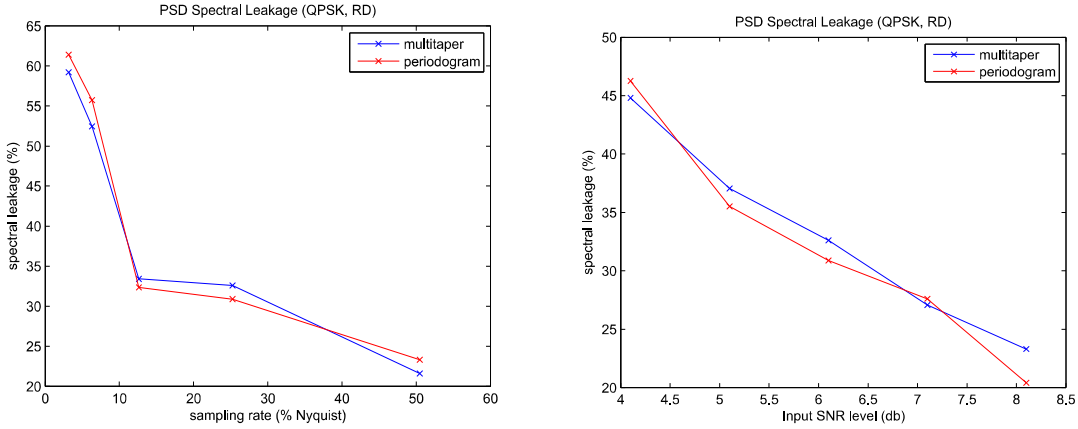

(a) (b)

Figure 5.14: PSD spectral leakage vs (a) sampling rate and (b) input SNR with QPSK signal and for classical RD (periodogram) and MT-RD (multitaper).

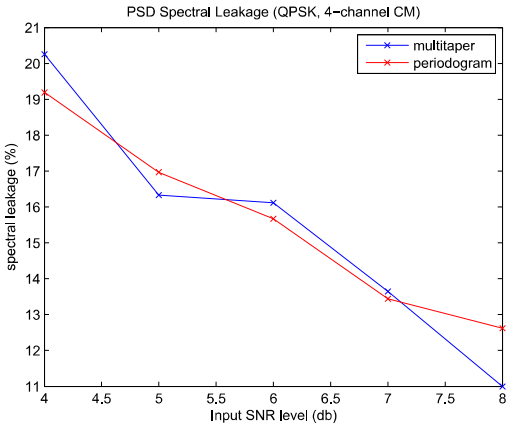

Figure 5.15: PSD spectral leakage vs input SNR for classical CM and MT-CM architectures.

The reason for this lack of improvement is due to the PSD structure of a QPSK signal and indeed, digitally modulated signals in general. Their PSD is characterised by a main lobe centred at a carrier frequency, with side lobes distributed across the spectrum. These side lobes are spectral leakage, but constitute part of the signal spectrum so the MT method cannot act upon such signals in the same way as with narrowband signals to reduce leakage and thus increase sparsity, since it is a

consistent spectral estimator that exhibits low bias and variance compared to the periodogram. The consequence is that the MT-based architectures cannot increase sparsity and thus CS performance for digitally modulated signals, as apparent in Figure 5.16. where the PSD graphs derived from both classical RD and MT-RD are depicted.

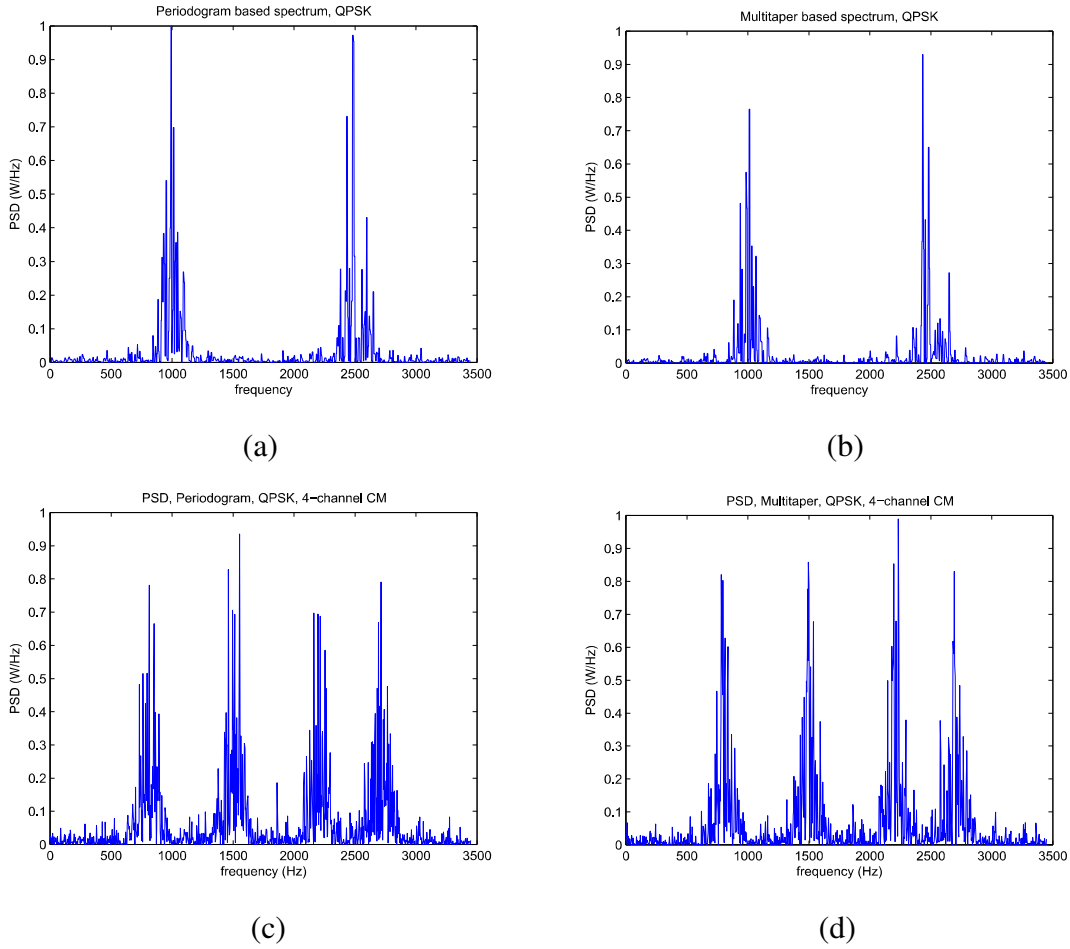

Figure 5.16: Recovered normalised PSD of QPSK signal for (a) classical RD, (b) MT-RD, (c) classical CM and (d) MT-CM.

5.5 Summary

This Chapter has presented the novel MT-based CS model, which embeds the MT spectral estimator to both RD and CM architectures. The parameters of the MT method, the Slepian sequences and their associated eigenvalues, are seamlessly integrated to the RD and CM, in order to present two new CS architectures. Since the MT method is non-parametric, there is no dependence, reliance on, or burden to the

signal transmission side, namely the PU. Both novel architectures were found to provide enhanced performance compared with their classical counterparts, in regards PSD spectral leakage against sub-Nyquist sampling rate, when the signals employed are narrowband, such as AM and chirp. They have also exhibited enhanced robustness against input noise. However, for digitally modulated signals, the MT method does not provide enhanced CS performance, due to the fact that the MT being a consistent estimator does not reduce side lobe leakage, since for such signals the side lobes are part of the true signal spectrum.

In Chapters 4 and 5, the common property of all the signals employed, regardless of structure, was their sparsity in the frequency domain. As discussed in Chapter 2, as CR improves spectrum utilization, signal sparsity may not be sufficient for efficient CS performance. In addition, there are signals which are not frequency sparse, but instead exhibit sparsity in a different domain. The next Chapter will thus investigate alternative signal sparsity basis domains other than Fourier for CS.

Chapter 6

A Walsh-Hadamard based Compressive Sensing model

6.1 Introduction

Novel CS models applicable to both the classical RD and CM architectures have been presented in Chapters 4 and 5 respectively. While the precolouring concept was employed in Chapter 4 and the MT in Chapter 5, in both cases the signals involved exhibit sparsity in the Fourier (frequency) domain. This frequency sparsity, as discussed in Section 2.4, is typical with the wireless signals in open-spectrum networks where the spectrum is underutilised (Haykin, 2005; Federal Communications Commission, 2002; McHenry, 2005) and only a small portion of the spectrum is heavily used. However, there are two issues of concern with sparsity in the frequency domain: Firstly, as CR techniques find their way in the future wireless networks, the spectrum utilization will continuously improve, with the consequence being the reduction of the sparsity level of the relevant wireless signals (Sun et al., 2013). Hence, the performance of the CS techniques will deteriorate as well. The second issue is that there are wireless signals which are not considered frequency sparse, like CDMA, as mentioned in Chapter 1.

Therefore, it is essential to investigate possible sparsity basis for signals of interest other than Fourier, and subsequently develop a corresponding CS model, which then is to be applied to the existing CS architectures namely the RD and the CM. In this Chapter a novel *Walsh-Hadamard - based compressive sensing* model will be presented. For specific types of signals, the model provides improved CS performance by exploiting increased signal sparsity and noise reduction compared with Fourier, in the so called Walsh-Hadamard (WH) or *sequency domain*. The new model along with a discussion of the WH transform, *sequency sparsity* and CDMA are presented in

Section 6.2, while *Sections 6.3* and *6.4* present the simulation setup and critical results discussion respectively. Finally, *Section 6.5* concludes this Chapter.

6.2 The WH-CS Model

Almost all the CS techniques and applications in the field of telecommunications assume that the signals are sparse in the frequency domain, thus the sparsity basis is the DFT matrix. This sparsity is due to the underutilization of the spectrum resources, an issue discussed in Section 2, where it was also mentioned the CS could effectively be employed in spectrum sensing for CR to provide solution to the spectrum underutilization. As the successful application of CR in wireless networks increases, the spectrum will be more efficiently utilised, with the consequence the respective signals becoming less sparse. This will have an impact on the performance of the CS architectures, which will deteriorate if less sparse signals are involved, unless they acquire more signal samples. However, the latter comes at the cost of lower efficiency and increased computational complexity.

Another issue is that there are cases where wireless signals are not frequency sparse like those involved in the CDMA access scheme. In CDMA spreading codes are used for channelization and interference avoidance purposes. The result is the signal is spread over a bandwidth wider than would be required if other access schemes were involved (Ipatov, 2005). These codes are taken from the rows of the *Hadamard* matrix. This matrix along with the relevant WH transform and their relation with CDMA will be discussed in the following sub-Section.

6.2.1. The WH Transform and Sequency Sparsity

The WH transform (WHT) acts upon a discrete signal and decomposes it into a set of orthogonal functions called Walsh functions (Beauchamp & Debnath, 1979; Beauchamp, 1975). These functions represent the discrete signal just like the trigonometric functions represent a continuous function in the Fourier analysis (Walsh, 1923). The Walsh functions are rectangular waveforms and can only take two

values, +1 and -1, unlike the sine and cosine functions, which are continuous and can take any value within [-1,+1] (Weisstein, 2017; Tzafestas, 1985). An important property of a Walsh function is *sequency*, which is measured by the number of zero-crossings of its corresponding time-domain waveform (Weisstein, 2017), therefore the unit of sequency is the Hz. Sequency in the WH domain can be viewed as the equivalent of frequency in the Fourier domain.

The Walsh functions populate the rows of a Hadamard matrix, which is the equivalent of the DFT matrix in Fourier analysis. Just as each row of the DFT matrix corresponds to a sine/cosine function with specific frequency, each row of the Hadamard matrix corresponds to a Walsh function with a unique sequency. Unlike the DFT matrix which exists for every order N, that it is of NxN dimensions, the Hadamard matrices can exist only for orders being multiples of 4 (A. Hedayat & Wallis, 1978; Ipatov, 2005; Beauchamp & Debnath, 1979). The reason for this is that binary functions such the Walsh are orthogonal only when their length is a multiple of 4 (Hadamard, 1893; Ipatov, 2005).

A very popular algorithm for recursively building the Hadamard matrices is the Sylvester rule (Sylvester, 1867; Ipatov, 2005; Seberry et al., 2005). If the Hadamard matrix H_N of order N exists, then the Hadamard matrix H_{2N} of order $2N$ can be constructed as:

$$H_{2N} = \begin{bmatrix} 1 & 1 \\ 1 & -1 \end{bmatrix} \otimes H_N = \begin{vmatrix} H_N & H_N \\ H_N & -H_N \end{vmatrix} \qquad (6.1)$$

where $\otimes$ denotes the Kronecker product (Strang, 2016).

According to the Sylvester algorithm, one can start with Hadamard $H_1=[1]$. Then from 6.1 the Hadamard H_2 is:

$H_2 = \begin{vmatrix} 1 & 1 \\ 1 & -1 \end{vmatrix} \otimes [1] = \begin{bmatrix} [1] & [1] \\ [1] & -[1] \end{bmatrix} = \begin{bmatrix} 1 & 1 \\ 1 & -1 \end{bmatrix}$, then from H_2 the Hadamard H_4 is constructed as:

$$H_4 = \begin{bmatrix} H_2 & H_2 \\ H_2 & -H_2 \end{bmatrix} \otimes \begin{bmatrix} 1 & 1 \\ 1 & -1 \end{bmatrix} = \begin{bmatrix} 1 & 1 & 1 & 1 \\ 1 & -1 & 1 & -1 \\ 1 & 1 & -1 & -1 \\ 1 & -1 & -1 & 1 \end{bmatrix},$$

$$H_8 = \begin{bmatrix} H_4 & H_4 \\ H_4 & H_4 \end{bmatrix} \otimes \begin{bmatrix} 1 & 1 \\ 1 & -1 \end{bmatrix} = \begin{bmatrix} 1 & 1 & 1 & 1 & 1 & 1 & 1 & 1 \\ 1 & -1 & 1 & -1 & 1 & -1 & 1 & -1 \\ 1 & 1 & -1 & -1 & 1 & 1 & -1 & -1 \\ 1 & -1 & -1 & 1 & 1 & -1 & -1 & 1 \\ 1 & 1 & 1 & 1 & -1 & -1 & -1 & -1 \\ 1 & -1 & 1 & -1 & -1 & 1 & -1 & 1 \\ 1 & 1 & -1 & -1 & -1 & -1 & 1 & 1 \\ 1 & -1 & -1 & 1 & -1 & 1 & 1 & -1 \end{bmatrix}.$$

In general, the elements of H_N are given by:

$$(H_N)_{i,j} = (-1)^{i \cdot j}, \; i, j = 0, 1 \ldots, N\text{-}1 \qquad (6.2)$$

where $i \cdot j$ is the dot product of the binary representations of i,j (Agaian et al., 2011) . In this way a Hadamard matrix of any order $N=2^m$ for $2 \leq m \in \mathbb{N}$ can be constructed. The rows of a Hadamard matrix generated as above are arranged in the so-called natural order (Beauchamp, 1975; Kanjilal, 1995). They can also be arranged in increasing sequency order. In this thesis the sequency ordered matrices will be considered from now on, so to be in accordance with the rows of the DFT matrix which are also arranged in increasing frequency order.

The WH transform of a discrete signal x of length N is given by the following equation (Beauchamp, 1975):

$$h = H_N x \quad \text{(forward)} \qquad (6.3.a)$$

$$x = H_N^{-1} h \quad \text{(inverse)} \qquad (6.3.b)$$

where H_N is the Hadamard matrix of order N and vector h is the representation of x in the WH/sequency domain. From (6.3.b) signal vector x can also be expanded as:

$$x = \sum_{i=0}^{N-1} h_i r_i^{H_N} \qquad (6.4)$$

with coefficients h_i being the i^{th} element of h and $r_i^{H_N}$ the i^{th} row of H_N. It is evident from (6.4) that x is generated by the rows of H_N, each one of them characterised by a unique sequency equal to i, just as a signal in the Fourier/sequency domain is generated by the rows of the DFT matrix, each one corresponding to a single frequency. The coefficients h_i weight the corresponding row/sequency according to the contribution in the generation of x. The concept of sparsity in the sequency domain is also straightforward from (6.4) and. A signal is k-sparse in the sequency domain when all but k of the h_i coefficients are zero or close to zero. The k rows (Walsh functions) with their respective non-zero coefficients convey the sequency content of the signal x.

A CDMA signal is encoded with a channelization code thereby assigned a specific user channel associated with the code, which corresponds to a Walsh function (Ipatov, 2005; Rgheff, 2007). To illustrate this, a simple data signal of four bits [1, 0, 0, 1] is considered, which is encoded with a Walsh function u=[1, -1], the latter being a row of Hadamard H_2. The encoding rule is that if the data bit is 1 it is encoded to the function u=[1 -1] and if it is 0 to $-u$ [ref]. Therefore the encoded signal will be [1, -1, -1, 1, -1, 1, 1, -1], which is actually a row of the Hadamard H_8. According to (6.3.b) and (6.4), the signal is written respectively as:

$$\begin{bmatrix}1 & -1 & -1 & 1 & -1 & 1 & 1 & -1\end{bmatrix} = H_8^{-1}h = \begin{bmatrix}1 & 1 & 1 & 1 & 1 & 1 & 1 & 1\\ 1 & 1 & 1 & 1 & -1 & -1 & -1 & -1\\ 1 & 1 & -1 & -1 & -1 & -1 & 1 & 1\\ 1 & 1 & -1 & -1 & 1 & 1 & -1 & -1\\ 1 & -1 & -1 & 1 & 1 & -1 & -1 & 1\\ 1 & -1 & -1 & 1 & -1 & 1 & 1 & -1\\ 1 & -1 & 1 & -1 & -1 & 1 & -1 & 1\\ 1 & -1 & 1 & -1 & 1 & -1 & 1 & -1\end{bmatrix} \cdot \begin{bmatrix}0\\0\\0\\0\\0\\1\\0\\0\end{bmatrix} \quad (6.5.a),$$

$$\begin{bmatrix}1 & -1 & -1 & 1 & -1 & 1 & 1 & -1\end{bmatrix} = \sum_{i=0}^{8-1} a_5 r_5^{H_8} = \\ = 1 \cdot \begin{bmatrix}1 & -1 & -1 & 1 & -1 & 1 & 1 & -1\end{bmatrix} \quad (6.5.b)$$

where H_8 is arranged in increasing sequency order.

From this example, it is shown that the CDMA encoded signal of length 8 is constructed from only one Walsh function characterised by a unique sequency value being in this example equal to 5, hence the signal is sparse in the WH domain. Therefore, CS techniques could be applied in order to extract the dominant Walsh functions/sequences of the signal and thereby identify the occupied channels in a CDMA communications network. This is the equivalent of the frequency spectrum sensing in CR, with the difference that now the sensing process is performed in the sequency domain. The following two sub-Sections 6.2.2 and 6.2.3 present the application of a novel WH-CS model to RD and CM architectures respectively.

6.2.2 The RD and CM versions of the WH-CS Model

The RD architecture so far exploits signal frequency sparsity in the frequency/Fourier domain and recovers signal PSD. The sparsity basis is the DFT matrix, which is an orthonormal basis, a requirement dictated by the CS theoretical framework discussed in Section 2.4.2. Similarly, in order to perform CS exploiting signal sequency sparsity in the WH domain, the respective basis must be an orthonormal Hadamard-based matrix. Form the example in 6.2.1, it is concluded that the Hadamard matrix discussed

can be a sparse basis in the sequency sparse signals like CDMA. In regards to the orthonormal basis, it can be observed that the Euclidean norm of each of the rows of an $N \times N$ Hadamard matrix H_N is $\sqrt{N}$. Hence, WHT $N \times N$ matrix H can be defined as:

$$H = \frac{1}{\sqrt{N}} H_N \tag{6.6}$$

Therefore, while the equation that expresses the sampling function of the RD will remain the same:

$$y = \Phi x \tag{6.7}$$

with y being the output $K \times 1$ vector after sampling x of length N samples and Φ being the $K \times N$ measurement matrix with $K<N$, the recovery process employs the $N \times N$ Hadamard matrix H and the $N \times 1$ vector h which is the representation of x in the sequency domain:

$$y = \Phi x = \Phi H^{-1} h = G_H h \tag{6.8}$$

with $G_H = \Phi H^{-1}$.

The matrix G_H satisfies the RIP property (Tropp et al., 2010; Baraniuk et al., 2017), thus (6.8) can be solved for the sequency vector h with CS recovery algorithms. As in the Fourier/frequency domain, the vector P_H termed as the *Sequency Power Spectrum* (SPS) of $x(t)$ can also be calculated as $P_H=|h|^2$. The sequency power spectrum is analogous to the PSD in the frequency domain. In this way the integration of the WHT matrix is implemented, leading to the introduction of the *novel WH-RD architecture*, the block diagram of which is shown in the following Figure 6.1.

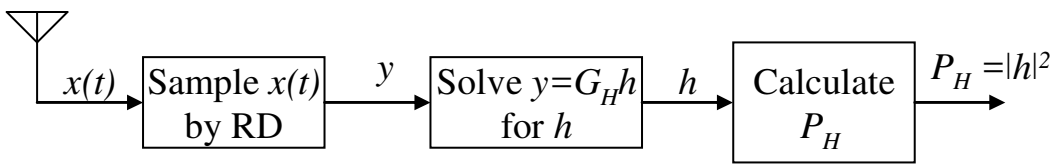

Figure 6.1: Block diagram of the WH-RD architecture.

The corresponding pseudo code for the WH-RD is given in the Algorithm 6.1.

Algorithm 6.1: Pseudo code for the WH-RD

Inputs: signal $x(n)$ of length N samples.

Variables: M - number of measurements or equivalently length of $y(n)$ output of sub-Nyquist sampling, H- the $N \times N$ WHT matrix, A- the $M \times N$ measurement matrix.

Outputs: P_H of $x(n)$

1: ***Initialise*** M, H

2: ***Construct*** Φ.

3: ***Calculate*** $y=\Phi x$

4: ***Calculate*** $G_H=AH^{-1}$

5: ***Apply*** l_1 minimisation algorithm to solve $y=G_H h$ for h.

6: ***Calculate*** $P_H = |h|^2$.

7: **END**

Comparing the above RD architecture with the classical one that exploits frequency sparsity, the major difference is the type of the sparsity basis employed. The theoretical frameworks in both cases have similarities, since they exploit sparsity in some domain to perform sub-Nyquist sampling and employ matrices satisfying the RIP property to perform recovery.

In a similar way the CM-based architecture is introduced. Recalling the CM discussion in previous Chapters, and assuming a J-channel CM, the vector form of the equation which gives the output of the CM is:

$$y = \sum_{j=1}^{J} \Phi_j x_j \tag{6.9}$$

with x_j being the j^{th} of the J channels and Φ_j being a NxN diagonal matrix, with the main diagonal being populated by iid entries from a Rademacher distribution, as was

the case in Chapters 4 and 5. Assuming that the signals x_j have length of N samples and considering that the sparsity basis for each of them is the $N \times N$ DFT matrix H, they can be written according to (6.3.b):

$$x_j = H^{-1} h_j \tag{6.10}$$

Based on the above equation (6.10) and recalling (4.17) and (5.13), (6.9) becomes:

$$y = \sum_{j=1}^{J} \Phi_j x_j = [\Phi_1 H^{-1}, \Phi_2 H^{-1}, .., \Phi_J H^{-1}] \begin{bmatrix} h_1 \\ h_2 \\ . \\ . \\ h_J \end{bmatrix} =$$

$$= G_H^{CM} \begin{bmatrix} h_1 \\ h_2 \\ . \\ . \\ h_J \end{bmatrix} \tag{6.11}$$

where G_H^{CM} is the result of concatenating matrices $\Phi_j H^{-1}$ and h_j are the sequency vectors for each respective x_j. In a manner analogous to the Fourier-based CM architectures previously presented, the sparsity basis is now a $JN \times JN$ block diagonal matrix with $N \times N$ WHT basis H along the diagonal. Moreover, the derives a vector q_H, which is the combined representation of these signals $x_1, x_2, .., x_J$ in the sequency domain. The CS problem for a CM architecture is thus the recovery of q_H, solving the following equation using CS techniques:

$$y = G_H^{CM} q_H \tag{6.12}$$

The block diagram of the WH-CM is shown in Figure 6.2, while the corresponding pseudo code given in the Algorithm 6.2.

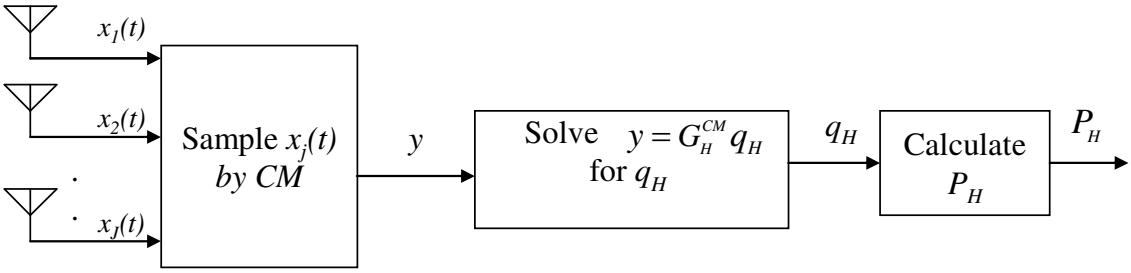

Figure 6.2: Block diagram of the WH-CM architecture.

Algorithm 6.2: Pseudo code for the WH-CM

Inputs: signals $x_j(n)$ of length N samples, $j=1,..,J$.

Variables: H- the $N \times N$ WHT matrix, Φ_j – the $N \times N$ measurement matrices, $j=1,..,J$.

Outputs: Combined P_H of $x_j(n)$, $j=1,..,J$

1: ***Initialise*** H.

2: ***Construct*** Φ_j, $j=1,..,J$.

3: ***Calculate*** $y = \sum_{j=1}^{J} \Phi_j x_j$.

4: ***Calculate*** matrices $\Phi_j H^{-1}$, $j=1,..,J$.

5: ***Construct*** G_H^{CM} by ***concatenating*** matrices $\Phi_j H^{-1}$, $j=1,..,J$.

6: ***Apply*** l_1 minimisation algorithm to solve $y = G_H^{CM} q_H$ for q_H.

7: ***Calculate*** $P_H = |q_H|^2$.

8: **END**

In this Section, the WHT and sequency sparsity were discussed before the presentation of the applications of the WH-CS model, namely the WH-RD and WH-CM architectures. The employment of the WHT matrix as sparsity basis permits the said architectures to recover signals like CDMA, which are not sparse in the

frequency/Fourier domain. The block diagram of the WH-CS model is shown in Figure 6.3.

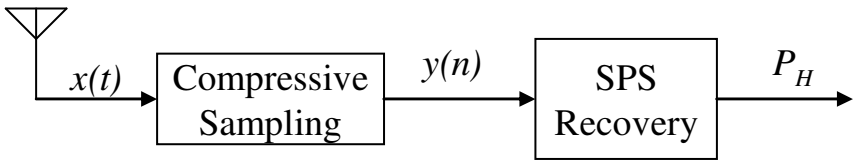

Figure 6.3: Block diagram of the generic WH-CS model.

The next Section presents the simulation setup for the two versions of the WH-CS model, while Section 6.4 critically analyses their respective performances.

6.3 Simulation Setup

At first, CDMA encoded test signals are compared in regards to sparsity in frequency and sequency domains and their behaviour will be investigated and analyzed. Initially simple CDMA encoded test signals will be considered where only the channelization code is applied. Subsequently, CDMA encoded signals which are also scrambled are employed (Ipatov, 2005). The signal sparsity will be investigated in both baseband and passband versions. Then for the above mentioned signals, the performance of the WH-RD and WH-CM architectures will be compared against their classical Fourier-based counterparts. Moreover, the encoding and scrambling functions of a CDMA forward link (Ipatov, 2005) are simulated and the signal sensing performance of the WH-RD and WH-CM architectures is investigated and critically analyzed.

The signals considered and simulated in order to examine their sparsity behaviour are the following:

a. Baseband CDMA test signals, where the data are QPSK modulated before being encoded by a Walsh function for channelization purposes. The rationale for the QPSK modulation is that it is used by all the mobile networks employing CDMA technology (Rgheff, 2007).

b. The passband version of the previous CDMA signals, where after channelization, the signals are modulated by a carrier hence frequency up-conversion takes place.

c. CDMA signals, where after the QPSK modulation of the data and the channelization by a Walsh function, the signals are further encoded by scrambling codes. In this project codes generated by PN sequences are considered, although other sequences such as Gold and Kasami could also be employed in CDMA networks (Ipatov, 2005; Torrieri, 2005); Rgheff]. The scrambling codes are employed to secure signal separation between different base stations of a CDMA network, therefore they are unique for each of them (Ipatov, 2005; Torrieri, 2005; Rgheff, 2007).

The signals parameters are shown in Table 3.2. Binary data of length equal to 64 samples are encoded with one of the 32 available codes of length 32 (derived from a 32x32 Hadamard matrix), to form a signal with 2048 samples. Then the CDMA signal is scrambled before frequency up-conversion takes place.

As in the previous Chapters, the functions of the involved CS architectures, namely the classical RD and the CM as well as the WH-RD and WH-CM are simulated. Firstly, the recovered PSD/SPS graphs pertaining to the 3 signal types described above are visually compared and evaluated. As discussed in Section 3.4, this is a way to reveal signal features, in this case the signal sparsity in different domains.

Then, the said architectures are compared under the criterion of system SNR against sampling rate. This was also defined and discussed in Section 3.4. The rationale to employ system SNR is that in this case the purpose is to solely evaluate the architectures for their ability to reconstruct the original signal under different the sparsity bases employed.

Finally, the ability of the WH-architectures to perform sensing for sequency sparse signals is investigated in the following two simulations:

The first one pertains to the forward link of CDMA-based mobile network (Ipatov, 2005). At a base station (BS) a QPSK signal is encoded, scrambled, frequency up-converted and transmitted to a mobile station (MS) receiver, equipped with a WH-RD

architecture which performs channel sensing, hence it identifies which of the CDMA channels are occupied or not.

It is assumed that only up to 4 of the 32 available CDMA channels of one BS are active, so the incoming signal to the MS is sparse in the WH domain. A different number of active channels could be equally applicable, with sparsity being the factor affected, that is more active channels less sparsity. It is noted that since in CDMA the users occupy channels instead of frequency bands, the term channel sensing is used instead of spectrum sensing. In CDMA all the users share and occupy most of the available bandwidth and the identification of the available frequencies is not applicable. The users are distinguished and identified by the channelization code described in 6.2.1. The fact that the BS transmission makes use of most of the available spectrum is also the reason the WH-CM is not suitable to be employed in these experiments. Since the CDMA channels are not distinguished by frequency, the antennas of the WH-CM will receive the same input channel, thus there is no reason for the employment of parallel structures like WH-CM or the multi-channel version of the RD mentioned in Chapter 4.

Hence, a second simulation scenario is required to investigate the channel sensing capability of the WH-CM. In this simulation two BS are assumed which transmit signals like those described above, but over different bandwidths. The BS signals feed the respective inputs of a 2-channel WH-CM.

6.4 Simulation Results Discussion

The validation of algorithms 6.1 and 6.2, which respectively correspond to the WH-RD and WH-CM architectures is firstly undertaken, where it is assumed each input signal is CDMA-encoded, QPSK modulated with two active Walsh codes. The active sequency threshold is set at 20dB relative to the maximum energy value and sparsity is measure across a range of input SNR and at a sampling rate 25.25% of Nyquist. Figures 6.4 and 6.5 reveal that for both algorithms, the signal sparsity in the WH (sequency) domain is significantly enhanced compared to the Fourier (frequency) domain. The green curves show sparsity of the original non-sampled signal in the frequency domain. The red curves show reduced sparsity when CS is applied in the

frequency domain due to performance degradation incurred by CS. Since the signal sparsity is notably increased as depicted by the blue curves, there is a significant denoising effect, when CS is performed in the WH domain due to the inherent structure of the CDMA-encoded signals described in Section 6.2.

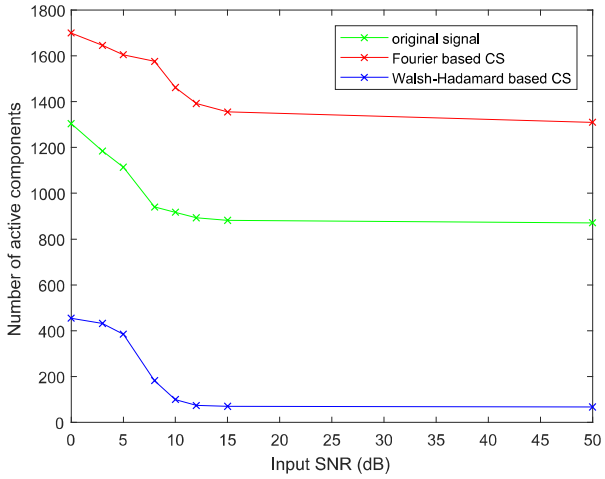

Figure 6.4. The effect of WH-based CS in signal sparsity of CDMA encoded QPSK signals using algorithm 6.1.

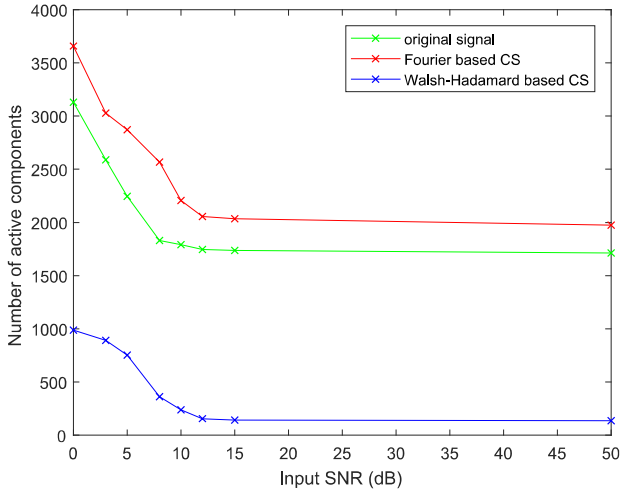

Figure 6.5. The effect of WH-based CS in signal sparsity of CDMA encoded QPSK signals using algorithm 6.2.

The next experiment presents and analyses the results pertaining to the sparsity behaviour of the baseband version of one CDMA encoded QPSK test signal, where the code is a Walsh function of length 32. Figure 6.6 depicts the PSD and SPS graphs of this signal. The bases employed were the $N \times N$ DFT and $N \times N$ WHT matrices respectively with $N=2048$.

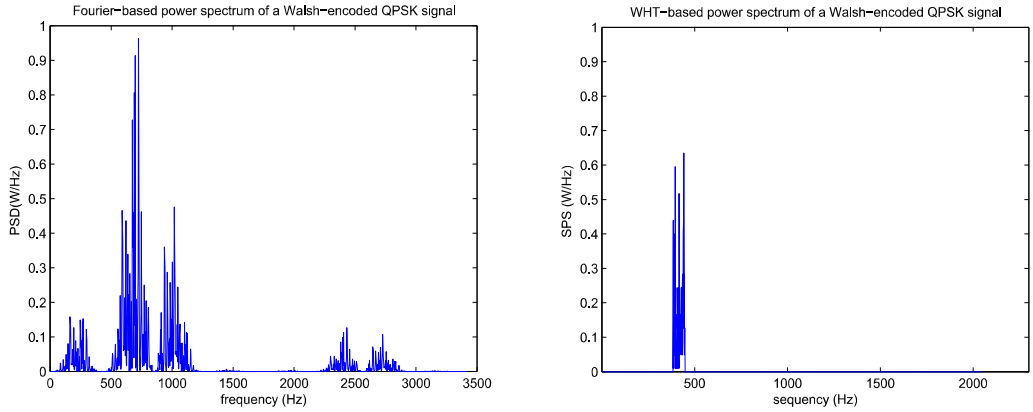

(a) (b)

Figure 6.6: Normalised PSD (a) and SPS (b) of the baseband version of a Walsh-encoded QPSK signal.

It is apparent that the signal sparsity in the sequency domain is much more pronounced than in the Fourier domain. This is due to the effect of the encoding with the Walsh code. The latter modifies the original data of the QPSK as described in Section 6.2.1, so that each data bit is transformed to the Walsh code itself or its opposite sign counterpart. This process can also be viewed as modulation of a Walsh function by the signal data.

As Figure 6.6.b reveals, the signal SPS can be represented by a limited number of Walsh functions being rows of the $N \times N$ WHT matrix, clustered in a specific sequency band, which corresponds to the 32 length Walsh code. Since there are 32 available codes over a total width of 2048Hz, each band has a width of only 64Hz. On the other hand, the encoding process causes the original signal to spread in frequency, hence sparsity in the Fourier domain decreases as shown in Figure 6.4a, since more frequencies contribute in the formation of the signal PSD.

In the next experiment, the same CDMA encoded QPSK test signal is considered, which has now been scrambled by a PN sequence. The respective signal PSD and SPS graphs are displayed in Figure 6.7. It is apparent that the signal is not sparse to either Fourier or WH domains. This is due to the fact that the PN sequence has white noise-like characteristics and spreads the signal (Proakis, 2003) so that almost all the frequencies within the signal bandwidth are present in the respective PSD.

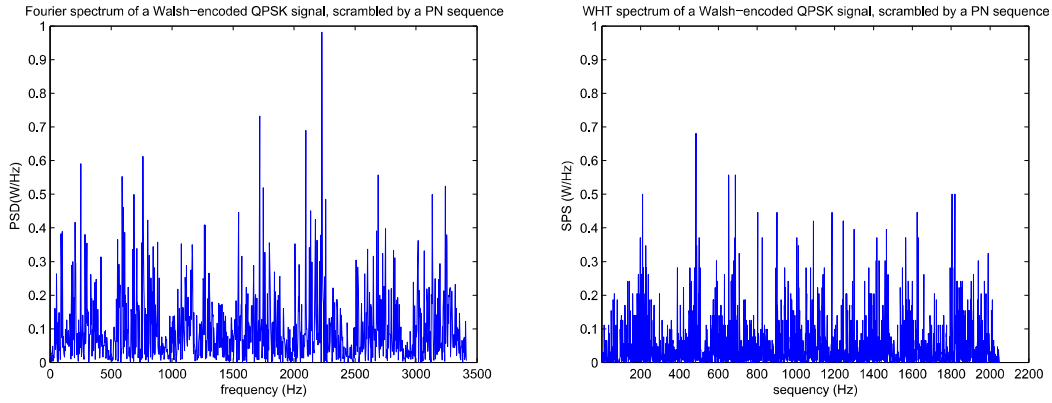

(a) (b)

Figure 6.7: Signal PSD (a) and SPS (b) for a CDMA encoded and scrambled QPSK signal.

Next, the QPSK signal is frequency up-converted after being encoded with a Walsh code, to form the passband version of the CDMA signal. The relevant PSD and SPS graphs shown in Figure 6.8 reveal that the sparsity of the passband signal is reduced in both Fourier and WH domains. The signal is now more complicated due to the frequency up-conversion and a significant number of frequency and sequency components are required for its representation in the respective domains.

From the above it is concluded that in both domains sparsity is larger for the baseband version when the signal has only passed through the channelization process with a Walsh, without being scrambled and frequency up-converted. It is also noted that for the baseband version in particular, the sparsity in the WH domain is much more pronounced than the respective one in the Fourier domain. Therefore, the CS architectures will provide superior performace if they exploit WH domain sparsity instead of Fourier. This is confirmed in Figure 6.9a, where the system SNR performances of the classical RD and WH-RD architectures are compared. Across different sampling rates below Nyquist, the system SNR is indeed consistently higher

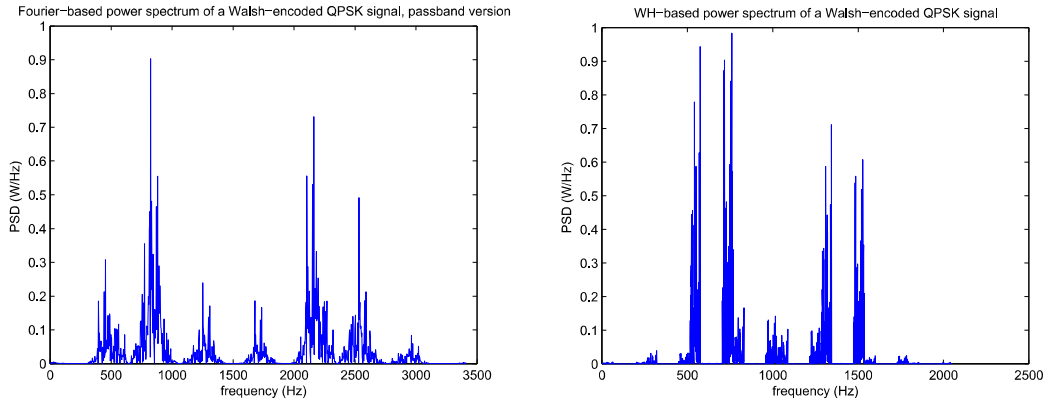

(a) (b)

Figure 6.8: Normalised PSD (a) and SPS (b) of the passband version of a Walsh-encoded QPSK signal.

in the WH-RD case than the classical counterpart. This is due to the much higher sparsity the signal exhibits in the WH domain. The same is also valid for the WH-CM architecture, as shown in Figure 6.9b, where the system SNR is calculated for different number of input channels. Again the WH-CM provides superior performance than its Fourier based counterpart. The reason for the decaying performance with increasing channel number is that sparsity decreases as more channels contribute to the formation of the combined SPS of the input signals.

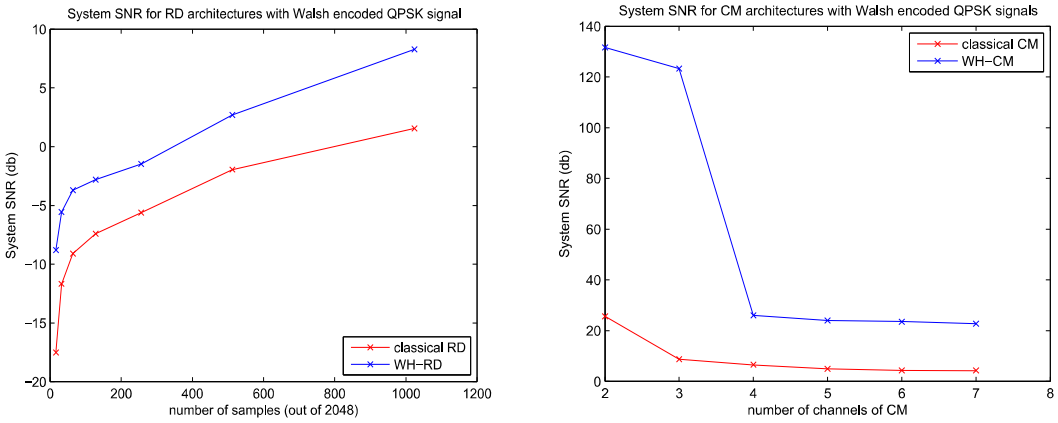

(a) (b)

Figure 6.9: Comparison of system SNR performance for (a) classical RD vs WH-RD and (b) classical CM vs WH-CM architectures.

Since the WH sparsity can be exploited at the baseband version of a CDMA encoded signal, the MS receiver must first perform down-conversion and

descrambling of the incoming forward link signal of the CDMA mobile network before the channel sensing by the WH-RD architecture. Descrambling and down-conversion are carried out in the analog domain (Rgheff, 2007; Proakis, 2003), in a way similar to the signal multiplication by a chipping sequence in the case of the RD architectures. Hence there is no need for signal digitization and sampling above Nyquist rate, which could negate the positive effects of CS.

Figure 6.10a shows the PSD graphs of such an incoming forward link signal to the MS receiver, where no CS has taken place. It is clear that the PSD occupying a large portion of the spectrum does not provide any information regarding the active and non-active CDMA channels therefore it is of no use for channel sensing for CR purposes. In fact, the knowledge of the frequency spectrum of a CDMA signal is not suitable for CR sensing, since the information regarding occupied and non-occupied bands is useless for identification of the active channels. On the other hand the SPS graph in Figure 6.10.b clearly reveals the active (occupied) channels. The active channels can also be identified when the SPS is derived by the WH-RD architecture, even when the measurement samples taken are as few as 32, as shown in Figure 6.11 thanks to the signal sparsity in the WH domain.

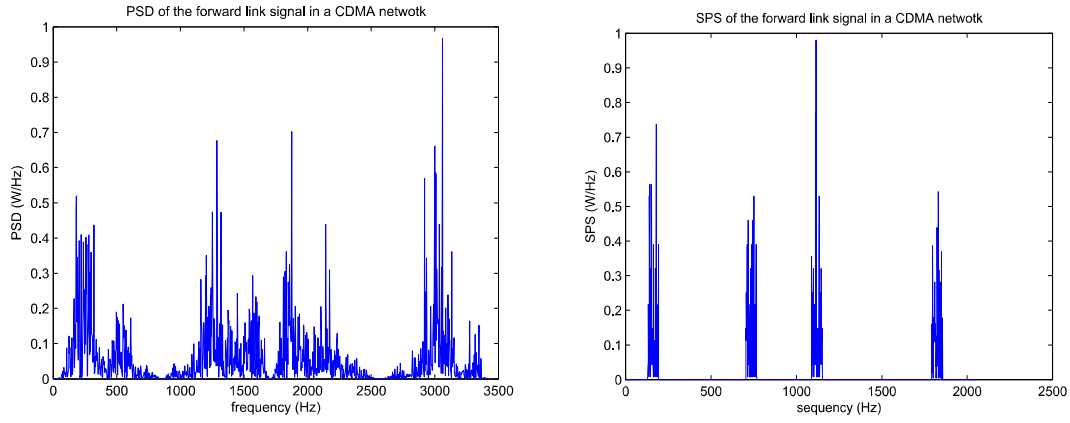

(a) (b)

Figure 6.10: The PSD (a) and SPS (b) graphs for a CDMA forward link signal with 4 active channels.

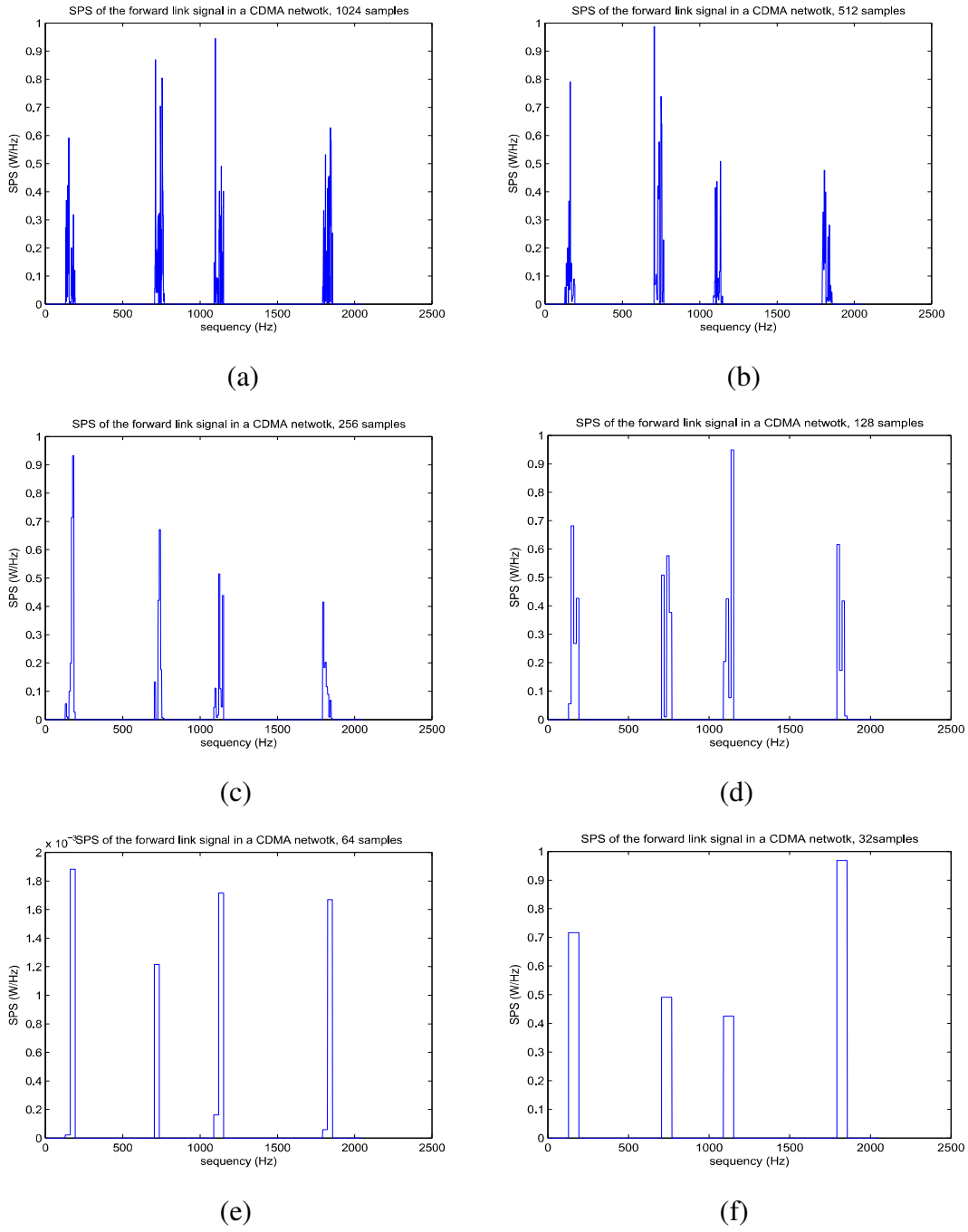

Figure 6.11: SPS graphs of CDMA forward link signal derived by a WH-RD architecture with (a) 1024, (b) 512, (c) 256, (d) 128, (e) 64 and (f) 32 measurements.

The SPS of the combined signal from 2 BS derived by a 2-channel WH-CM, is shown in Figure 6.12a. It is apparent that the 8 active CDMA channels are clearly identifiable, while the respective PSD shown in Figure 6.12b, as in the previous set of experiments, cannot provide any information useful for channel sensing.

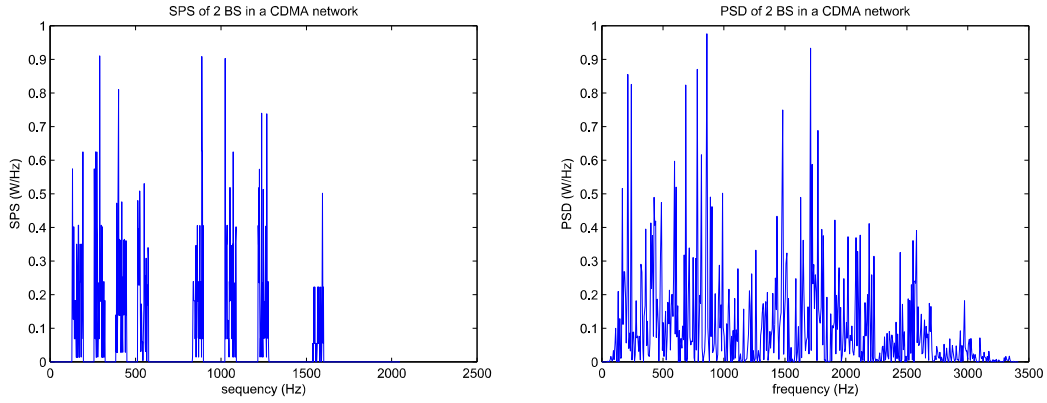

(a) (b)

Figure 6.12: The SPS (a) and PSD (b) graphs for 2 CDMA forward link signals with 8 active channels.

It must be noted however that in this scenario the WH-CM will not be suitable if each CDMA BS transmits over the same bandwidth, since as explained in Section 6.3., the antennas of the WH-CM will receive the same input. Moreover, even if the BS transmitted over different bands of the CDMA network, the combined SPS graph would not be able to assign an active channel to its corresponding BS, because all the BS use the same set of Walsh functions for coding. Therefore each BS signal must be guided to separate architectures.

A final observation common in all Figures 6.10, 6.11 and 6.12 is the denoising effect the signals experience, which is linked to their enhanced sparsity in the WH domain.

The WH-CS model presented in this Chapter enables channel sensing for CDMA encoded signals which are sequency sparse, thereby extended the concept of CS beyond the Fourier domain. There are however limitations pertaining to the fact that the sparsity holds for the baseband version only. Considering that the AR-CS and MT-CS models exploit frequency sparsity, a motivation arises to investigate the integration of all the presented models. A generic framework will therefore be presented in the next Chapter.

6.5 Summary

This Chapter presented a novel WH-CS compressive sensing model which is applicable in both single channel and multi-channel versions that is the WH-RD and WH-CM architectures respectively. The model extends the CS concept to take advantage of sparsity basis other than Fourier and consequently to signals like CDMA, for which the Fourier sparsity basis is not applicable due to their spread spectrum nature. The WH-RD and WH-CM architectures provide enhanced performance against their Fourier based counterparts for signals employed in CDMA networks and in particular their baseband and descrambled version. Also due to the structure of these signal types the WH based architectures perform channel sensing instead of frequency spectrum sensing.

The next Chapter will investigate and propose a generic CS framework, which will incorporate the three CS models presented in the previous Chapters, enabling it to handle a wide range of signal types employed in CR networks.

Chapter 7

Integration of the AR, MT and WH based Models into a Generic CS Framework

7.1 Introduction

In the previous Chapters 4, 5 and 6 novel CS models were presented, respectively based on AR filter, the MT method and the WH transform. All models were found to be suitable for specific types of signals only. In particular, the AR-based CS model is suitable for digitally modulated signals of the QAM family, not being able to exploit the favourable properties of the MT method when the AR filter coefficients are not available. On the other hand the MT-based CS model is suitable for narrowband modulation only and its design does not permit to effectively use an AR filter even if the relevant coefficients were available. As for the WH-based WH-CS model, it is specifically suited for signals sparse in the WH domain and not in the Fourier.

As far as the AR-based CS model is concerned, its performance has not been investigated with access schemes like OFDM, which is widely proposed in CR network standards such as LTE-Advanced and IEEE 802.11af, as discussed in Section 3.3.3. Moreover, if the AR-based CS model is to be employed for spectrum sensing for CR purposes, it has to perform classification of the spectral bands (Hossain & Bhargava, 2007; Haykin et al., 2009) and even under the existence of three possible classification states instead of two, as mentioned in Section 2.3.2.3.

The above provided the motivation to investigate ways to integrate the three novel CS models into a generic framework in order to widen the range of applicable signals. To this end, the unification of the AR-based CS and MT-based CS will be first presented to form a *unified* CS (UNI-CS) model, followed by a discussion of spectral classification and then the formation of the generic framework from the UNI-CS and

WH-CS. It is noted that the UNI-CS and consequently the generic framework are applicable to both RD and CM.

The UNI-CS model, the spectral classification discussion and the generic framework will be presented in *Section 7.2*. The simulation setup and critical results discussion are presented in *Sections 7.3* and *7.4* respectively. Finally a summary of the key findings from this model are provided in *Section 7.6*.

7.2 The UNI-CS Model

Looking at equations (4.14), (4.21) and (5.8), (5.14) it is concluded the operations of the AR-based CS and MT-based CS models are determined by either matrices C or S respectively being applied in the signal recovery stage. S is signal independent because MT is a non-parametric spectrum estimator, with the constituent elements depending only on the slepian sequences and their eigenvalues, which are entirely defined by the signal length and bandwidth resolution (Haykin et al., 2009).

This means the elements of the MT recovery matrices G_{MT} , G_{MT}^{CM} of the MT-RD and MT-CM respectively, can be stored for reuse in the same manner the elements of the recovery matrix G, are in (Ragheb et al., 2008). This will have the effect of a permanent integration of the MT spectrum estimator, hence endowing the RD and CM with a permanent performance improvement when dealing with narrowband signals and no degradation in the case of digitally modulated ones.

C is not signal independent, nevertheless in the absence of the AR filter coefficients it relaxes to the unitary matrix I, as it can be deduced from (4.9), (4.10) for $\alpha_k=0$. In such a case, even if it is integrated into the MT-RD or MT-CM structures, it will not affect their operation. Only when there is a set of non-zero coefficients the precolouring effect will take place.

Next step therefore is to integrate precolouring to the MT-RD and MT-CM architectures and subsequently determine the recovery matrix for the resulting designs, which will combine both MT and precolouring. Assuming that matrix S is stored in the RD, then according to (5.7), (5.8), (5.9) the MT-RD performs

recovery of the MT version of the Fourier transform f_{MT} of the signal $x_{MT}=Sx$ by solving:

$$y = Ax = AS^{-1}F^{-1}f_{MT} = G_{MT}f_{MT} \qquad (7.1)$$

for f_{MT}. In a similar fashion and according to (4.8), (4.13) and (4.14) the AR-RD performs the recovery of the coloured version of the Fourier transform f_c of the signal $x_C=Cx$ by solving:

$$y = AC^{-1}F^{-1}f_C = G_C\ f_C \qquad (7.2)$$

for f_c. It follows that if precolouring is to be applied to x_{MT} instead of x then its precoloured version x_{CMT} will be:

$$x_{CMT} = Cx_{MT} = CSx \qquad (7.3)$$

with its Fourier transform being:

$$f_{CMT} = Fx_{CMT} = FCx_{MT} = FCSx \qquad (7.4)$$

Based on (7.4), a unified RD-based architecture, termed UNI-RD, recovers the coloured-MT version f_{CMT} by first taking the measurement vector $y=Ax$ and then solving the following equation

$$y = Ax = AS^{-1f}C^{-1}F^{-1}f_{CMT} = G_{CMT}f_{CMT} \qquad (7.5)$$

for f_{CMT}, with $G_{CMT} = AS^{-1}C^{-1}F^{-1}$ being the *precolouring-multitaper* (PM-MT) recovery matrix. The block diagram of UNI-RD is shown in Figure 7.1. Its operation

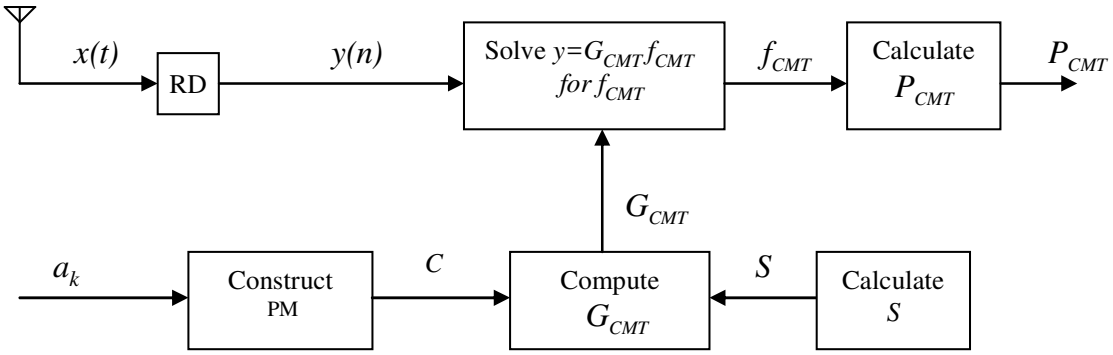

Figure 7.1: Block Diagram of the UNI-RD architecture.

is determined by the presence of the AR coefficients. In their presence, where it is assumed a digital modulation is present, the benefits of precolouring are exploited. In the absence of the AR coefficients, C relaxes to the unitary matrix, therefore precolouring is not active and the benefits of the MT spectrum estimation are derived. The corresponding pseudo code for the UNI-RD architecture is given in the algorithm 7.1.

Algorithm 7.1: Pseudo code for the UNI-RD architecture

Inputs: signal $x(n)$ of length N samples

Variables: M- number of measurements or equivalently length of $y(n)$, p- the AR filter order, F- the $N \times N$ DFT matrix, A- the $M \times N$ measurement matrix, W- the resolution of the MT estimator.

Outputs: P_{CMT} of $x(n)$

---

1. **Initialise** M, F, p, W
2. ***Calculate*** AR filter coefficients α_k from $x(n), p$
3. ***Construct*** A
4. ***Construct*** S from (5.5)
5. **Calculate** $y(n)=Ax(n)$
6. ***Construct*** C from (4.10)
7. **Calculate** $G_{CMT} = AS^{-1}C^{-1}F^{-1}$
8. ***Apply*** l_1 minimisation algorithm to solve $y = G_{CMT} f_{CMT}$ for f_{CMT}
9. ***Calculate*** $P_{CMT} = \left| f_{CMT} \right|^2$

10. **END**

A multi-channel version of the UNI-RD is also presented in Figure 7.2. For this thesis the single-channel UNI-CS architectures employ the same matrix S, though apparently the design requirements could dictate the use of different matrices. Therefore as in the *i*PM-RD case, the individual UNI-RD architectures are defined by the respective measurement and recovery matrices.

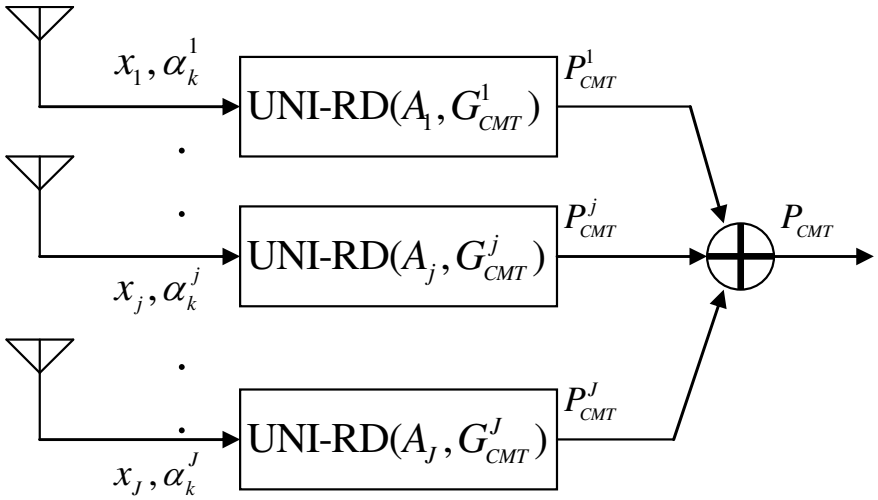

Figure 7.2: Block Diagram of the multi-channel UNI-RD architecture, with J channels.

As for the CM architecture, the integration of precolouring and MT is attained in an analogous manner to that of the RD. For each input signal x_j to the CM, the corresponding PM matrices C_j are calculated, while the elements of the MT matrix S could be generated and made available for reuse by every channel, as mentioned in Section 2.2. Applying (7.4) to each of the signals x_j, a coloured-MT version of the corresponding Fourier transform can be derived:

$$f_{CMTj} = Fx_{CMTj} = FCx_{MTj} = FC_jSx_j \qquad (7.6)$$

Based on (7.6) the output of the CM in (5.12) is expressed as follows:

$$y = \sum_{j=1}^{J} \Phi_j x_j = [\Phi_1, \Phi_2, .., \Phi_J] \begin{bmatrix} x_1 \\ x_2 \\ . \\ . \\ x_J \end{bmatrix} = [\Phi_1, \Phi_2, .., \Phi_J] \begin{bmatrix} S^{-1}C_1^{-1}F^{-1}f_{CMT_1} \\ S^{-1}C_2^{-1}F^{-1}f_{CMT_2} \\ . \\ . \\ S^{-1}C_J^{-1}F^{-1}f_{CMT_J} \end{bmatrix} =$$

$$= [\Phi_1 S^{-1}C_1^{-1}, \Phi_2 S^{-1}C_2^{-1}, .., \Phi_J S^{-1}C_J^{-1}] \begin{bmatrix} F^{-1} & & & & \\ & F^{-1} & & & \\ & & . & & \\ & & & . & \\ & & & & F^{-1} \end{bmatrix} \begin{bmatrix} f_{CMT_1} \\ f_{CMT_2} \\ . \\ . \\ f_{CMT_J} \end{bmatrix} =$$

$$= [\Phi_1 S^{-1}C_1^{-1}F^{-1}, \Phi_2 S^{-1}C_2^{-1}F^{-1}, .., \Phi_J S^{-1}C_J^{-1}F^{-1}] \begin{bmatrix} f_{CMT_1} \\ f_{CMT2} \\ . \\ . \\ f_{CMTJ} \end{bmatrix} =$$

$$= [G_{CMT_1}, G_{CMT_2}, .., G_{CMT_J}] q_{CMT} = G_{CMT}^{CM} q_{CMT} \qquad (7.7)$$

where G_{CMT}^{CM} being the *precolouring-multitaper* (PM-MT) recovery matrix for the unified CM-based architecture, termed UNI-CM, and vector q_{CMT} the combined PM-MT representation of the signals $x_1, x_2, .., x_J$ in the Fourier domain. Therefore the UNI-CM, recovers the coloured-MT version q_{CMT} by first taking the measurement vector y and solving afterwards (7.7) employing CS algorithms. The block diagram of the UNI-CM architecture is shown in Figure 7.3.

The corresponding pseudo code for the UNI-CM architecture is given in the algorithm 7.2.

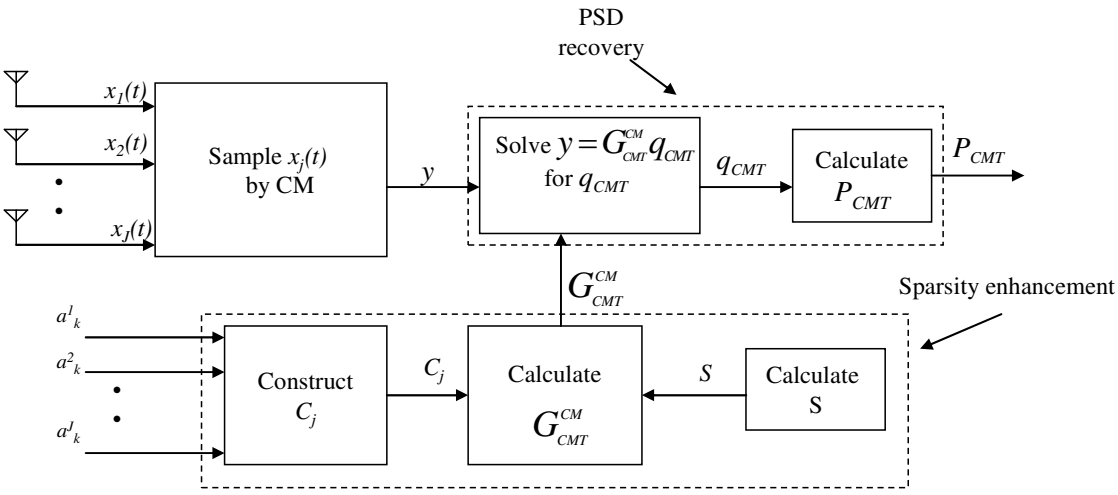

Figure 7.3: Block Diagram of the UNI-CM architecture.

Algorithm 7.2: Pseudo code for the UNI-CM architecture

Inputs: signals $x_j(n)$ of length N samples, $j=1,..,J$

Variables: p- the AR filter order, F- the $N \times N$ DFT matrix, Φ_j- the $N \times N$ measurement matrices, $j=1,..,J$, W- the resolution of the MT estimator.

Outputs: Combined P_{CMT} of $x_j(n)$, $j=1,..,J$

1: ***Initialise*** F, p

2: ***Calculate*** AR filter coefficients a_k^j from $x_j(n)$, p, $j=1,..,J$

3: ***Construct*** Φ_j, $j=1,..,J$

4: **Calculate** $y = \sum_{j=1}^{J} \Phi_j x_j$

5: ***Construct*** S from (5.5)

6: ***Construct*** C_j from (4.10), $j=1,..,J$

7: ***Calculate*** $G_{CMT_j} = \Phi_j S^{-1} C_j^{-1} F^{1}$, $j=1,..,J$

8: **Construct** G_{CMT}^{CM} by **concatenating** matrices G_{CMT_j}, $j=1,..,J$

9: ***Apply*** l_1 minimisation algorithm to solve (7.7) for q_{CMT}

10: ***Calculate*** $P_{CMT} = \left| q_{CMT} \right|^2$

11: **END**

So far in this Section the UNI-CS model, shown in Figure 7.4, has been presented. It is applicable to both RD and CM, and capable of processing wideband and narrowband signal types as a result of the seamless integration of both precolouring and MT methods. A discussion on spectral classification now follows.

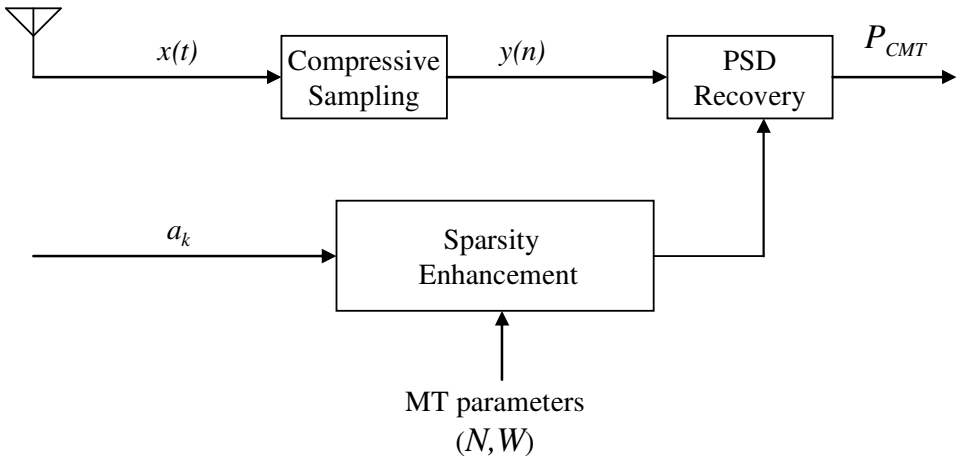

Figure 7.4: Block diagram of the generic UNI-CS model.

7.2.1 Spectral Classification

As discussed in Section 2.3.2, a major task in CR is spectrum sensing, which pertains to the assignment of a state to the spectral bands/frequencies regarding their occupancy status. This assignment process is called spectral classification and the signal PSD is the basis for it.

In Section 2.3.2 it was also discussed that if the spectral classification assumes the existence of only two occupancy states, then the SU in a CR network will miss the opportunity to exploit the so-called gray areas of the spectrum. In these areas the signal of PU is present but weak to be of use, rendering the relevant channel useful for a CR SU. However, with the consideration of only two occupancy states, the gray spectral bands are identified as occupied and not as opportunities for the SU, apparently impacting the efficient use of the spectrum available for a CR network.

In the light of the above mentioned pertaining to the existence of the gray spectral bands, a novel spectral classification procedure is proposed, where all three possible utilization states of a spectral band are considered. To assign a frequency band into

one of the three states, two energy/power thresholds T_1 and T_2 must be defined which respectively determine the existence of either a vacant or occupied frequency. Intermediate values characterize the gray spectral areas. T_1 is set to the average input noise level, so at a specific frequency, if the average energy within the corresponding spectral band is lower than T_1, only noise is present and the frequency is classified as vacant and available for a SU to access in a CR network. T_1 level is given by

$$T_1 = \frac{P_{total}}{1 + 10^{\frac{SNR}{10}}} \tag{7.8}$$

Hence it is a function of the signal input SNR and P, the latter being the total signal plus noise power over bandwidth B. Both SNR and P can be measured with conventional analog test equipment.

To set T_2, as signals of interest are generally frequency sparse, the average signal power can be very low, much closer to the noise level T_1 than the average power within occupied bands, hence it is not a good candidate for determining T_2. Instead the *root mean square* (RMS) value of the signal PSD is used, since it gives values greater than the average power, closer to that of the occupied bands. Actually the sparser the signal is, the lower the RMS value of its PSD. If the average energy within a spectral band is higher than T_2, then the band is classified as occupied and unavailable for SU access.

In general the spacing between T_1 and T_2 is location-specific. For example, it will be notably narrower in a building than in an outdoor line-of-sight environment (Haykin, 2007). In this thesis communications in an open environment are assumed.

The next step is to determine the energy within each band. The bandwidth B of a sparse signal with known PSD from a CS architectures like the UNI-RD or UNI-CM, is scanned at a resolution Δf to determine the average energy within spectral bands of width b (the bandwidth per carrier), such that $B=N\Delta f$ and $b=m\Delta f$, where m and N are positive integers. N is the number of samples which if the signal would have been sampled at the Nyquist rate, while m denotes the number of frequency resolutions

within the band. It is assumed the occupancy status assigned to a specific band, applies to all the individual frequencies of width Δf within this band, so if a band is occupied, all frequencies within this band are considered occupied and none can be used by a SU as a carrier frequency. The energy within a band having a centre frequency f_i is given by:

$$E(f_i) = \sum_{i-\frac{m}{2}+1}^{i+\frac{m}{2}} P(f_i)\Delta f \qquad (7.9)$$

where $i = \frac{m}{2},..,N-\frac{m}{2}$.

A *frequency classification vector* is now formed comprising entries corresponding to the frequencies f_i, by assigning the value 1 for an occupied frequency, 0 for vacant and ½ for gray. A *reference vector* is also introduced, which represents the real occupancy status within B, where active carrier frequencies along with these around them and for a width equal to b are assigned the value 1, while all other frequencies are 0. In the ideal case, the status of the bands is always known so there are no gray frequencies, and they are all either occupied or vacant. The accuracy of the spectral classification process is measured by comparing the frequency classification and reference vectors, using their Euclidean distance. The lower the Euclidean distance between the vectors, the higher the classification accuracy and the relevant performance of a CS structure like the UNI-RD and UNI-CM, which have derived the PSD.

The next section presents a generic CS framework, which encompasses both the UNI-CS and WH-CS models.

7.2.2 A Generic CS Framework

The UNI-CS model described above is applicable to frequency sparse signals only. In order to widen the range of applicable CR related signals and include those being sparse in the WH domain such the CDMA encoded ones, the WH-CS model has to be integrated to the UNI-CS.

The two models and in particular their recovery stages are designed to process signals which are sparse in a specific domain only, therefore the UNI-CS is not able to handle sequency sparse signals while the WH-CS model is not able to handle the frequency sparse ones. To achieve this, the two sparsity basis matrices, that is the DFT and WHT respectively, would have to be integrated to one. However, this is not feasible since they represent completely different domains hence the integration cannot be implemented by unifying the two models to one. Instead, both are to function in parallel, as shown in Figure 7.5 depicting the generic CS framework. Since UNI-CS and WH-CS models have been found to be applicable to RD and CM, the same also holds for the framework, the function of which is described as follows.

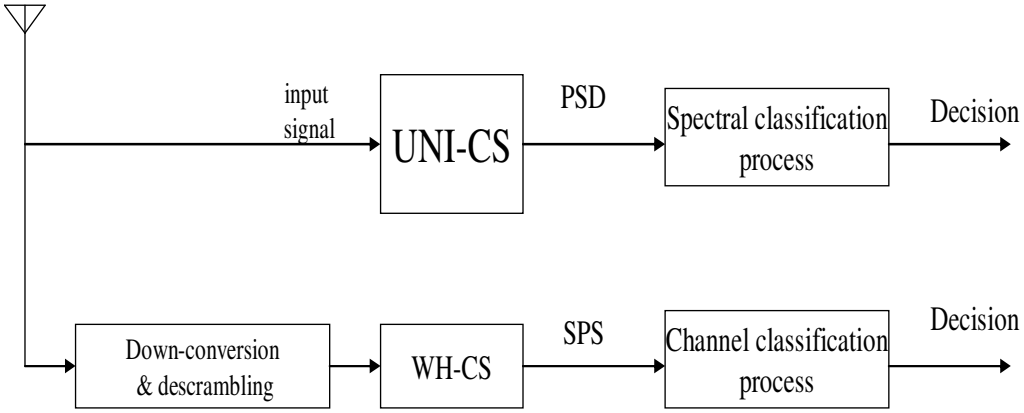

Figure 7.5: The Generic CS Framework.

As observed in Figure 7.5, the input signal is fed to both models. There are three possibilities regarding the input signal types as far sparsity is concerned:

a. The signal is frequency sparse only and there is no CDMA encoding: In this case the UNI-CS will be able to derive the respective PSD and a spectral classification decision will be taken, which would be exploited by a SU in a CR network. Since the signal is not CDMA, it is not recognisable by the descrambling process, so it will be virtually filtered out. Hence the WH-CS model and the channel classification will not derive any information for potential SU in a CR setting.

b. The signal is CDMA encoded, hence sparse only in the sequency domain: As discussed in Chapter 6, such signals occupy a large portion of the available bandwidth and they are not frequency sparse. Therefore, in this case the UNI-CS and the subsequent spectral classification is unable to identify any pronounced frequency bands occupied by a PU. On the other hand, the WH-CS model and the respective channel classification will be able to extract the active CDMA channels, so in this case the information from the WH-CS model and the channel classification process can be utilised by a SU in a CR network, while this does not hold for the outcome from the spectral classification.

c. Both signal types of a. and b. are present at the input to the framework: Since the CDMA signal is spread throughout the frequency spectrum and its energy present in each frequency is very low (Rgheff, 2007), the overall frequency sparsity is not affected. Hence the dominant components of the frequency sparse signal will still be pronounced in the combined PSD and the spectral classification information could still be exploited by the SU in a CR network. As for the combined SPS, it will still be able to depict the dominant sequency components of the CDMA input, since the non-encoded frequency sparse signal will be filtered out by the descrambling process. Therefore, the channel classification information can be used by a SU in a CR network.

In conclusion, the presented generic CS framework, applicable to both RD and CM, can process both frequency and sequency sparse signals simultaneously and independently, regardless of the types of sparsity that exist within the input signal. The independent function of the branches permits a modular framework structure, which adds flexibility to its design. Each of the branches provides useful outcomes for the SU only if the portion of constituent of the input signal which has the appropriate sparsity type.

The next Section presents the simulation setup for both RD and CM versions of the framework, with Section 7.4 then critically analysing their respective performances.

7.3 Simulation Setup

As discussed in Section 7.2.2. the UNI-CS and WH-CS branches of the generic framework operate independently and provide useful outcomes for signals having frequency and sequency sparsity respectively. For the WH-CS, its performance has already been investigated and analysed in Chapter 6. In regards to the UNI-CS, the findings in Chapters 4, 5 reveal that it is suitable for both digital and analog modulation schemes, since it is the unification of the AR-based CS and MT-based CS models. However, it has not been tested for more complicated and closer to real world signals such as OFDM access schemes.

To this end, the performance of the UNI-CS will be critically evaluated in comparison with the traditional RD and CM architectures when the signals involved are based on OFDM. The first simulation scenario considers two OFDM channels, corresponding to respective PU signals. The signals are received by a potential CR receiver that derives the combined signal PSD employing either the classical RD and CM architectures or the respective UNI-RD and UNI-CM ones. It is assumed that the AR filter coefficients for each OFDM channel are available to either a multi-channel version of the UNI-RD or the UNI-CM. Moreover, the CR receiver can sense a sparse spectrum bandwidth B of approximately 34MHz and 43MHz for the LTE and 802.11af standards respectively. For the AR coefficients in particular, simulations were performed for both 4^{th} and 8^{th} AR filter orders, so to investigate the performance improvement when transitioning from 4^{th} order CS architectures to 8^{th} ones regardless the added filter latency discussed in Section 4.4. As with the simpler digital modulation schemes discussed in Chapter 4, the positions of the OFDM channels within B are unknown. The OFDM signal parameters are shown in Table 3.2.

For this scenario, the comparison of the classical RD and CM architectures against their counterparts UNI-RD and UNI-CM respectively is made with the same metrics employed in Chapters 4, 5, that is PSD spectral leakage against sampling rate and input SNR.

The second scenario pertains to the spectral classification performance of the CS architectures. Both UNI-RD and UNI-CM are respectively compared with their classical counterparts RD and CM. As discussed in Section 7.2.1, the characteristics of the spectral classification is the bandwidth B, the resolution Δf at which the latter is

scanned and the width $b=m\Delta f$ of the spectral band in which the average signal energy is calculated. For this scenario, b is the OFDM channel bandwidth, so the value of m is equal to the number of the sub-carriers in an OFDM channel that is 144 for 802.11af and 181 for LTE. The performance metric is the similarity between the frequency classification vector and reference vector and is the reciprocal of their Euclidean distance, as discussed in Section 3.4. The corresponding classification vectors for each of the RD, 4th order UNI-RD and 8th order UNI-RD are compared with the reference vector to derive the respective similarities across different input SNR values. The same procedure is also followed for the CM based architectures, classical CM, 4th order UNI-CM and 8th order UNI-CM.

7.4 Simulation Results Discussion

As in the previous three Chapters, algorithms 7.1 and 7.2, which correspond respectively to the UNI-RD and UNI-CM architectures, are firstly validated using the sparsity metric. The signals employed are OFDM LTE, and the active frequency threshold is set at 20dB relative to the maximum energy value, with the sparsity being measured across a range of input SNR and the sampling rate set at 12.5% of the Nyquist frequency.

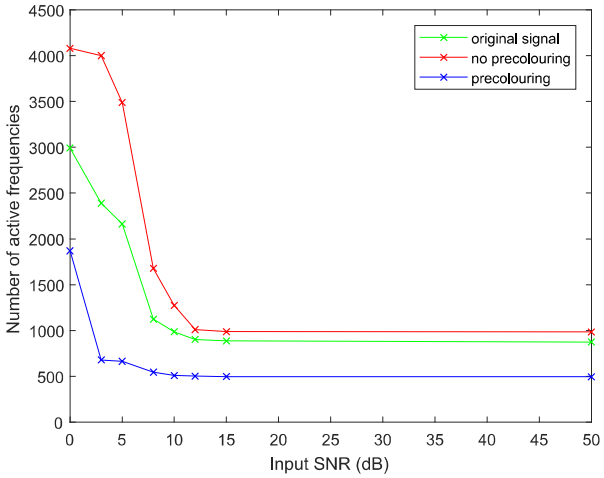

Figure 7.6. The effect of precolouring on sparsity of an OFDM signal using algorithm 7.1.

The results in Figures 7.6 and 7.7 are respectively for algorithms 7.1 and 7.2. As with the sparsity measurements in Chapters 4, 5 and 6, they reveal that when precolouring is applied (blue curves) signal sparsity is enhanced and there is a significant noise reduction. In contrast, with no precolouring (red curves) the CS progressively degrades compared with the original signal (green curves) due to the sub-Nyquist sampling.

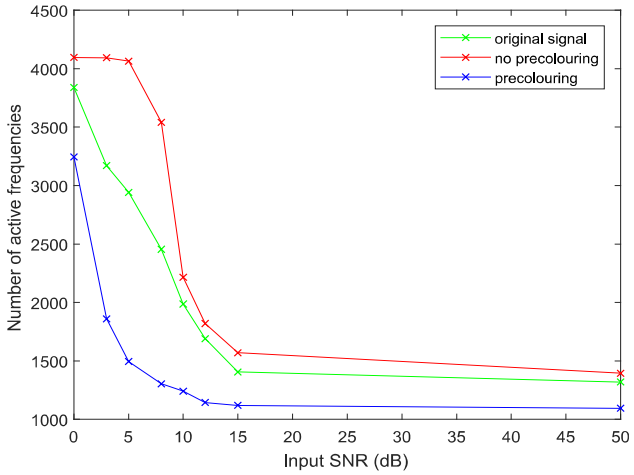

Figure 7.7. The effect of precolouring on sparsity of an OFDM signal using algorithm 7.2.

Next this Section analyses the results pertaining to the comparison of the RD and the UNI-CS for both LTE Advanced and 802.11af. The PSD spectral leakage against sampling rate is shown in Figure 7.8, with input SNR set to 8.1dB (Werther & Minihold, 2013; Flores et al., 2013). It is evident that for both standards the resulting PSD spectral leakage for the 4^{th} order UNI-RD is consistently lower across the range of sampling rates, providing an overall spectral leakage improvement approximately 33% with both standards taken into account. In the UNI-RD case the average spectral leakage is always lower than 20%, while it is always above 15% for its classical RD counterpart. The 8^{th} order UNI-RD provides a further spectral leakage improvement of approximately 11% compared with the 4^{th} order counterpart. The robustness of the UNI-CS compared to the RD is also manifested in Figure 7.9, where the spectral leakage against input different input SNR levels is depicted. The sampling rate is chosen at 25.25% of Nyquist rate. As in Figure 7.8, the spectral leakage is always lower in the case of the 4^{th} order UNI-RD, with an average improvement about 50% with both standards taken into account. The 8^{th} order UNI-RD provides a further

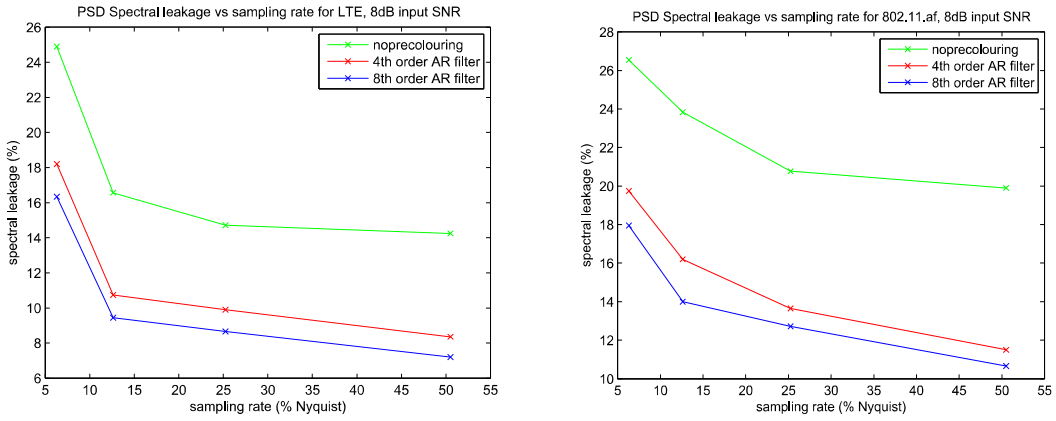

(a) (b)

Figure 7.8: PSD spectral leakage vs sampling rate for (a) LTE Advanced, (b) 802.11af standards, with RD, UNI-RD 4th order and UNI-RD 8th order employed.

spectral leakage improvement of approximately 13% compared with the 4th order counterpart. The improvement is more enhanced with progressively lower input SNR values, while with higher input SNR the three graphs converge. This happens because the precolouring effect is more pronounced when noise becomes significant and the signal dynamic range is reduced, which is not the case when input SNR gets larger values and the noise content and the signal dynamic range are reduced.

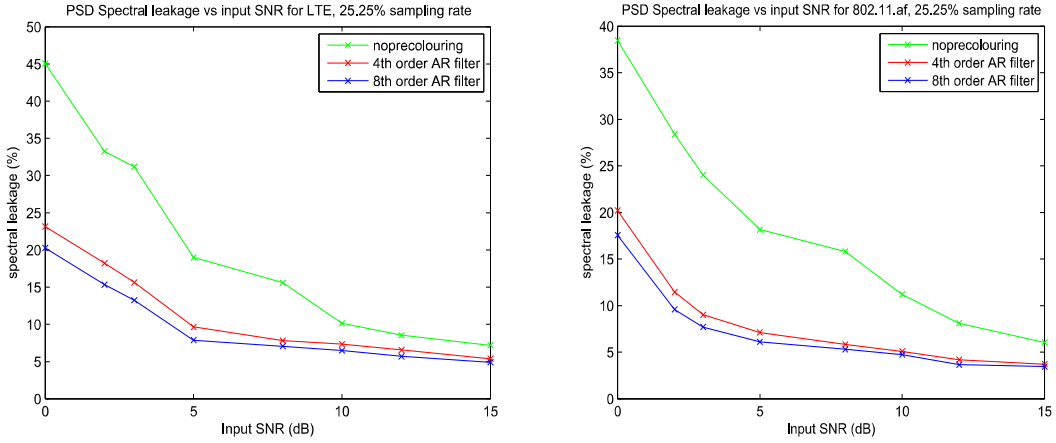

(a) (b)

Figure 7.9: PSD spectral leakage vs input SNR for (a) LTE , (b) 802.11af standards, with RD, UNI-RD 4th order and UNI-RD 8th order employed.

The spectral leakage improvement is also evident when the classical CM and the UNI-CM architectures are employed. The latter provides enhanced robustness as it is

shown in Figure 7.10. When the 4th order UNI-CM is compared with the CM, the PSD spectral leakage improvement against input SNR is approximately 48% with both standards considered. The 8th order UNI-CM provides a further spectral leakage improvement of approximately 15% compared with the 4th order counterpart. As with the RD and UNI-RD, the graphs converge as the input SNR takes larger values.

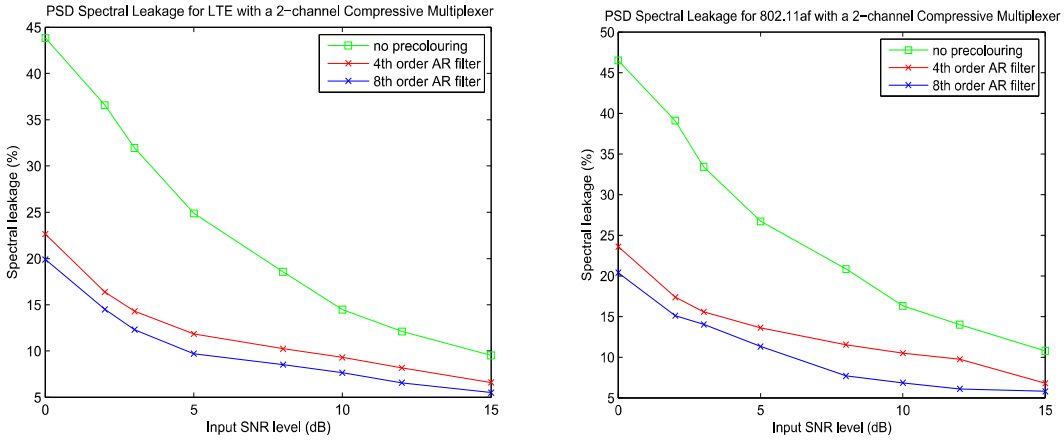

(a) (b)

Figure 7.10: PSD spectral leakage vs input SNR for (a) LTE (b) 802.11af standards, with CM, UNI-CM 4th order and UNI-CM 8th order employed.

The enhanced performance of the UNI-CS is due to the nature of the OFDM signals. The relevant sub-carriers employ digital modulation schemes hence the benefits of precolouring apply to them as well, giving emphasis to the dominant frequencies within the bandwidth B, while attenuating the weaker ones. This is further illustrated in Figures 7.11 and 7.12 where the PSDs of the LTE Advance and 802.11af standards are respectively displayed. The input SNR is set to 0dB in order to clearly show the robustness of precolouring method while the sampling rate is indicatively chosen at approximately 25.25% of Nyquist although other rates could have been employed. From Figures 7.11a and 7.12a where the PSD graphs for the classical RD and the 4th order UNI-RD are presented, it is apparent that the spectral leakage is higher in the case of the RD than the UNI-RD. Further improvement is noticed when the 8th order UNI-RD is employed as shown in Figures 7.11b and 7.12b where the graphs corresponding to the 4th order and 8th order UNI-RD are shown.

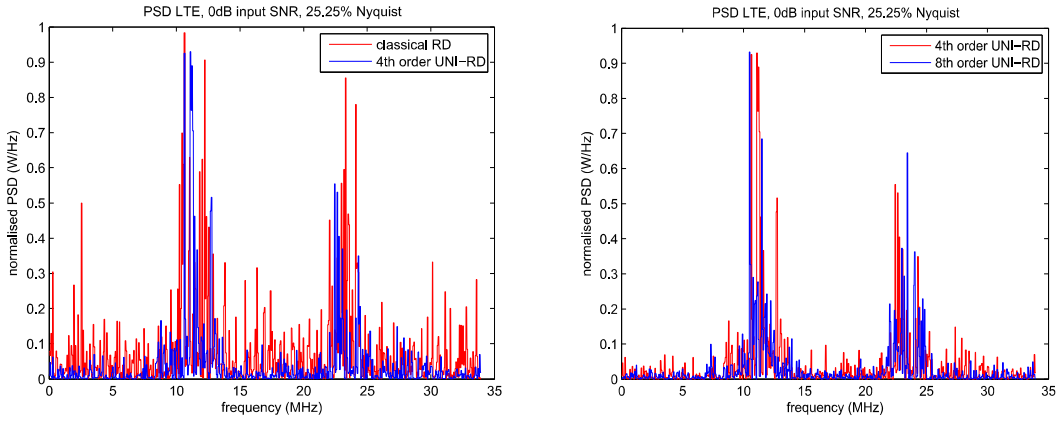

(a) (b)

Figure 7.11: Comparison of PSD graphs for (a) classical RD, 4th order UNI-RD and (b) 4th order UNI-RD and 8th order UNI-RD with LTE signals.

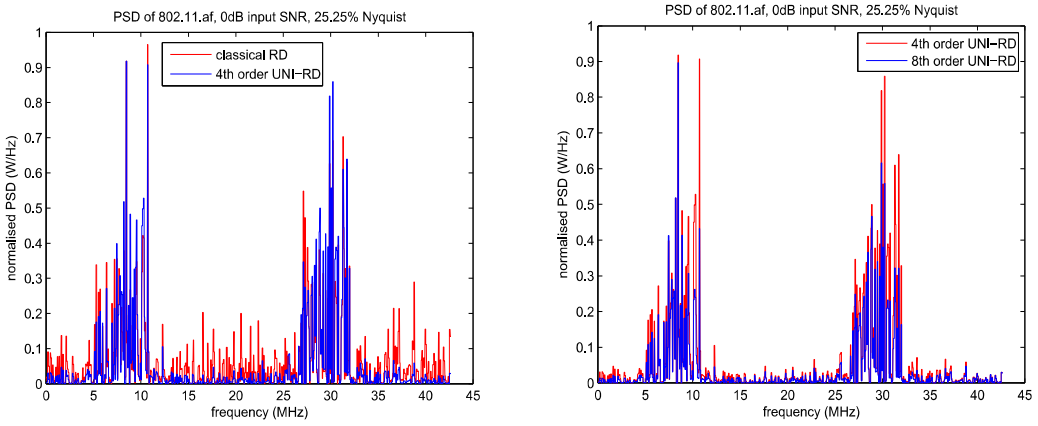

(a) (b)

Figure 7.12: Comparison of PSD graphs for (a) classical RD, 4th order UNI-RD and (b) 4th order UNI-RD and 8th order UNI-RD with 802.11.af signals.

Next, the spectral classification performance of the UNI-RD and UNI-CM architectures is investigated and critically analysed. The similarities for the RD based architectures and for both LTE Advanced and 802.11.af are shown in Figure 7.13. The graphs reveal the enhanced classification performance that is achieved with the CS architectures based on precolouring. For both 4th and 8th order UNI-RD, the similarity is larger across the entire range of input SNR values. Moreover, when SNR reaches -3dB the RD similarity graph reaches a steady state lowest value of approximately 0.025. From this it is inferred that the RD-based classification collapses below this

-3dB threshold. The 4th order UNI-RD reaches this steady state condition at the same threshold, however it performs better for larger SNR values as the graphs reveals.

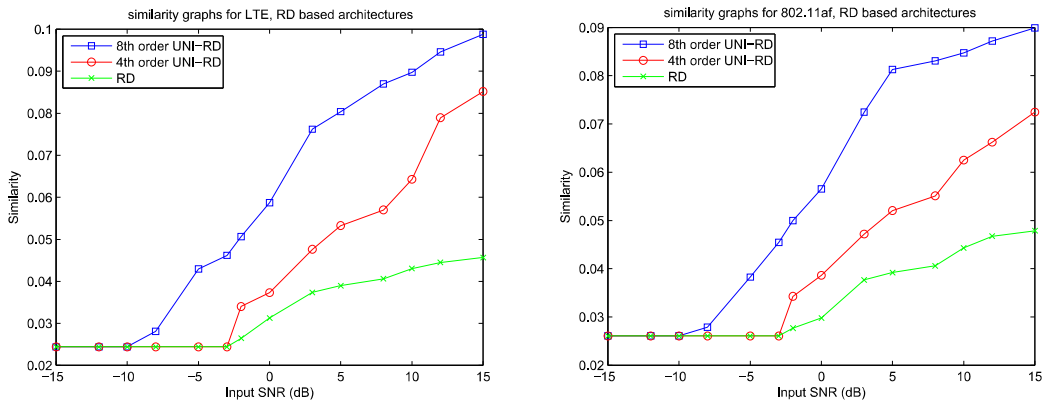

(a) (b)

Figure 7.13: Comparison of spectral classification performance of RD, 4th order UNI-RD and 8th order UNI-RD, (a) LTE and (b) IEEE.802.11.af.

The 8th order UNI-RD proves to be more robust since it reaches its steady state at -10 dB. The remarks above are also valid for the CM, 4th order UNI-CM and 8th order UNI-CM, as it is revealed from their respective similarity graphs depicted in Figure 7.14.

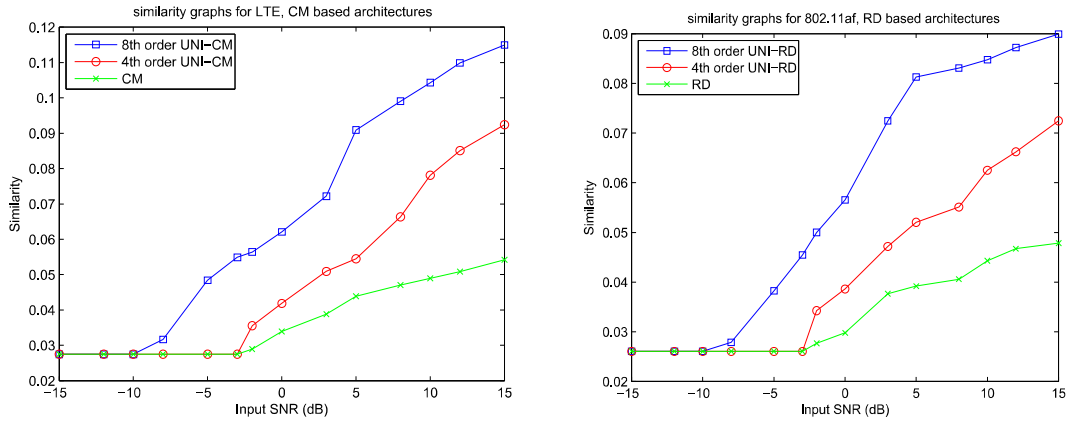

(a) (b)

Figure 7.14: Comparison of spectral classification performance of CM, 4th order UNI-CM and 8th order UNI-CM for (a) LTE and (b) 802.11af.

In summary, by virtue of its two parallel and independently operating branches, the generic CS framework is adept at processing a diverse range of sparse signals that

comprise digital and narrowband modulations and also different access schemes including OFDM and CDMA. This has been achieved by employing two different sparsity bases. The first is a modified DFT matrix tailored according to the structure of the signals to be processed by the UNI-CS model. It incorporates both sparsity bases that are employed in the AR-based CS and MT-based CS models. The second basis is the WHT matrix which expands the concept of sparsity beyond the Fourier domain so to include signals sparse in the WH/sequency domain.

7.5 Summary

This Chapter has presented a generic CS framework, which incorporates the contributions of this Thesis presented and discussed in the previous Chapters 4, 5 and 6. It seamlessly integrates the AR-based CS and MT-based CS models into the UNI-CS model, while the nature of the signals involved permitted the incorporation of the WH-CS model as well, as a separate and independent branch of the framework. Both frequency and sequency sparse signals are applicable, while the framework can be implemented with either employing RD or CM based architectures. The framework carries all the advantages of the individual models is comprised of, while it provides the additional benefit of flexibility by not limiting its function to specific types of signals. Moreover, its modular structure gives design flexibility, while providing a way forward for future enhancements by adding more branches in order to exploit sparsities in other domains. To this end, the next Chapter presents some ideas for future extensions of the CS framework based on the findings from this Thesis.

Chapter 8

Conclusion

Today's world is experiencing an unprecedented proliferation of wireless devices and services. This fact, coupled with the further significant anticipated growth, has led to a continuously increasing demand for higher transmission rates in wireless communications and networks. This is a great challenge given the limited availability of radio spectrum and the problem becomes even more acute by a rigid regulatory framework and large spectrum underutilisation. The latter has prompted regulators to promote the concept of opportunistic spectrum access, which allows *secondary users* (SU) to access unoccupied bands licensed to *primary users* (PU). *Cognitive radio* (CR) technology offers an attractive solution to the spectrum underutilisation, but encounters major challenges like high sampling rates and low number of available samples due to the stringent timing requirements. *Compressive sensing* (CS) is a new signal acquisition paradigm for signals being sparse in some domain, which has the potential to address the above issues by acquiring few measurements at sampling rates well below Nyquist. However, existing CS architectures, such as the random demodulator (RD) and the compressive multiplexer (CM), have limitations pertaining to the applicable signal types, the spectrum estimation methods employed, the identification of the occupancy status of spectral bands and the exclusive reliance on frequency sparse signals. This provided the context for the research question addressed in this project.

This thesis has presented a novel, generic, flexible and robust CS framework that enhances CS performance and addresses the above mentioned limitations of the CS architectures. The framework is the most important scientific contribution being able to process a wide range of signals encountered in wireless networks. It employs the *discrete Fourier transform* (DFT) matrix as the sparsity basis which is accordingly modified to increase frequency sparsity and thereby enhance performance pertaining to a diverse range of digital and analog modulations as well as access schemes like the

orthogonal frequency division multiple access (OFDMA). It expands the concept of sparsity beyond the frequency domain by utilising the *Walsh-Hadamard transform* (WHT) matrix as the sparsity basis so to include sequency sparse signals within a *code division multiple access* (CDMA) scheme. The new framework has been critically evaluated for a range of test signals as well as signals whose parameter settings are wireless network compliant such as those defined in current CR network standards such as LTE-Advance and IEEE 802.11af. The new framework integrates the following suite of innovative models:

a. A new autoregressive with CS (AR-CS) model capable of operating in both single and multi-channel modes and is applicable to both RD and CM architectures. It employs AR filtering to precolour the signal thereby increasing frequency sparsity and consequently enhancing CS performance. The precolouring process is seamlessly integrated to the model with the modification of the DFT matrix to form a new frequency sparsity basis. While the AR method is parametric and the model assumes *a priori* knowledge of the AR coefficients, this is not a major obstacle since such coefficients can be easily derived by the PU for speech coding purposes. Rigorous simulations with various digital modulation schemes, confirm that the AR-CS model exhibits superior spectral leakage and robustness performance compared with the classical RD and CM architectures.

b. A new multitaper with CS (MT-CS) model which embeds a variant of the MT method. The model employs the parameters of the MT method to modify the DFT matrix and create a new MT-based Fourier basis. The non-parametric nature of the MT method permits its seamless integration into the existing CS architectures without imposing either any computational burden or requiring cooperation from the PU. While simulation results have shown the MT-CS model provides both improved CS and robustness performance, these benefits are achieved for analogue modulation schemes, while for digital modulation schemes equivalent CS performance of signals is achieved compared with the classical RD and CM counterparts.

c. Given their signal sparsity enhancements focus on different modulation classes, the AR-CS and MT-CS models in (a) and (b) are combined to create the unified CS (UNI-CS) model. This embraces the advantages of both individual models by seamlessly integrating the AR and MT methods. UNI-CS has also been critically evaluated as a spectral classifier, and its ability to identify the occupancy status of a frequency band which is vital for spectrum sensing in CR applications. Moreover UNI-CS is a more robust spectral classifier, since it consistently provides more accurate spectral classification compared to its classical counterparts across a range of input SNR values.

d. Finally, the novel Walsh-Hadamard with CS (WH-CS) model considers signals that are sparse in domains other than frequency. In particular, sequency sparse signals, such those arising in the CDMA scheme. To this end, the WH-CS model exploits sequency sparsity using a WHT matrix as a sparse basis instead of a DFT. Simulation results have shown that while the frequency-based models are not able to recover the sequency sparse CDMA signals, the WH-CS model is capable of achieving channel sensing by successfully recovering CDMA signals and thereby more accurate identification of CDMA channel status.

In summarising, the new generic CS framework makes a notable contribution to the field of efficient spectral/channel sensing for the diverse range of signals encountered in today's wireless networks and CR-based standards. It offers a flexible and robust solution for enhanced CR spectrum sensing, which is both seamlessly extendible to other potential sparsity domains as well as also being embedded into different CS architectures to enhance their performance.

Chapter 9

Future Work

There are a number of rich opportunities to enhance and extend the generic CS framework presented in this thesis thereby affording new research directions. Since the framework consists of individual components, any enhancement will by its nature relate to specific blocks. Some potential new research pathways will now be reviewed.

a. While two CS architectures have been exploited for this generic CS framework, other existing CS architectures were highlighted in Section 2.4.3. These are based on the frequency sparsity and utilize the DFT matrix as the sparsity basis. Consequently it would be insightful to study the applicability of these particular architectures to the generic CS framework and to critically evaluate their performance under the alternative sparsity bases presented in this thesis. This could lead to enhancing both the scope and performance of the new framework by exploiting the distinctly advantageous features of these particular CS architectures.

b. The modulation types employed in this thesis were digital modulations such as QPSK, BPSK and 16/64QAM, as well as analog modulations like AM and chirp. In regards to access schemes, OFDMA and CDMA were used. There are also nonlinear modulation schemes (Proakis & Salehi, 2008) which are also encountered in wireless communications including such as the *Gaussian minimum shift keying* (GMSK) which is used in the GSM mobile phone standard. Moreover, there are other access technologies such as the *sparse code multiple access* (SCMA) which is a potential candidate for the 5G standard (Zhang Dong, 2016; Chen et al., 2016). Therefore, the scope of the generic CS framework can be

widened if research is undertaken to directly investigate the application of these other modulation schemes in the new CS framework

c. The UNI-CS model of the framework employs both parametric and non-parametric methods, namely the AR and MT spectrum estimation methods respectively. There are also other methods which are of interest. Firstly, there are more sophisticated parametric spectrum estimation methods considered suitable for signals which can be represented by the harmonic model, such as the Pisarenko, MUSIC and ESPRIT method (Manolakis et al., 2005), which have exhibited better resolution and better frequency estimation characteristics that the AR method (Marple, 1987). It is also noted that the harmonic signal model is suitable for the RD, as mentioned in Section 2.4.3. There is also the FB non-parametric spectrum estimator, which has been proposed for CR spectrum sensing (Farhang-Boroujeny, 2008a). Furthermore, FB multicarrier is a candidate modulation scheme for 5G communications (Banelli et al., 2014). Therefore, the performance of the framework could be enhanced and its scope extended if research is undertaken to investigate the application of the said methods in the framework.

d. The generic CS framework has exploited signal sparsity in the Fourier and WH domain. There are however, other domains in which various types of signals can exhibit sparsity, such as the various families of wavelet transforms (Mallat, 1999), curvelet transforms (Starck et al., 2010), and the Karhunen-Loève transform (Mallat, 1999). It would be beneficial to explore strategies for integrating some of these sparse bases into the generic CS framework and also investigate the levels of sparsity of wireless signals with respect to them The discrete wavelet transform in particular can potentially be exploited in OFDM (Ali, 2011), though the major design challenge would be to determine the most appropriate mother wavelet function to be applied for these signals types.

e. Finally, new application domains where the developed CS framework could be applicable include energy sensing performance of unlicensed (SU) access to TV White Space (Martin, 2017), while CS has been recently employed in physical layer attack detection algorithms (Fragkiadakis et al., 2012; Maric et al., 2017;

Huang et al., 2016), so the new framework thesis could be utilised to enhance performance for example for wormhole attack prevention techniques such as that proposed in (Karlsson, 2017).

References

3GPP (2010) *Technical Specification Group Radio Access Network; Evolved Universal Terrestrial Radio Access (E-UTRA); Further advancements for E-UTRA physical layer aspects*, TR 36.814 V9.0.0, ETSI.

3GPP (2016) *Technical Specification Group Radio Access Network; Evolved Universal Terrestrial Radio Access (E-UTRA); Physical channels and modulation*, TS 36.211 V13.2.0, ETSI.

3GPP (2017) "The Mobile Broadband Standard", [online] Available from: http://www.3gpp.org (Accessed 25 July 2017).

3GPP (2014) *Universal Mobile Telecommunications System (UMTS); LTE; EVS Codec General Overview*, TS 26.441 version 12.0.0, ETSI.

A. Hedayat, A. and Wallis, W. (1978) "Hadamard Matrices and Their Applications", *The Annals of Statistics*, 6(6), pp. 1184-1238.

Afif Osseiran, Jose F. Monserrat, J. and Patrick Marsch, P. (2016) *5G Mobile and Wireless Communications Technology*, 1st ed. Cambridge University Press.

Agaian, S., Sarukhanyan, H., Egiazarian, K. and Astola, J. (2011) *Hadamard Transforms*, 1st ed. SPIE Press.

Akaike, H. (1974) "A new look at the statistical model identification.", *IEEE Trans. Automatic Control*, 19, pp. 716-723.

Akaike, H. (1970) "Statistical predictor identification", *Annals Inst. Statistical Mathematics*, 22, pp. 203-217.

Akyldiz, I., Lee, W., Vuran, M. and Mohanty, S. (2006) "NeXt generation/dynamic spectrum access/cognitive radio wireless networks: A survey", *Computer Networks Journal*, 50, pp. 2127-2159.

Ali, A. (2011) "Discrete Wavelet Transform Based Wireless Digital Communication Systems", 1st ed. In Olkkonen, J. (ed.), *Discrete Wavelet Transforms - Theory and Applications*, Intech.

Amini, P., Kempter, R. and Farhang-Boroujeny, B. (2006) "A comparison of alternative filter bank multicarrier methods in cognitive radios", In *Software Defined Radio Conference*, Orlando, USA, 13-17 November.

Arianandа, D., Lakshmanan, M. and Nikookar, H. (2009) "A survey of spectrum sensing techniques for cognitive radio", *2nd International Workshop on Cognitive Radio and Advanced Spectrum Management*, pp. 74-79, Denmark, 18-20 May.

Banelli, P., Buzzi, S., Colavolpe, G., Modenini, A., Rusek, F. and Ugolini, A. (2014) "Modulation Formats and Waveforms for 5G Networks: Who Will Be the Heir of OFDM?", *IEEE Signal Processing Magazine*, 31(6), pp. 80-92.

Baraniuk, R., Davenport, M., DeVore, R. and Wakin, M. (2007) *A simple proof of the restricted isometry property principle for random matrices*, Constructive Approximation, [online] Available from: http://dsp.rice.edu/cs/jlcs-vo3.pdf. (Accessed 22 July 2017).

Baraniuk, R., Davenport, M., Duarte, M. and Hegde, C. (2017) *An Introduction to Compressive Sensing*, CONNEXIONS, [online] Available from: http://cnx.org/content/col11133/1.5 (Accessed 18 July 2017).

Baraniuk, R. (2007) "Compressive sensing: Lecture notes", *IEEE Signal Processing Magazine*, 24(4), pp. 118–124.

Beauchamp, K. and Debnath, L. (1979) "Walsh Functions and Their Applications", *IEEE Transactions on Systems, Man, and Cybernetics*, 9(1), pp. 67-87.

Beauchamp, K. (1975) *Walsh Functions and Their Applications*, Academic Press.

Ben Letaief, K. and Zhang, W. (2007) "Information Theoretic Analysis of Cognitive Radio Systems", 1st ed. In Hossain, E. and Bhargava, V. (ed.), *Cognitive Wireless Communication Networks*, Springer.

Blumensath, T. and Davies, M. (2009) "Iterative hard thresholding for compressive sensing", *Applied and Computational Harmonic Analysis*, 27(3), pp. 265–274.

Boccuzzi, J. (2008) *Signal Processing for Wireless Communications*, 1st ed. McGraw Hill.

Bostian, C., Kaminski, N. and Fayez, A. (2016) *Cognitive Radio Engineering*, 1st ed. Scitech/IET.

Boyd, S. and Vanderberghe, L. (2004) *Convex Optimization*, 1st ed. Cambridge University Press.

Braione, P., Denaro, G. and Pezzè, M. (2012) "On the Integration of Software Testing and Formal Analysis", 1st ed. In Meyer, B. and Nordio, M. (ed.), *Empirical Software Engineering and Verification*, Springer.

Broderson, R., Wolisz,, A., Cabric, D., Mishra,, S. and Willkomm,, D. (2004) *CORVUS: A cognitive radio approach for usage of virtual unlicensed spectrum*, Submitted at the University of Berkeley, [online] Available from: https://pdfs.semanticscholar.org/776b/57fd1f0992d6cb70753623d99a1bee66a2da.pdf (Accessed 18 July 2017).

Brown, T. (2005) "An Analysis of Unlicensed Device Operation in Licensed Broadcast Service Bands", *Proc. IEEE 1st Symp. Dynamic Spectrum Access Networks*, pp. 11-29, Baltimore, USA, 8-11 November.

Bruckstein, A., Donoho, D. and Elad, M. (2009) "From sparse solutions of systems of equations to sparse modeling of signals and images", *Society for Industrial and Applied Mathematics*, 51(1), pp. 34–81.

Cabric, D., Mishra, M. and Brodersen, R. (2004) "Implementation issues on spectrum sensing for cognitive radios.", *Proceedings of 38th Asilomar Conference on Signals, Systems and Computers*, Vol 1, pp. 772-776, Pacific Grove, USA, 7-10 November.

Cabric, D., Tkachenko, A. and Brodersen, R. (2006) "Spectrum sensing measurements of pilot, energy and collaborative detection", *IEEE Military Communications Conference*, pp. 1-7, Washington, D.C,, USA, 23-25 October.

Candès, E. and Romberg, J. (2017) "l1 Magic, a collection of MATLAB routines for solving the convex optimization programs central to compressive sampling.", [online] Available from: https://statweb.stanford.edu/~candes/l1magic/ (Accessed 23 July 2017).

Candès, E. and Romberg, J. (2005) "Practical signal recovery from random projections", *SPIE 17th International Symposium on Electronic Imaging III*, 5674, pp. 76-86, Bruges, Belgium, 23-27 May.

Candès, E. and Tao, T. (2005) "Decoding by linear programming," IEEE Transactions on Information Theory", *IEEE Transactions on Information Theory*, 51(12), pp. 4203–4215.

Candès, E. and Tao, T. (2006) "Near optimal signal recovery from random projections: Universal strategies", *IEEE Transactions on Information Theory*, 52(12), pp. 5406-5425.

Candès, E. and Wakin, M. (2008) "An introduction to compressive sampling", *IEEE Signal Processing Magazine*, 25(2), pp. 21-30.

Candès, E., Romberg, J. and Tao, T. (2006) "Robust uncertainty principles: Exact signal recovery from highly incomplete frequency information", *IEEE Transactions on Information Theory*, 52(2), pp. 489-509.

Candès, E. (2006) "Compressive Sampling", *Proceedings of International Congress of Mathematicians*, 3, pp. 1433–1452.

Candès, E., Romberg, J. and Tao, T. (2006) "Stable signal recovery from incomplete and inaccurate measurements", *Comm. Pure Appl. Math*, 59(8), pp. 1207-1223.

Carvalho, N., Cidronali, A. and Gómez-Garcia, R. (2015) *White Space Communication Technologies*, 1st ed. Cambridge University Press.

Chen, S., Donoho, D. and Saunders, M. (1998) "Atomic decomposition by basis pursuit", *SIAM Journal on Scientific Computing*, 20(1), pp. 33-61.

Chen, Y., Bayesteh, A., Wu, Y., Han, S., Taherzadeh, M., Chen, D. and Ma, J. (2016) "SCMA: A Promising Non-Orthogonal Multiple Access Technology for 5G Networks", *IEEE 84th Vehicular Technology Conference*, pp. 1-6, Montreal, Canada, 18-21 September.

CISCO (2017b) *Cisco Visual Networking Index: Forecast and Methodology, 2016-2011,* CISCO, [online], Available from: http://www.cisco.com/c/en/us/solutions/collateral/service-provider/visual-networking-index-vni/complete-white-paper-c11-481360.htm l(Accessed 13 July 2017).

CISCO (2016) *Cisco Visual Networking Index: Global Mobile Data Traffic Forecast Update, 2015-2020, CISCO,* [online], Available from: http://www.cisco.com/c/dam/m/en_in/innovation/enterprise/assets/mobile-white- paper-c11-520862.pdf (Accessed 13 July 2017.

CISCO (2017a) *Cisco Visual Networking Index: Global Mobile Data Traffic Forecast Update, 2016-2012, White Paper,* [online], Available from: http://www.cisco.com/c/us/solutions/collateral/service-provider/visual-networking-index-vni/mobile-white-paper-c11-520862.html (Accessed 18 July 2017).

CISCO (2017c) *The Zettabyte Era: Trends and Analysis*, 1st ed. CISCO, [online] Available from: http://www.cisco.com/c/en/us/solutions/collateral/service- provider/visual-networking-index-vni/vni-hyperconnectivity-wp.html (Accessed 20 July 2017).

CTIA (2016) *Background on CTIA's Wireless Industry Survey*, CTIA, [online] Available from: http://ttps://ctia.org/docs/default-source/default-document- library/ ctia_survey_ye_2015_graphics.pdf?sfvrsn=0 (Accessed 18 July 2017).

Dahlman, E., Parkvall, S. and Skold, J. (2014) *4G: LTE/LTE-Advanced for Mobile Broadband*, 2nd ed. Elsevier.

Daubechies, I., Defrise, M. and DeMol, C. (2004) "An iterative thresholding algorithm for linear inverse problems", *Comm. Pure Appl. Math*, 57(11), pp. 1413–1457.

Davenport, M. and Wakin, M. (2010) "Analysis of orthonormal matching pursuit using the restricted isometry property", *IEEE Transactions on Information Theory*, 56(9), pp. 4395–4401.

Davenport, M., Laska, J., Boufounos, P. and Baraniuk, R. (2009) *A simple proof that random matrices are democratic*, Rice University, TREE.

De Almeida, E., De Carvalho, P., Cordeiro, P. and Vieira, R. (2008) "Experimental study of a wavelet-based spectrum sensing technique", *42nd Asilomar Conference on Signals, Systems and Computers*, pp. 1552-1556, Pacific Grove, USA, 26-29 October.

De Nardis, L. and Di Benedetto, M. (2007) "Overview of the IEEE 802.15.4/4 standards for low data wireless personal data networks", *4th Workshop on Positioning, Navigation and Communication*, pp. 285-289, Hannover, Germany, 22 March.

DeNardis, L. (2011) *Opening Standards: The Global Politics of Interoperability (The Information Society Series)*, 1st ed. MIT Press.

DeVore, R. (1998) "Nonlinear approximation", *Acta Numerica*, 7, pp. 51-150.

Divakaran, K., Manikandan, N. and Hari, S. (2011) "Wavelet based spectrum sensing techniques for cognitive radio-A survey", *International Journal of Computer Science and Information Technology (IJCSIT)*, 3(2), pp. 123-137.

Donoho, D. and Elad, M. (2003) "Optimally sparse representation in general (non orthogonal) dictionaries via l1 minimization", *Proceedings of the National Academy of Science,*, 100(5), pp. 2197–2202.

Donoho, D. and Huo, X. (2001) "Uncertainty principles and ideal atomic decomposition", *IEEE Transactions on Information Theory*, 47(7), pp. 2845–2862.

Donoho, D., Vetterli, M., DeVore, R. and Daubechies, I. (1998) "Data compression and harmonic analysis", *IEEE Transactions on Information Theory*, 44(6), pp. 2435–2476.

Donoho, D. (2006) "Compressed sensing", *IEEE Transactions on Information Theory,*, 52(4), pp. pp. 1289–1308.

Donoho, D. (2004) *Compressed sensing*, Technical Report, Stanford University.

Donoho, D. (1995) "Denoising by shift-thresholding", *IEEE Transactions on Information Theory*, 41(3), pp. 613-627.

Doyle, L. (2009) *Essentials of Cognitive Radio*, Cambridge University Press.

Duarte, M. and Eldar, Y. (2011) "Structured Compressed Sensing: From Theory to Applications", *IEEE Transactions on Signal Processing*, 59(9), pp. 4053-4085.

Elad, M. and Bruckstein, A. (2002) "A generalized uncertainty principle and sparse representation in pairs of bases", *IEEE Transactions on Signal Processing*, 48(9), pp. 2558–2567.

Elad, M. (2010) *Sparse and Redundant Representations: From Theory to Applications in Signal and Image Processing*, 1st ed. Springer.

Eldar, Y. and Kutyniok, G. (2012) *Compresses Sensing, Theory and Applications*, 1st ed. Cambridge University Press.

Eldar, Y. and Mishali, M. (2009) "Beyond bandlimited sampling", *IEEE Signal Processing Magazine*, 26(3), pp. 48–68.

Farhang-Boroujeny, B. and Kempter, R. (2008) "Multicarrier communication techniques for spectrum sensing and communications in cognitive radio", *IEEE Communications Magazine*, 48(4), pp. 80–85.

Farhang-Boroujeny, B. (2008) "A square-root Nyquist (M) filter design for digital communication systems", *IEEE Transactions on Signal Processing*, 56(5), pp. 2127–2132.

Farhang-Boroujeny, B. (2008) "Filter bank spectrum sensing for cognitive radios", *IEEE Transactions on Signal Processing*, 56(55), pp. 1801-1811.

Farhang-Boroujeny, B. (2003) "Multicarrier modulation with blind detection capability using cosine modulated filter banks", *IEEE Transactions on Communications*, 51(12), pp. 2057-2070.

FCC (2015) *Amendment of the Commission's Rules with Regard to Commercial Operations in the 3550-3650 MHz Band*, [online] Available from: https://apps.fcc.gov/edocs_public/attachmatch/DA-15-955A1.pdf (Accessed 9 December 2017).

FCC (2002) *Spectrum policy task force*, ET Docket 02-135.

FCC (2004) *Unlicensed operation in the TV broadcast bands*, ET Docket 04-186.

Fette, B. (2009) *Cognitive Radio Technology*, 2nd ed. Elsevier.

Fette, B. (2004) "Technical Challenges and Opportunities", *Conference on Cognitive Radio*, pp. Las Vegas, USA, 15-16 March.

Flores, A., Guerra, R., Knightly, E., Ecclesine, P. and Pandey, S. (2013) "IEEE 802.11af: A standard for TV white space spectrum sharing", *IEEE Communications Magazine*, 51(10), pp. 92-100.

Fornassier, M. and Rauhut, H. (2015) "Compressive Sensing", In Scherzer, O. (ed.), *Handbook of Mathematical Methods in Imaging*, Springer.

Fragkiadakis, A., Nikitaki, S. and Tsakalides, P. (2012) "Physical-layer intrusion detection for wireless networks using compressed sensing", *IEEE 8th International Conference on Wireless and Mobile Computing, Networking and Communications*, pp. 845-852, Barcelona, Spain, 8-10 October.

Gardner, W. and Brown, W. (1987) "Spectral correlation of modulated signals: Part II-Digital modulation,", *IEEE Transactions on Communications*, 35(6), pp. 595-601.

Ghasemi, A. and Sousa, E. (2008) "Spectrum Sensing in Cognitive Radio Networks: Requirements, Challenges and Design Trade-offs", *IEEE Communications Magazine*, 46(4), pp. 32-39.

Goldsmith, A. (2005) *Wireless Communications*, 1st ed. Cambridge University Press.

Grayver, E. (2013) *Implementing Software Defined Radio*, 1st ed. Springer.

Guizani, M., Chen, H. and Wang, C. (2015) *The Future of Wireless Networks: Architectures, Protocols, and Services*, 1st ed. CRC Press.

Hadamard, J. (1893) "Résolution d'une question relative aux déterminants", *Bull. Sci. Math*, 17, pp. 240-246.

Harms, A., Bajwa, W. and Calderbank, R. (2013) "A constrained random demodulator for sub-Nyquist sampling", *IEEE Transactions on Signal Processing,*, 61(3), pp. 707-723.

Harris, F. (2004) *Multirate Signal Processing for Communication Systems*, 1st ed. Prentice Hall.

Hayashi, K., Nagahara, M. and Tanaka, T. (2013) "A User's Guide to Compressed Sensing for Communications Systems", *IEEE Transactions of Communications*, E96-B(3), pp. 685-712.

Haykin, S., Thomson, D. and Reed, H. (2009) "Spectrum Sensing for Cognitive Radio", *Proceedings of the IEEE*, 97(5), pp. 849-877.

Haykin, S. (2005) "Brain-empowered wireless communications", *IEEE Journal on Selected Areas in Communications*, 23(2), pp. 2-1-220.

Haykin, S. (2007) "Fundamental Issues in Cognitive Radio", 1st ed. In Hossain, E. and Bhargava, V. (ed.), *Cognitive Wireless Communication Networks*, Springer.

Hossain, E. and Bhargava, V. (2007) *Cognitive Wireless Communication Networks*, Springer.

Huang, Y., Jin, L., Huang, K., Lu, H. and Kang, X. (2016) "Performance analysis of the encryption method based on compressed sensing at the physical layer", *19th International Symposium on Wireless Personal Multimedia Communications*, pp. 188-193, Shenzhen, China, 14-16 November.

Ian F. Akyildiz, I., Lo, B. and Balakrishnan, R. (2011) "Cooperative spectrum sensing in cognitive radio networks: A survey", *Physical Communication*, 4, pp. 40-62.

IEEE 802.22 Working Group (2017) [online] Available from: IEEE 802.22, http://www.ieee802.org/22/. (Accessed 18 July 2017).

IEEE DySPAN (2017) "IEEE DySPAN Standards Committee (DySPAN-SC)", *Grouper.ieee.org*, [online] Available from: http://grouper.ieee.org/groups/dyspan/index.html (Accessed 9 December 2017).

Ikuma, T. and Pour, N. (2008) "A comparison of three classes of spectrum sensing techniques", *IEEE Globecom*, pp. 1-5, New Orleans, USA, 30 Nov-4 Dec.

Ipatov, V. (2005) *Spread Spectrum and CDMA, principles and applications*, 1st ed. John Wiley & Sons.

Israeli, E., Tsiper, S., Cohen, D., Shoshan, E., Hilgendorf, R., Reysenson, A. and Eldar, Y. (2014) "Hardware Calibration of the Modulated Wideband Converter", *Globecom, Cognitive Radio and Networks Symposium*, pp. 948-953, Austin, USA, 8-12 December.

Jain, R. (2014) "IEEE 802.22 Wireless Regional IEEE 802.22 Wireless Regional Area Networks", Presentation.

Kanjilal, P. (1995) *Adaptive Prediction and Predictive Control*, 1st ed. Peter Peregrinus/IET.

Karampoulas, D., Dooley, L. and Kouadri, S. (2015) "A multitaper-random demodulator model for narrowband compressive spectral estimation", In *IEEE GlobalSIP*, pp. 1362-1366, Orlando, USA, 14-15 December.

Karampoulas, D., Dooley, L. and Kouadri, S. (2014) "Integration of a precolouring matrix in the random demodulator model for improved compressive spectrum estimation", In *IEEE GlobalSIP*, pp. 1209-1213, Atlanta, USA, 3-5 December.

Karampoulas, D., Dooley, L. and Mostéfaoui, S. (2013) "Precolouring in Compressive Spectrum Estimation for Cognitive Radio", In *IEEE EUROCON*, pp. 1715-1720, Zagreb, Croatia, 1-4 July.

Karampoulas, D., Kouadri, S. and Dooley, L. (2013) "A Novel Precolouring-Random Demodulator Architecture for Compressive Spectrum Estimation", In *IET Intelligent Signal Processing*, pp. 1-6, London, UK, 2-3 December.

Karlsson, J. (2017) "A Unified Wormhole Attack Detection Framework for Mobile AdHoc Networks", PhD, The Open University, UK.

Kasch, W., Ward, J. and Andrusenko, J. (2009) "Wireless network modeling and simulation tools for designers and developers", *IEEE Communications Magazine*, 47(3), pp. 120-127.

Keysight Technologies (2012) *LTE and the Evolution to 4G Wireless: Design and Measurement Challenges*, 2nd ed. Wiley.

Klumperink, E., Shrestha, R., Mensink, E., Arkesteijn, V. and Nauta, B. (2007) "Polyphase multipath radio circuits for dynamic spectrum access", *IEEE Communications Magazine*, 45(5), pp. 104-112.

Kolodzy, P. (2004) "Dynamic Spectrum Policies: Promises and Challenges", *CommLaw Conspectus*.

Kolodzy, P. (2001) "Next generation communications: Kick-off meeting", *Proceedings of Defense Advanced Research Projects Agency*.

Kotelnikov, V. (1933) "On the carrying capability of the ether and wire in telecommunications", *Izd. Red. Upr. Svyazi, RKKA*.

Kothari, C. (2004) *Research Methodology: Methods and Techniques*, 2nd ed. New Age Intern. Publishers.

Laska, J., Boufounos, P., Davenport, M. and Baraniuk, R. (2011) "Democracy in action: Quantization, saturation and compressive sensing", *Journal of Applied and Computational Harmonic Analysis*, 31(3), pp. 429-443.

Laska, J., Kirolos, S., Duarte, M., Ragheb, T. and Baraniuk, R. (2007) "Theory and implementation of an analog-to-information converter using random demodulation", *IEEE International Symposium on Circuits and Systems*, pp. 1959-1962, New Orleans, USA, 27-30 May.

Leon-Garcia, A. (1994) *Probability and Random Processes for Electrical Engineering*, 2nd ed. Addison-Wesley.

Lexa, M., Davies, M. and Thompson, J. (2012) "Reconciling Compressive Sampling Systems for Spectrally Sparse Continuous-Time Signals", *IEEE Transactions on Signal Processing*, 60(1), pp. 155-171.

Lundén, J., Koivunen, V. and Poor, H. (2015) "Spectrum Exploration and Exploitation for Cognitive Radio", *IEEE Signal Processing Magazine*, pp. 123-140.

Madisetti, V. (2010) *The Digital Signal Processing Handbook*, *Digital Signal Processing Fundamentals*, 2nd ed. CRC Press.

Malik, S., Shah, M., Dar, A., Haq, A., Khan, A., Javed, T. and Khan, S. (2010) "Comparative analysis of primary transmitter detection based spectrum sensing", *Australian Journal of Basic and Applied Sciences*, pp. 4522-4531.

Mallat, S. and Zhang, Z. (1993) "Matching pursuits with time-frequency dictionaries", *IEEE Transactions on Signal Processing*, 41(12), pp. 3397-3415.

Mallat, S. (1999) *A Wavelet Tour of Signal Processing*, Academic Press.

Mangia, M., Rovatti, R. and Setti (2011) "Analog-to-Information conversion of sparse and non-white signals: Statistical design of sensing waveforms", *IEEE International Symposium of Circuits and Systems*, pp. 2129-2132, Rio de Janeiro, Brazil, 15-18 May.

Manolakis, D. and Ingle, V. (2011) *Applied Digital Signal Processing*, Cambridge University Press.

Manolakis, D., Ingle, V. and Kogon, S. (2005) *Statistical and Adaptive Signal Processing*, 1st ed. Artech House.

Maral, G. and Bousquet, M. (2009) *Satellite Communications Systems, Systems, Techniques and Technology*, 3rd ed. Wiley.

Marcus, M. (2005) "Unlicensed cognitive sharing of TV spectrum: The controversy at the federal communications commission", *IEEE Communications Magazine*, Vol 43, pp. 24-25.

Maric, S., Biswas, A. and Reisenfeld, S. (2017) "A complete algorithm to diagnose and alleviate the effects of physical layer attacks", *International Conference on Signal and Systems*, pp. 29-34, Bali, Indonesia, 16-18 May.

Marks II, R. (1991) *Introduction to Shannon Sampling and Interpolation Theory*, 1st ed. Springer-Verlag.

Marple, S. (1987) *Digital Spectral Analysis with Applications*, 1st ed. Englewood Cliffs.

Martin, J. (2017) "A Cognitive TV White Space Access Framework", PhD, The Open University, UK.

Mathworks (2017) "MathWorks - Makers of MATLAB and Simulink", *Uk.mathworks.com*, [online] Available from: http://uk.mathworks.com (Accessed 25 July 2017).

McHenry, M. (2005) *NSF spectrum occupancy measurements project summary*, Shared Spectrum Company Report.

Miao, G. (2007) *Signal Processing in Digital Communications i*, 1st ed. Artech House.

Milligan, M. (2003) *Software Defined Radio: Architectures, Systems and Functions*, Wiley.

Mishali, M. and Eldar, Y. (2010) "From theory to practice: Sub-Nyquist sampling of sparse wideband analog signals", *IEEE Journal on Selected Topics on Signal Processing*, 4(2), pp. 375–391.

Mishali, M., Eldar, Y., Dounaevsky, O. and Shoshan, E. (2011) "Xampling: Analog to digital at sub-Nyquist rates,", *IET Circuits, Devices and Systems*, 5(1), pp. 8-20.

Mitola, J. and Maguire, G. (1999) "Cognitive radio: Making software radios more personal", *IEEE Personal Communications*, 6(4), pp. 13-18.

Mitola, J. (2006) *Cognitive radio architecture: The engineering foundations of radio XML*, Wiley.

Mitola, J. (2000) "Cognitive Radio: An integrated agent architecture for software defined radio", PhD, Royal Institute of Technology (KTH), Sweden.

Mitra, S. (2011) *Digital Signal Processing*, 4th ed. McGraw-Hill.

Mody, A. and Chouinard, G. (2010) "IEEE 802.22 Wireless regional area networks", *IEEE 802.22-10/0073r03*.

Mody, A., Blatt, S., Mills, D., Mcelwain, T., Thammakhoune, N., Niedzwiecki, J., Sherman, M., Myers, C. and Fiore, P. (2007) "Recent Advances in Cognitive Communications", *IEEE Comunication Magazine*, 45(10), pp. 54-61.

Muthukrishnan, S. (2005) "Data Streams: Algorithms and Applications", *Foundations and Trends in Theoretical Computer Science*, 1(2), pp. 117-236.

Natarajan, B. (1995) "Sparse approximate solutions to linear systems", *SIAM Journal on Computing*, 24(2), pp. 227-234.

Needell, D. and Vershynin, R. (2010) "Signal recovery from incomplete and inaccurate measurements via regularized orthogonal matching pursuit", *IEEE Journal of Selected Topics in Signal Processing*, 4(2), pp. 310-316.

Nekovee, M. (2010) "A Survey of Cognitive Radio Access to TVWhite Spaces", *International Journal of Digital Multimedia Broadcasting*, Volume 2010, [online] Available from: http://dx.doi.org/10.1155/2010/236568 (Accessed 18 July 2017).

Nekovee, M. (2006) "Dynamic spectrumaccess—concepts and future architectures", *BT Technology Journal*, 24(2), pp. 111-116.

NGMN Alliance (2015) *NGMN 5G White Paper*, [online] Available from: https://www.ngmn.org/uploads/media/NGMN_5G_White_Paper_V1_0.pdf (Accessed 20 July 2017).

NOKIA (2015) *3GPP Enhanced Voice Services (EVS) codec*, NOKIA Corporation.

Nutall, A. (1976) "Spectal Analysis of a Univariate Process with Bad Data Points, via Maximum Entropy and Linear Predictive Techniques", *Naval Underwater Systems Center*, Technical Report TR-5303.

Nyquist, H. (1928) "Certain topics in telegraph transmission theory", *Transactions AIEEE*, 47, pp. 617–644.

Ofcom (2012) *A Consultation on White Space Device Requirements*, TV White Spaces.

OFCOM (2016) *A framework for spectrum sharing*, [online] Available from: https://www.ofcom.org.uk/__data/assets/pdf_file/0028/68239/statement.pdf (Accessed 9 December 2017).

OFCOM (2015) *A framework for spectrum sharing*, [online] Available from: https://www.ofcom.org.uk/__data/assets/pdf_file/0032/79385/spectrum-sharing-framework.pdf (Accessed 9 December 2017).

Ofcom (2007) *Digital Dividend Reviews, A statement on our approach towards awarding the digital dividend*,.

Ofcom (2009) *Digital dividend: cognitive access Statement on licence-exempting cognitive devices using interleaved spectrum*, Ofcom, [online] Available from: https://www.ofcom.org.uk/__data/assets/pdf_file/0023/40838/statement.pdf (Accessed 21 July 2017).

Ofcom (2013) *Ofcom Spectrum Advisory Board Annual Report 2012 - 2013*,.

Oppenheim, A. and Schafer, R. (2009) *Discrete-Time Signal Processing*, 3rd ed. Pearson.

Papoulis, A. (1991) *Probabilities, Random Variables and Stochastic Processes*, 3rd ed. McGrawHill.

Parzen, E. (1974) "Some Recent Advances in Time Series Modeling", *IEEE Trans. Autom. Control*, 19, pp. 723-730.

Percival, D. and Walden, A. (1993) *Spectral Analysis for Physical Applications, Multitaper and Conventional Multivariate Techniques*, 1st ed. Cambridge University Press.

Petrou, M. and Petrou, C. (2010) *Image Processing: The Fundamentals*, 2nd ed.

Pillay, N. and Hu, H. (2013) "Eigenvalue-based spectrum sensing using the exact distribution of the maximum eigenvalue of a Wishart matrix", *IET Signal Processing*, 7(9), pp. 833-842.

Proakis, J. and Manolakis, D. (2006) *Digital Signal Processing; Principles, Algorithms and Applications*, 4th ed. Prentice Hall.

Proakis, J. and Salehi, M. (2008) *Digital Communications*, 5th ed. McGrawHill.

Proakis, J. (2003) *Wiley Encyclopedia of Telecommunications, Volume 5*, John Wiley & Sons.

Quan, Z., Cui, S., Sayed, A. and Poor, V. (2009) "Optimal Multiband Joint Detection for Spectrum Sensing in Cognitive Radio Networks", *IEEE Transactions on Signal Processing*, 57(3), pp. 1128-1140.

Rafael, R. and Woods, R. (2017) *Digital Image Processing*, 4th ed. Pearson.

Ragheb, T., Laska, J., Najati, H. and Kirolos, S. (2008) "A prototype hardware for random demodulation based compressive sensing analog-to-digital conversion", *51st Midwest Symposium on Circuits and Systems*, pp. 37-40, Knoxville, USA, 10-13 August.

Rahman, Q. and Ibnkahla, M. (2005) "Signal Processing for Future Mobile Communications Systems: Challenges and Perspectives", 1st ed. In Ibnkahla, M. (ed.), *Signal Processing for Mobile Communications Handbook*, CRC Press.

Rakesh, J., Vishal, W. and Dalal, U. (2010) "A survey of mobile WiMax IEEE 802.16m standard", *International Journal of Computer and Information Security*, 18(1), pp. 125-131.

Rawat, D., Yan, G. and Bajracharya, C. (2010) "Signal processing techniques for spectrum sensing in cognitive radios", *International Journal of Ultra Wideband Communications and Systems*, x(x/x), pp. 1-10.

Real Wireless (2015) *UK Spectrum Usage & Demand*, UK Spectrum Policy Forum.

Rgheff, M. (2007) *Introduction to CDMA Wireless Communications*, 1st ed. Elsevier.

Rissanen, J. (1983) "A Universal Prior for the Integers and Estimation by Minimum Description Length", *Ann. Stat.*, 11, pp. 417-431.

Riverbed (2017) "OPNET IS NOW PART OF RIVERBED STEELCENTRAL™ ", *Riverbed,* [online] Available from: https://www.riverbed.com/gb/products/steelcentral/opnet.html?redirect=opnet (Accessed 17 August 2017).

Romberg, J. (2009) "Multiple channel estimation using spectrally random probes", *Proc. SPIE Wavelets XIII*, 7446.

Romberg, J. (2007) "Sensing by random convolution", *2nd IEEE Workshop in Computational Advances in Multi-sensor Adaptive Processing*, pp. 137-140, St. Thomas, USA, 12-14 December.

Saltzberg, B. (1967) "Performance of an efficient data transmission system", *IEEE Transactions in Communications Technology*, 15(6), pp. 805-811.

Schaefer, H., Linz, T. and Spillner, A. (2014) *Software Testing Foundations*, 4th ed. Rocky Nook.

Schwartz, M. and Shaw, L. (1975) *Signal Processing: Discrete Spectral Analysis, Detection and Estimation*, 1st ed. McGraw Hill.

Scwhartz, M. (2005) *Mobile Wireless Communications*, 1st ed. Cambridge University Press.

Seberry, J., Wysocki, B. and Wysocki, T. (2005) "On some applications of Hadamard matrices", *Metrika*, 62(2-3), pp. 221–239.

Shannon, C. (1949) "Communication in the presence of noise", *Proceedings of Institute of Radio Engineers*, 37(1), pp. 10-21.

Shellhammer, S. (2008) "Spectrum sensing in IEEE 802.22", *IARP Workshop in Cognitive Information Processing,*, pp. 1-6, Santorini, Greece, 9-10 June.

Slavinsky, J., Laska, J., Davenport, M. and Baraniuk, R. (2011) "The Compressive Multiplexer for Multi-Channel Compressive Sensing", *ICASSP*, pp. 3980-3983, Prague, Czech Republic, 22-27 May.

Slepian, D. (1978) "Prolate spheroidal wave functions, Fourier analysis and uncertainty", *Bell Systems Technical Journal*, 57, pp. 1371–1430.

Smith, C. and Collins, D. (2007) *3G Wireless Networks*, 2nd ed. McGrawHill.

Stallings, W. (2014) *Data and Computer Communications*, 10th ed. Pearson.

Starck, J., Murtagh, F. and Fadili, J. (2010) *Sparse Image and Signal Processing. Wavelets, Curvelets and Morphological Diversity*, 1st ed. Cambridge University Press.

Stevenson, C. (2009) "IEEE 802.22: The First Cognitive Radio Wireless Regional Network Standard", *IEEE Communications Magazine*, pp. 133-138.

Strang, G. (2016) *Introduction to Linear Algebra*, 5th ed. Wellesley-Cambridge Press.

Subhedar, M. and Birajdar, G. (2011) "Spectrum sensing techniques for cognitive radio networks", *International Journal of Next-Generation Networks*, 3(2), pp. 37-51.

Sun, H., Laurenson, D. and Wang, C. (2010) "Computationally Tractable Model of Energy Detection Performance Over Slow Fading Channels", *IEEE Commun. Letters*, 14(10), pp. 924-926.

Sun, H., Nallanathan, A., Wang, C. and Chen, Y. (2013) "Wideband spectrum sensing for cognitive radio networks: A survey", *IEEE Wireless Communications*, 20(2), pp. 74-81.

Sylvester, J. (1867) "Thoughts on Orthogonal Matrices, Simultaneous Sign-Successions, and Tessellated Pavements in Two or More Colours, with Applications to Newton's Rule, Ornamental Tile-Work, and the Theory of Numbers", *Phil. Mag*, 34, pp. 461-475.

Taheri, O. and Vorobyov, S. (2011) "Segmented Compressed Sampling for Analog-to-Information Conversion: Method and Performance Analysis", *IEEE Transactions on Signal Processing*, 59(2), pp. 554-572.

Tandra, R. and Sahai, A. (2005) "Fundamental limits on detection in low SNR under noise uncertainty", *IEEE International Conference in Wireless Networks, Communications and Mobile Computing*, 1, pp. 464-469, Maui, USA, 13-16 June.

Tandra, R. and Sahai, A. (2008) "SNR walls for signal detection", *IEEE Journal of Selected Topics on Signal Processing*, 1(2), pp. 4-17.

Tang, H. (2005) "Some physical layer issues of wide-band cognitive radio systems,", *Proc. IEEE Int. Symposium on New Frontiers in Dynamic Spectrum Access Networks*, pp. 151-159, Baltimore, USA, 8-11 November.

Task Group 4 (2017) "IEEE 802.15 WPAN", [online] Available from: http://www.ieee802.org/15/pub/TG4.html (Accessed 24 July 2017).

Thomson, D. (1982) "Spectrum estimation and harmonic analysis", *Proceedings of the IEEE*, 20(9), pp. 1055-1096.

Tian, Z. and Giannakis, G. (2006) "A wavelet approach to wideband spectrum sensing for cognitive radios", *IEEE 1st International Conference on Cognitive Radio Oriented Wireless Networks and Communications*, pp. 1-5, Mykonos, Greece, 8-10 June.

Tian, Z. and Giannakis, G. (2007) "Compresses sensing for wideband cognitive radios", *IEEE International Conference on Acoustics, Speech and Signal Processing*, 4, pp. 1357–1360, Honolulu, USA, 16-20 April.

Tian, Z. (2008) "Compressed wideband sensing in cooperative cognitive radio networks", *IEEE Globecom*, pp. 1-5, New Orleans, USA, 30 Nov - 4 Dec.

Tkachenko, A., Cabric, D. and Brodersen, R. (2009) "Cyclostationary feature detector experiments using reconfigurable BEE2", *IEEE Proceedings of International Symposium on New Frontiers in Dynamic Spectrum Access Networks*, pp. 216-219.

Tomar, G., Bagwari, A. and Kanti, J. (2017) *Introduction to Cognitive Radio Networks and Applications.*, 1st ed. CRC Press.

Torrieri, D. (2005) *Principles of Spread-Spectrum Communication Systems*, 1st ed. Springer.

Tranter, W., Shanmugan, K., Rappaport, T. and Kosbar, K. (2003) *Principles of communication systems simulation with wireless applications*, 1st ed. Prentice Hall.

Tropp, J. and Needell, D. (2009) "CoSaMP: Iterative signal recovery from incomplete and inaccurate samples", *Applied and Computational Harmonic Analysis*, 26(3), pp. 301-321.

Tropp, J., Gilbert, A. and Strauss, M. (2006) "Algorithms for simultaneous sparse approximation. Part I: Greedy pursuit", *Journal of Signal Processing*, 86(3), pp. 572–588.

Tropp, J., Laska, M., Duarte, M., Romberg, J. and Baraniuk, R. (2010) "Beyond Nyquist: Efficient Sampling of Sparse Bandlimited Signals", *IEEE Transactions on Information Theory*, 56(1), pp. 520-544.

Tropp, J., Wakin, M., Duarte, M., Baron, D. and Baraniuk, R. (2006) "Random filters for compressive sampling and reconstruction 872–875", *IEEE Proceedings of International Conference of Acoustics, Speech and Signal Processing (ICASSP)*, pp. 872–875, Toulouse, France, 14-19 May.

Tropp, J. (2004) "Greed is good: Algorithmic results for sparse approximation", *IEEE Transactions on Information Theory*, 50(10), pp. 2231–2242.

Tsaig, Y. and Donoho (2004) *Extensions of compressed sensing*, Technical Report, Stanford University.

Tuttlebee, W. (2002) *Software Defined Radio: Origins, Drivers and International Perspectives.*, Wiley.

Tzafestas, S. (1985) *Walsh Functions in Signal and Systems Analysis and Design*, 1st ed. Van Nostrand Reinhold.

Ulrich, T. and Clayton, R. (1976) "Time Series Modeling and Maximum Entropy", *Phys. Earth Planet. Inter.*, 12, pp. 188-200.

Unser, M. (2000) "Sampling-50 years after Shannon", *Proceedings of IEEE*, 88(4), pp. 569–587.

Vaidyanathan, P. (1993) *Multirate Systems and Filter Banks*, Prentice-Hall.

Walden, R. (1999) "Analog-to-digital converter survey and analysis", *IEEE Journal of Selected Areas in Communications*, 17(4), pp. 539–550.

Walden, R. (1999) "Performance trends for analog-to digital converter", *IEEE Communications Magazine,*, 37(2), pp. 96-101.

Walsh, J. (1923) "A closed set of normal orthogonal functions", *American Journal of Mathematics*, 45, pp. 5-24.

Wang, S., Bao, J., Shen, B., Huang, Q. and Chen, Q. (2014) "Eigenvector based cooperative wideband spectrum sensing for cognitive radios", *Proceedings of IEEE International Conference on Ubiquitous and Future Networks*, pp. 346-351.

Webb, W. (2012) *Understanding Weightless*, 1st ed. Cambridge University Press.

Weisstein, E. (2017) "Walsh Function", *MathWorld--A Wolfram Web Resource*, [online] Available from: http://mathworld.wolfram.com/WalshFunction.html (Accessed 24 July 2017).

Werther, O. and Minihold, R. (2013) *LTE: System Specifications and Their Impact on RF & Base Band Circuits*, Application Note, Rohde & Schwarz.

Whittaker, E. (1915) "On the functions which are represented by the expansions of the interpolation theory", *Proceedings of the Royal Society*, Sec. A(35), pp. 181–194.

Y. Lu, Y., Guo, W., Wing, X. and Wang, W. (2011) "Distributed streaming compressive spectrum sensing for wide-band cognitive radio networks", *73rd IEEE Vehicular Technology Conference*, pp. 1-5, Budapest, Hungary, 15-18 May.

Yu, L., Hong, S. and Zhao, H. (2009) "The performance analysis of spectrum sensing algorithms based on wavelet edge detection,", *1st International Conference on Wireless Communications, Networking and Mobile Computing*, pp. 1-4, Beijing, China, 24-28 September.

Yu, Z. and Hoyos, S. (2009) "Compressive spectrum sensing front-ends for cognitive radios", *IEEE International Conference on Systems, Man and Cybernetics*, pp. 1899–1904, San Antonio, USA, 11-14 October.

Yu, Z., Hoyos, S. and Sadler, B. (2008) "Mixed-signal Parallel Compressed Sensing and Reception for Cognitive Radio", *ICASSP*, pp. 3861-3864, Las Vegas, USA, 31 Mar - 04 Apr.

Yucek, T. and Arslan, H. (2009) "A Survey of Spectrum Sensing Algorithms for Cognitive Radio Applications", *IEEE Communications Surveys & Tutorials*, 11(1), pp. 116-130.

Zeng, Y. and Liang, Y. (2009) "Spectrum-sensing algorithms for cognitive radio based on statistical covariances", *IEEE Transaction on Communications*, 57(6), pp. 1784-1793.

Zhang Dong, Z. (2016) *Up in the air with 5G*, 1st ed. Huawei Publications, [online] Available from: http://www.huawei.com/en/publications/communicate/80/up-in-the-air-with-5g (Accessed 26 July 2017).

Zhao, L., Chen, X. and Zhang, G. (2011) "A novel spectrum sensing algorithm based on compressive sensing for cognitive radio", *IEEE Workshops of International Conference on Advanced Information Networking and Applications*, pp. 243-246, Singapore, 22-25 March.

Zheng, H. and Cao, L. (2007) "Decentralized Spectrum Management Through User Coordination", 1st ed. In Hossain, E. and Bhargava, V. (ed.), Springer.